UNIVERSIDAD MICHOACANA DE SAN NICOLÁS DE HIDALGO

FACULTAD DE INGENIERÍA ELÉCTRICA

DIVISIÓN DE ESTUDIOS DE POSGRADO

Power Quality State Estimation in Transient and Steady State

THESIS

Presented to obtain the degree of

DOCTOR OF SCIENCE IN ELECTRICAL ENGINEERING

by

RAFAEL CISNEROS MAGAÑA

Dr. Sc. J. AURELIO MEDINA RIOS

Thesis Advisor

Morelia, Michoacán, México December. 2013

POWER QUALITY STATE ESTIMATION IN TRANSIENT AND STEADY STATE

The Degree Examination Committee Members **approve** the **Doctorate in Sciences in Electrical Engineering** Thesis (Tesis de Doctorado en Ciencias en Ingeniería Eléctrica) of ***Rafael Cisneros Magaña***

Dr. Claudio R. Fuerte Esquivel
President of the Committee
(Presidente del Jurado)

Dr. J. Aurelio Medina Ríos
Advisor (Director de Tesis)

Dr. Antonio Ramos Paz
Committee Member (Vocal)

Dra. Elisa Espinosa Juárez
Committee Member (Vocal)

Dr. Gary W. Chang
External Examiner (Examinador Externo)
National Chung Cheng University, Taiwan

Dr. J. Aurelio Medina Rios
Head of the Division for Postgraduate Studies,
Electrical Engineering Faculty, UMSNH
(Jefe de la División de Estudios de Posgrado
de la Facultad de Ingeniería Eléctrica, UMSNH)

UNIVERSIDAD MICHOACANA DE SAN NICOLAS DE HIDALGO
December 2013

To my family: María Eva, Rafael Martín and Rebeca
For their understanding, motivation and help.

To my sisters: Ma. Remedios and Eva
For their unconditional help and support.

In memory of my dear parents:
Hermila Magaña Ruíz and Rafael Cisneros Magaña
For their education, advice, and example of perseverance in life.

In memory of my dear aunt and uncle:
Cleotilde and Martín Magaña Ruíz
For everything they did for me when I needed it.

Acknowledgments:

My acknowledgment and gratefulness to the Universidad Michoacana de San Nicolás de Hidalgo, Facultad de Ingeniería Eléctrica and the División de Estudios de Posgrado, thanks for the opportunity to continue postgraduate studies.

I gratefully acknowledge the Consejo Nacional de Ciencia y Tecnología CONACYT, México, thanks CONACYT for the financial assistance during my master and doctorate studies.

I like to express my appreciation and gratitude to Dr. J. Aurelio Medina Rios, supervisor of this work for his direction, invaluable support, incessant encouragement, motivation and friendship. Thanks for his advice, his guide and his permanent availability.

I am very grateful to Dr. Claudio Ruben Fuerte Esquivel, Dra. Elisa Espinosa Juárez and Dr. Antonio Ramos Paz, thanks for their comments, suggestions and observations to enhance this work. Thanks to Dr. Gary W. Chang of the National Chung Cheng University of Taiwan, R.O.C., external examiner of the present work and for his valuable comments.

My gratitude to Dr. Venkata Dinavahi for his guide, support and help during the research stay related with this project conducted at the University of Alberta, Canada.

I thank and acknowledge the academic staff of the División de Estudios de Posgrado of the Facultad de Ingeniería Eléctrica for their education, knowledge, continued collaboration and cooperation during my master and doctorate studies.

I am grateful to the administrative staff of the División de Estudios de Posgrado of the Facultad de Ingeniería Eléctrica, for their support and help.

Resumen

Esta tesis presenta una metodología que permite el análisis de la estimación de estado en dominio del tiempo en condiciones de estado estacionario y transitorio de los sistemas de potencia, con referencia al campo de calidad de la energía.

El objetivo principal es el desarrollo de la metodología mencionada en el dominio del tiempo por medio de la representación en espacio de estado del sistema de potencia. Se analiza el efecto de fenómenos adversos de calidad de energía, tales como la distorsión armónica, los armónicos variables en el tiempo, inter-armónicos, transitorios y depresiones de voltaje.

La estimación de estado examina aspectos como la ubicación de las mediciones para obtener una observabilidad adecuada del sistema y mediciones con ruido. La descomposición en valores singulares se utiliza para verificar la observabilidad del sistema durante la estimación de estado y la solución de casos sobre, normal y bajo determinados.

La solución del sistema se obtiene mediante la incorporación de técnicas numéricas computacionales eficientes, tales como los métodos de Newton para obtener el estado estacionario periódico basado en el mapa de Poincaré y la extrapolación al ciclo límite. La diferenciación numérica y una versión mejorada en base a la simetría de media onda de las señales se aplican en casos de estudio para resolver la estimación del estado de calidad de la energía, proporcionando una condición inicial conveniente para los métodos de filtro de Kalman, normal, extendido y unscented. Estos filtros se aplican a la solución de casos de estudio de la estimación de estado en el dominio del tiempo sobre armónicos, interarmónicos, transitorios y depresiones de voltaje.

El algoritmo del filtro de Kalman se implementa utilizando técnicas de procesamiento en paralelo; una configuración CPU-GPU ejecuta el procesamiento en paralelo bajo la plataforma CUDA y la biblioteca CUBLAS para evaluar cada paso de tiempo el filtro de Kalman. El sistemas de potencia se replican para analizar sistemas más grandes y verificar el efecto de la velocidad comparando el tiempo de ejecución del código C ++ secuencial y las soluciones paralelas CPU-GPU aplicadas para resolver la estimación de estado de la calidad de energía.

Los resultados obtenidos a partir de la estimación de estado de la red eléctrica se validan comparándolos con los obtenidos mediante el simulador PSCAD/EMTDC ampliamente utilizado y aceptado por la industria eléctrica.

Finalmente se obtienen conclusiones sobre los estudios realizados y se sugieren direcciones para continuar el trabajo de investigación desarrollado en el campo de la estimación de estado de la calidad de energía.

Abstract

This thesis presents a methodology that allows the analysis of the time domain state estimation under transient and steady state conditions of power systems, with reference to the power quality field.

The main objective is to develop the mentioned time domain methodology by means of a state space representation of the power systems. The effect of adverse power quality phenomena is analyzed, such as harmonic distortion, time varying harmonics, inter-harmonics, transients and voltage sags.

The state estimation examines aspects such as the location of measurements to obtain an adequate system observability, and noisy measurements. The singular value decomposition is used to verify the system observability during the state estimation and the solution of over, normal and undetermined cases.

The system solution is obtained by incorporating efficient computational numerical techniques, such as the Newton methods to obtain the periodic steady state based on the Poincaré map and extrapolation to the limit cycle. Numerical differentiation and an enhanced version based on the half wave symmetry of the waveforms are applied in case studies to solve the power quality state estimation, and provide a convenient initial state condition for the Kalman filter methods, normal, extended and unscented. These filters are applied to the time domain state estimation solving case studies about harmonics, interharmonics, transients and voltage sags.

The Kalman filter algorithm is implemented using parallel processing techniques; a CPU-GPU configuration executes the parallel processing under the CUDA platform and the CUBLAS library to evaluate each time step of the Kalman filter. Power networks are replicated to analyze larger systems and verify the effect on the speed up comparing the execution time of the sequential C++ code and the CPU-GPU parallel solutions applied to solve the power quality state estimation.

The obtained results from the electrical network state estimation are validated by comparing them against those obtained from a simulator widely used and accepted by the power industry such as the PSCAD/EMTDC.

Finally conclusions are drawn about the conducted studies and directions are suggested to continue the research work developed in the power quality state estimation field.

Power Quality State Estimation in Transient and Steady State

Table of Contents

List of Acronyms and Symbols

Alternating current ..... AC
Angle ..... θ
Apparent power ..... S
Application program interface ..... API
Artificial neural network ..... ANN
Basic Linear Algebra Subprograms ..... BLAS
Brute Force ..... BF
Capacitance C
CUDA Basic Linear Algebra Subprograms ..... CUBLAS
Compute Unified Device Architecture ..... CUDA
Column orthogonal matrix (SVD) ..... $\mathbf{U}$
Derivative of state variable vector at time $t+h$ ..... $\dot{\mathbf{x}}_{t+h}$
Direct current ..... DC
Direct transmission matrix ..... $\mathbf{D}$
Discrete Fourier Transform ..... DFT
Distortion Index ..... DIN
Electric Arc Furnace ..... EAF
Electromagnetic Transient Program ..... EMTP
Electromagnetic Transients including DC ..... EMTDC
Enhanced Numerical Differentiation ..... END
Error vector ..... $\mathbf{e}$
Estimate a posteriori error covariance matrix at time k ..... $\mathbf{P}_k$
Estimate a posteriori state variable vector ..... $\hat{\mathbf{x}}^+$
Estimate a priori error covariance matrix at time k ..... $\mathbf{P}_k^-$
Estimate a priori state variable vector ..... $\hat{\mathbf{x}}^-$
Estimate state variable vector ..... $\hat{\mathbf{x}}$
Extended Kalman filter ..... EKF
Fast Fourier Transform ..... FFT
Flexible alternating current transmission system ..... FACTS
Frequency ..... f
Genetic algorithms ..... GA
Global positioning system ..... GPS
Graphics Processing Unit ..... GPU
Harmonic current ..... I_h
Harmonic order ..... X_h
Harmonic state estimation ..... HSE
High voltage direct current ..... HVDC
Impedance ..... Z
Index ..... J
Inductance L
Infinite ..... ∞, inf
Input variable vector ..... $\mathbf{u}$
Inputs matrix ..... $\mathbf{B}$
Instantaneous current i
Instantaneous voltage v
Integration step ..... h
Kalman filter ..... KF
Kalman filter gain ..... $\mathbf{G}$, $\mathbf{K}$
Kilovolt ..... kV
Kilovoltamper ..... kVA
Kilowatt ..... kW

Kirchhoff's current law ..... KCL
Kirchhoff's voltage law ..... KVL
Least squares ..... LS
Magnetic flux ..... ψ
Measurement noise covariance matrix ..... $\mathbf{R}_k$
Measurement noise vector ..... $\mathbf{w}_k$
Measurement vector ..... $\mathbf{z}$
Measurements matrix ..... $\mathbf{H}$
Median ..... μ
Megawatt ..... MW
Null space coefficient vector ..... k_i
Null space of A matrix ..... *null*[**A**]
Null space vector ..... $\mathbf{x}_{ni}$
Number of measurements ..... *m, me*
Number of state variables ..... *n, nsv*
Numerical differentiation ..... ND
Ordinary differential equation ..... ODE
Output variable vector ..... $\mathbf{y}$
Outputs matrix ..... $\mathbf{C}$
Parallel Kalman filter ..... PKF
Period ..... T
Power factor ..... PF
Power system computer aided design ..... PSCAD
Power quality state estimation ..... PQSE
Power quality ..... PQ
Probability of Δx_k ..... $P_{\Delta xk}$
Process noise covariance matrix ..... $\mathbf{Q}_k$
Process noise vector ..... $\mathbf{v}_k$
Reactance X
Reactive power ..... Q
Real power ..... P
Residual vector ..... $\mathbf{r}$
Resistance ..... R
Rms current I
Rms voltage V
Row orthogonal matrix (SVD) ..... $\mathbf{V}$
Singular value decomposition ..... SVD
Standard deviation ..... σ
State matrix ..... $\mathbf{A}$
State transition matrix ..... $\mathbf{\Phi}$
State variable vector at time $t+h$ ..... $\mathbf{x}_{t+h}$
State variable vector difference ..... $\Delta\mathbf{x}$
State variable vector of a particular solution ..... $\mathbf{x}_p$
State variable vector ..... $\mathbf{x}$
Static compensator ..... STATCOM
Static var compensator ..... SVC
Subspace dimension ..... N
Supervisory Control and Adquisition Data ..... SCADA
Switching function ..... s
Telephone Influence Factor ..... TIF
Thyristor controlled reactor ..... TCR
Thyristor firing angle ..... α
Time Domain Harmonic State Estimation ..... TDHSE
Time step ..... Δt

Time ..... t
Total Demand Distortion..... TDD
Total Harmonic Distortion ..... THD
Transient state estimation..... TSE
Unified power quality state estimation ..... UPQSE
Unscented Kalman filter ..... UKF
Uninterruptible power supply..... UPS
Variance ..... σ^2
Variation..... Δ
Very large scale integration..... VLSI
Voltage sags state estimation ..... VSSE
Weighted Least Squares..... WLS
Wide Area Measurement System ..... WAMS

List of Figures

List of Tables

List of Publications

Indexed by Journal Citation Reports (JCR), published papers:

1. **Time Domain Harmonic State Estimation Based On The Kalman Filter Poincaré Map and Extrapolation to the Limit Cycle,** Medina, A., Cisneros-Magaña Rafael, IET Generation, Transmission & Distribution, volume 6, issue 12, December 2012, pp. 1209-1217.

2. **Time Domain Transient State Estimation Using Singular Value Decomposition Poincaré Map and Extrapolation to the Limit Cycle,** Rafael Cisneros-Magaña, Aurelio Medina, International Journal of Electrical Power and Energy Systems, volume 53, December 2013, pp. 810-817.

Indexed Conference Papers by ISI Thompson, published papers:

1. **Power Quality Transient Phenomena using a State Space Wind Park Dynamic Model,** Cisneros-Magana, R., Medina, A.; IET Conference on Renewable Power Generation (RPG 2011), Edinburgh, UK, September 6-8, 2011.

2. **Parallel Kalman Filter Based Time-Domain Harmonic State Estimation,** Rafael Cisneros-Magaña, Aurelio Medina, Venkata Dinavahi, IEEE North American Power Symposium (NAPS 2013), Manhattan, KS, USA, September 22-24, 2013.

Indexed by Journal Citation Reports (JCR), under review:

1. **Dynamic Harmonic State Estimation using The Extended Kalman Filter in Networks with Nonlinear Loads**, Rafael Cisneros-Magaña, Aurelio Medina, Electric Power Components and Systems.

2. **Efficient Time Domain Power Quality State Estimation using The Enhanced Numerical Differentiation Newton Type Method**, Rafael Cisneros-Magaña, Aurelio Medina, Juan Segundo-Ramírez, International Journal of Electrical Power & Energy Systems.

3. **Time Domain Voltage Sags State Estimation using The Unscented Kalman Filter in Nonlinear Power Networks,** Rafael Cisneros-Magaña, Aurelio Medina, IET Generation, Transmission & Distribution.

Chapter 1

Power Quality State Estimation: Introduction

1.1 Introduction

The state estimation takes a state space model and a measurement model to determine the power quality in an electrical power system.

The growing complexity and the size of the actual power systems make unfeasible to completely monitor its transient or steady state operation. The state estimation has been used since the final years of 60´s, in addition with fundamental frequency power flow studies based in ideal conditions of operation, i.e., sinusoidal waveforms for voltages and currents, of constant magnitude and frequency, as well as the balanced operation condition [Monticelli 1999], [Abur & Exposito 2004]. However, actually the concept of power quality considers the implicit deviation of the ideal sinusoidal waveforms due to the following phenomena:

a) Under and over-voltage magnitudes in steady state.
b) Voltage amplitude variations, peak or *rms* value (depressions or sags and temporary over-voltages or swells).
c) Harmonics and inter-harmonics.
d) Voltage fluctuations or flicker.
e) Transients.

The power quality accurate evaluation depends on each case in particular and the problem to be considered [Heydt 1991], and therefore is required a different type of Power Quality State Estimation (PQSE) for each phenomenon. The frequency domain state estimation can be considered as a particular case of PQSE, since it considers possible under and over-voltages, harmonic distortion and transients.

The constant development and complexity of power systems, and as a natural consequence, the increased use of nonlinear devices, as well as uncommon but undesirable occurrence of various failures in the system make necessary to consider the extension of state estimation techniques, to account for various adverse effects on power quality, such as those previously mentioned in items a) to e), in order to identify adverse power quality sources, nature and magnitude, to quickly decide corrective actions and thus improve the power quality, so that fast and efficient estimation methods are required.

During operation of power systems, disturbances occur due to failures, switching generators, transformers, lines and loads, lightning, among others. The effects of these disturbances propagate through the network and degrade the power quality affecting the normal operation of the equipment connected to the system, also affecting the measurement and protection equipment, causing interference in communication and control equipment [Emanuel 2000].

It is clear that the cost of measuring instruments for assessing the power quality would be prohibitive if attempted to install them to monitor the entire system, so naturally emerges the need to use state estimation

techniques. The fundamental objective of the PQSE is to determine the location and magnitude of the source that adversely affects the power quality and the associated quality indices at unmonitored nodes in the power system. Various events are currently identified under the term of power quality and have been considered separately. For example, harmonic state estimation (HSE) [Heydt 1989, Meliopoulos *et al.* 1994, Du *et al.* 1996, Du *et al.* 1999], transient state estimation (TSE) [Yu and Watson 2007], and voltage sags state estimation (VSSE) [Espinosa-Juarez and Hernandez 2007]. This research is intended to develop a unified power quality state estimation technique (UPQSE) in the time domain that can consider and solve individual problems of power quality as previously mentioned.

The solution to this problem is obtained by applying numerical methods and efficient computational techniques, such as Newton methods based on Poincaré map and extrapolation to the limit cycle and parallel processing. In the state estimation process the representation of time-varying harmonics, identification and detailed representation of nonlinear loads and conventional sources, optimal placement of measurements and analysis of erroneous data are considered.

1.2 State of the Art

The state estimation uses a measurement equation:

$$\mathbf{z} = \mathbf{h}(\mathbf{x}) + \mathbf{e} \tag{1.1}$$

Where **x**, **z** and **e** and are the state, measurement and error vectors respectively, and **h** is a function vector relating measurements to state variables, in the present work is used the matrix-vector notation, matrices are represented with uppercase, boldface, no cursive; vectors with lowercase, boldface, no cursive; variables with normal, cursive and numbers with normal, no cursive.

For the frequency domain state estimation, nodal voltage magnitudes, injections and flows of real and reactive power are used as measurements and the state variables are the voltage phasors, resulting in a nonlinear measurement equation [Grainger and Stevenson 1996]. With an appropriate choice of state variables and measurements, a linear equation can be derived for cases of HSE and TSE when the power system model is linear. For this case, the Kalman filter can be applied; however, for representation with nonlinear models, the HSE and TSE can use algorithms as the extended and unscented Kalman filters.

1.2.1 Harmonic State Estimation

The state estimation begins to be applied to power systems in the early 70's with the work [Schweppe *et al.* 1970] applied to estimate the voltage phasors in the frequency domain by measuring injections and power flows and nodal voltage magnitudes. In the early 90's this technique began to be used to estimate the harmonic flows in the network; the main topics were the system model, measurement model, state estimation solution, observability and implementation [Kanao *et al.* 2005].

In [Meliopoulos *et al.* 1994] an algorithm is proposed for state estimation in power systems based on a multi-phase model and to estimate multi-frequency harmonics and distortion in the waveform. [Matair *et al.* 2000] proposes a measurement model based on current injections, line currents and nodal voltages. A method

for optimally locating the measurements to assess the HSE based in a sequential elimination is proposed in [Farach *et al.* 1993]. A methodology for the HSE implementation including algorithms and software development, object-oriented models, graphical interface and database was proposed by [Du *et al.* 1998].

The time domain state estimation can be evaluated with measurements coming from a periodic steady state system condition, which can be obtained using the extrapolation to the limit cycle. The state estimator represents the power system by means of a state space model and an observable measurement model.

The Kalman filter has been applied in the dynamic time-domain HSE in [Ma and Girgis 1996], there have been articles in reference to the state estimation using the KF to address the noise in the measurements, the filter divergence, the covariance matrices and different models of measurements [Kennedy *et al.* 2003].

The nonlinear electrical components and loads generate harmonics, the impact of harmonics flow in electrical networks is diverse, e.g., damage to capacitor banks and incorrect operation of equipment, such as braking of motors, negative sequence currents in generators and communications interference are effects of harmonics. However, the reduction of the equipment lifetime is not obvious for many years and the increase in losses is difficult to assess.

The main objective of the HSE is to estimate the level of harmonics starting with limited harmonic measurements data possibly contaminated with noise. There are three issues involved: the choice of the state variables, the criteria and the selection of the measurement points and the quantities to be measured.

When the state variables are known, they completely determine the system. In the frequency domain, harmonic voltage phasors in all nodes are usually chosen as state variables, since they allow the evaluation of harmonic currents in lines, and the harmonic currents injected into the nodes in parallel components. For the HSE, harmonic voltages and currents are measured quantities, as these are the amounts that the power quality meters supply and the accuracy of harmonic power measurements is low. Based on the measured voltage and current harmonics and the node harmonic voltages, a linear measurement equation can be defined:

$$\mathbf{z} = \mathbf{H}\mathbf{x} \tag{1.2}$$

Initially the HSE used the normal equation approach [Du *et al.* 1996], [Du *et al.* 1999] and a separate procedure for observability analysis to determine the possibility of solving the measurements equation [Watson *et al.* 2000]. However, unlike the problem of state estimation at fundamental frequency, the time domain measurements equation for HSE in most cases is under-determined, so this approach declines the use of the normal equation. The use of the singular value decomposition allows the assessment of a particular solution and the inspection of null space vectors supplies information about the observability of the system [Arrillaga *et al.* 2000], [Yu *et al.* 2004], [Matair *et al.* 2000], [Madtharad *et al.* 2003].

The HSE initial formulations begin with the primitive admittance matrices for each component and using the node-branch connection matrices to form the nodal admittance matrix of the system, currently this matrix is formed directly by reading the parameters of the components, and can be adjusted examining the type and the connections of new elements.

Figure 1.1 illustrates the framework of the HSE, this framework is the inverse of the corresponding harmonic propagation where harmonic sources are unknown and harmonic levels in the system are determined by using a limited number of harmonic measurements. It should use a three-phase model as necessary to describe asymmetric conditions, such as mutual coupling circuit, and impedance imbalance of currents injected into the nodes. The HSE of partially or completely observable systems requires synchronized phasor measurements of voltage and current harmonics performed at different points in the system when the study is carried out in the frequency domain, a solution for each harmonic is required, HSE requires discrete value measurements at each time step when the study is conducted in the time domain, these discrete values show the voltage or current waveforms including the harmonic content over a number of cycles and are sensed and converted A/D from the power system or from a time domain system simulation.

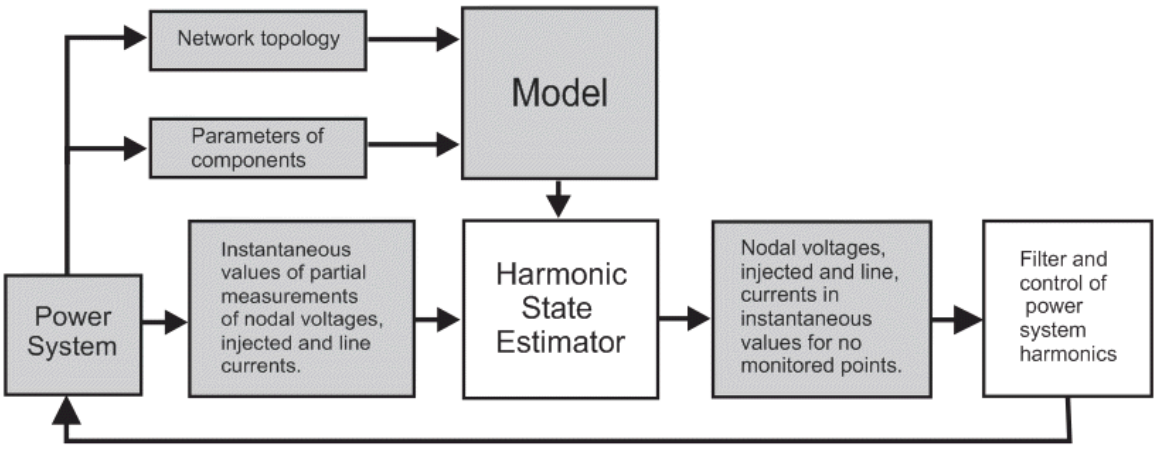

Figure 1.1 Time Domain Harmonic State Estimation Framework

A harmonic state estimator based on the network topology, is formulated from the admittance matrix to harmonic frequencies and the location of measurements [Arrillaga *et al.* 2000]. Measurements of voltage and current harmonics in selected nodes and lines are sent to a control center for estimating the spectra of nodal voltages, the currents injected into the nodes and line currents in the whole network or in selected positions.

The position of measurement points is assumed symmetric (e.g., three phases or without connection on possible measurement locations). However, this requirement restricts the search of optimal locations of measurement points in three-phase asymmetrical networks.

Existing algorithm implementation in practice depends on the timing of measurements. One option is to use the global positioning system (GPS) for synchronizing the measurements.

Two HSE approaches are the maximum observable subsystem for a given set of measurements, and the minimum number of measurements required for the observability of a given system. The HSE can be implemented in real time if the measurements are continuous and the processing speed is high enough; [Miller and Dewe 1992] presents an implementation of harmonic analysis. Harmonic monitoring instruments and the

estimator may be integrated into a system of wide area measurement system WAMS [Wilson 2007] or into a supervisory control and data acquisition system (SCADA).

1.2.2 Transient State Estimation

The state estimation techniques have been applied from the early 70's [Schweppe *et al.* 1970]. In [Ueda *et al.* 1975] the use of a nonlinear transient state estimator of a synchronous machine connected to infinite bus is presented, where the estimation models are formed by a set of nonlinear differential equations, which are discretized by a Taylor series; the solution is made for each cycle. [Ueda *et al.* 1977] applies the extended Kalman filter to the estimation of transients in a system of three generators, important details are the numerical method for solving the discretized equations and the evaluation of the filter gain. The TSE is solved in [Yu and Watson 2007] using a state space model, an over-determined model of measurements and the normal equation, the estimated transient is generated by a sudden loss of load. In other contribution, TSE is applied with partial measurements under a fault condition represented in state space [Watson and Yu 2008].

Electromagnetic transient studies can be performed using programs such as EMTP [Dommel 1969], [EMTPTB 1981], ATP [ATP 2002], PSCAD/EMTDC [PSCAD 2005] among others, modeling the possible conditions, so that the results can be compared to measurements of the simulated condition available to identify possible transients origins. However, this method is time consuming and often do not reach acceptable results. Moreover fault locators are used in analyzing the transmission lines based on current and voltage measurements made at the line terminals, labeling this time information via the GPS system, thus improving this approach with more measurements, it can be considered as an estimator that provides estimates of the entire system. Voltage depressions is the most common disorder affecting consumers, so that the extension of the estimation techniques in steady state to transient phenomena is desirable, so the HSE can be extended to TSE and VSSE.

The HSE formulation can use instantaneous or phasor quantities in Equation (1.1). This is because in steady-state operation, the system behavior can be represented by voltage and current phasors or by instantaneous values in the time domain. Otherwise, as the switching events and failures result in transient variations, which may be modeled using phasors, alternatively instantaneous values are required in the time domain TSE formulation. Application of estimation techniques to TSE determines the transient behavior in unmonitored nodes and provides an alternative method to locate system disturbances from partial measurements. The development of the TSE measurements equation requires a model of the system.

The TSE can be seen as a transient simulation reverse process [Abur and Exposito 2004], [Tan *et al.* 2005]. Figure 1.2 shows this relationship, the main objective is to calculate the best state estimate under a transient condition where partially measurements are being monitored. An electrical system can be state space represented by a first order Ordinary Differential Equations (ODE) set and the output equation. The state estimation measurement equation ($\mathbf{z}=\mathbf{Hx}$) is formulated based on the state space model; each measurement defines an equation to set up this equation [Watson 2010], [Yu and Watson 2007]. The framework for the TSE is shown in Figure 1.3. From the TSE results, it is possible to identify the disturbance location by

inspecting the current and voltage mismatches within the network. TSE can be used to quickly locate the disturbances to take appropriate corrective actions [Arrillaga *et al.* 2000], [Watson and Yu 2008].

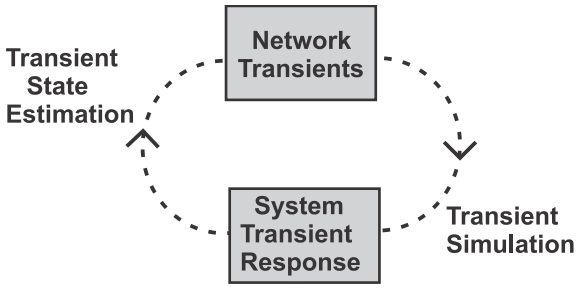

Figure 1.2 Reverse process relating the transient simulation and transient state estimation.

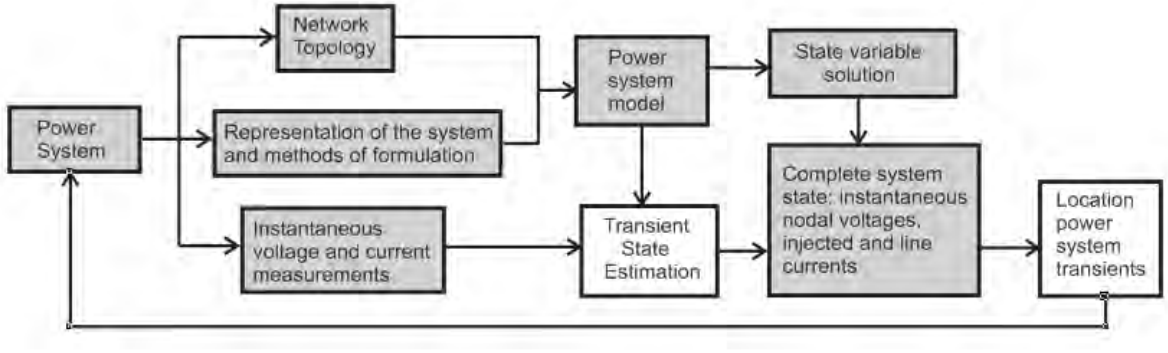

Figure 1.3 Framework of Transient State Estimation

1.2.3 Voltage Sags State Estimation

The voltage sags state estimation (VSSE) computes voltage sags occurred at unmonitored nodes, from voltage sags known in a limited number of monitored nodes.

The magnitude of the voltage depressions on remote nodes due to a fault or by the start of a machine depends on the topology and the parameters of the network.

[Espinosa-Juarez and Hernandez 2007] shows the implementation of a voltage sags state estimator using the measurement equation and adding a vector of measurement error, to carry out the analysis and vary the number of measurements, so that the estimation is solved for systems over, normal and under determined based on state variables. The range of the monitoring system is the area where if a fault occurs, the monitoring system will detect the specified low voltage limits; this feature is important for the estimation of voltage depressions [Bollen *et al.* 1998].

1.3 Motivation Behind the Present Research

Currently the identification of disturbances which affect the power quality is often a complex problem and its solution takes too long times, especially when the problem is intermittent. The PQSE is useful in this case

since it provides power quality indices in a given network, this allowing to adjust those rates and ensures compliance with the requirements of the standards, as well as meet the demand for service within the quality limits. Trends in the power quality indices can be observed in time so to make decisions according to the problems that arise during system operation. By comparing with other systems, the application of state estimation techniques can be found to improve power quality. Rapid identification both in location and magnitude of an effect that influences the power quality can help minimize its impact. The intermittent troubles can be still readily identifiable with the power quality state estimation.

The electrical load characteristics have changed with the increase of nonlinear loads using semiconductor devices, at low, medium and high voltage. The power quality and its associated issues have become important, this has originated an increased interest in assessing existing indices of power quality in power networks. On the other hand, there has been a reduction in the cost of equipment for power quality monitoring, which has resulted in a greater number of monitors installed in the networks, which collect data to assess the power quality. The main objective should be to have enough information of the system level quality and identify the location and magnitude of sources of disturbances that affect the power quality. This requires synchronization of the measurements to be sent to a control center, which might be done by signaling through the global positioning system (GPS), and then run a PQSE algorithm to find the location and magnitude of disturbances and indexes of power quality (PQ) in unmonitored nodes and components.

The improved power quality measurement instruments and data communication in the future means greater availability of data both in quantity and quality, which can be applied to PQSE, to optimize its implementation, development and operation.

Diverse events are currently identified under the power quality state estimation which have been separately considered. For example, Harmonic State Estimation (HSE) [Heydt 1989], [Meliopoulos *et al.* 1994], [Du *et al.* 1996], [Du *et al.* 1999]; Transient State Estimation (TSE) [Yu and Watson 2007], and Voltage Sags State Estimation (VSSE) [Espinosa-Juárez and Hernandez 2007]. The aim of this work is to develop a time domain state estimation technique for Unified Power Quality State Estimation (UPQSE). The solution to this problem can be obtained by applying numerical and computational efficient techniques such as Newton-based methods Poincaré map and extrapolation to the limit cycle [Semlyen and Medina 1995] and parallel processing [Owens *et al* 2008]. In the state estimation process the representation of time-varying harmonics, interharmonics, identification and detailed representation of nonlinear loads, and noise measurements are considered.

1.4 Objectives

- Main objective: to develop a methodology for the state estimation studies and analyzes under conditions of steady and transient state of power systems, with particular emphasis to the field of power quality. In particular, considering the effect of adverse events such as harmonic distortion, time-varying harmonics, inter-harmonics, transients and voltage sags.

- To develop the digital tools to allow the power system studies associated with the power quality state estimation. The state estimation accounts for issues associated with location of meters, and noisy measurements.
- To incorporate in the solution process, numerical and computational efficient techniques, such as Newton methods, Poincaré map and extrapolation to the limit cycle, and parallel processing techniques based on the use of CPU-GPU systems under the CUDA platform and the CUBLAS library.

1.4.1 Contributions

The main contributions of this work can be summarized as follows:

- A unified general time domain methodology that allows the analysis of state estimation under conditions of transient and steady state of electrical systems with particular emphasis to the field of power quality and adverse events listed above.
- Development and implementation of simulation tools based on the proposed methodology for power quality state estimation, consideration of noisy measurements, as well as efficient numerical and computational techniques, such as Newton methods based on Poincaré map and extrapolation to the limit cycle and use of GPU parallel processing to implement the KF algorithm to solve PQSE.

1.5 Methodology

The methodology of this research work is the implementation of the power quality state estimation for the following processes and their use in different case studies to experiment and analyze the results:

1.- Harmonic State Estimation (HSE).

2.- Transient State Estimation (TSE).

3.- Voltage Sags State Estimation (VSSE).

4.- Observability analysis, location of measurements and noise.

5.- Newton methods to obtain the periodic steady state based on the Poincaré map and extrapolation to the limit cycle in the solution of the ODE set modeling the system.

6.- Parallel processing techniques in the developed algorithms to reduce the execution time.

The unified power quality state estimation methodology applied in the case studies of this research work includes the following steps:

a).- Power system state space model definition using an ODE set to evaluate HSE, TSE or VSSE.

b).- ODE set solution to obtain the system actual response.

c).- Measurement model definition using the system output variables and observability analysis.

d).- Time domain state estimation solution using the state apace and measurement models; this solution can include data noise, Newton methods and parallel processing techniques.

e).- Compare the actual and estimated response to validate the state estimation response.

f).- Analysis of results to conclude about the actual and state estimation solutions, evaluate the state estimation error.

1.6 Thesis outline

Chapter 1 presents a review of the state of the art associated with the state estimation in power systems with particular reference to power quality and the numerical processing fundamentals. After this review of the state of the art, the methodology of the proposed project and the objectives to be achieved are established. The contributions of this investigation, the methodology in which is based and the description of chapters are given.

Chapter 2 presents the introduction and formulation of state estimation in power systems, techniques in transient and periodic steady state, the Kalman filter techniques applied to time domain state estimation, the singular value decomposition, the use of pseudo and virtual measurements, the optimal location of meters and the erroneous data analysis.

Chapter 3 describes the proposed power quality state estimation formulation, the state-space modeling of sources, identification load and systems, as well as the Newton techniques and extrapolation to limit cycle such as the numerical differentiation, the enhanced numerical differentiation and the parallel processing techniques.

Chapter 4 describes the HSE, presents simulations and case studies based on the proposed methodology with Kalman filter, extended Kalman filter and parallel Kalman filter, comparing the estimate harmonics and inter-harmonics results against the actual system response.

Chapter 5 applies the TSE with the proposed formulation in case studies of transient conditions, using the singular value decomposition, the application of conventional and enhanced numerical differentiation procedures, comparing and analyzing the results.

Chapter 6 presents the proposed methodology for time domain VSSE with case studies of short circuit faults, reviewing the sags distribution, voltage magnitude fluctuations, and the sags duration to determine and classify the transient voltage sags by means of the unscented Kalman filter algorithm.

Chapter 7 gives the general conclusions drawn from this research, addressing and suggesting ideas for further research to be done in the same field of knowledge.

Appendices are added to describe power quality phenomena, integration methods, nonlinear load models, test system parameters and the configuration of the measurement system.

Chapter 2

Power Systems Time Domain State Estimation

2.1 Introduction

The minimum set of variables at any instant of time t_0 to determine the future system state without the input variables before t_0 are known as state variables; these variables have a mathematical meaning from the view point of dynamics: the variables are required to specify the solution of differential equations representing the system [Kundur 1994]. The state variables of an electric circuit are the currents in the inductances (except those that form a cut set with other currents in the inductances and current sources) and the voltages on the capacitors (minus those that meshes with other capacitive voltages and voltage sources).

The mathematical process to estimate or approximate the state variables is called state estimation. Direct measurement of the state variables is possible although the state estimation is applied due to several reasons: In many cases there are numerous variables to be measured, current lines and nodal voltages so their direct measurement is not economical due to the cost and availability of meters, transducers and communication channels. A second reason which makes the direct measurement impractical is the inaccessibility of certain state variables such as the current in the rotor inductance of a rotating machine or the electrical variables in a distant part of the network, making difficult to measure and communicate to the control center. In cases where equivalent circuits are used containing state variables which do not physically exist, such as a Thevenin equivalent circuit may have an inductor, but may be impossible to measure the current because there is really no inductor. In these cases, mathematical modeling, calculation and the approximation are useful to determine the state variables through state estimation [Heydt 1991].

The above definition refers to the state variables in a dynamic sense. In many cases, the network is assumed under a periodic steady state, which leads to calculating the static state estimation, taking nodal voltages and angles of phase as state variables, with measurements of power flows, power injections and nodal voltage magnitudes.

The measurements redundancy may be useful to some extent due to communication failures, or errors in the transducers and significant measurement noise. A state estimator is an alternative or supplement to direct measurement.

The time domain state estimation can be applied to determine fluctuations in the state variables such as harmonics, varying harmonics, inter-harmonics and transients; to find the origin and control these phenomena.

The main applications of power quality state estimation are:

+ Estimation of harmonic flows in the power network.
+ Estimation of harmonics at the points of common coupling.
+ Estimation of power quality indexes (THD, TDD, TIF) with on line data.
+ Estimating harmonics injected into the nodes to identify loads that cause power quality problems.

+ Mitigation of the effects of erroneous measurements on power quality.

+ Bad data identification and/or with noise.

+ Supplementary method of measurements.

2.1.1 Design stages of a state estimator.

The system identification formulates a mathematical model. This model has two parts: the state space model of the physical process and the measurement model of the sensor system. Then the observability and stability are verified; if the system is not observable or not stable, the model or the sensor system must be redesigned. After these tests the computational aspects are revised and the appropriate implementation is selected [Van der Heijden *et al.* 2004].

When the state estimator has been implemented, the consistency tests must be performed to validate the results. If they are not consistent, it is necessary to return to verify the previous stages, to refine the models or modify the implementation; the design cycle is illustrated in Figure 2.1 [Van der Heijden *et al.* 2004].

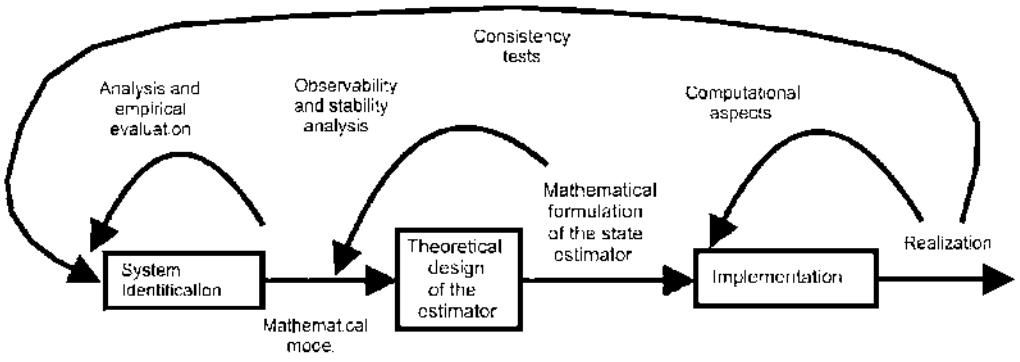

Figure 2.1 Design stages of state estimators.

Figure 2.2 shows the flowchart for the unified power quality state estimation, its main steps are model identification, observability analysis, erroneous or noisy data analysis, and application to harmonics, transients and voltage sags.

2.2 State Estimation Techniques

The main methods of state estimation are:

- Least Squares [Grainger and Stevenson 1996]. Minimizes the sum of the squares of errors between the actual and estimated values, requires a model of the system, supervisory and data acquisition systems; monitoring voltage, current and power, this method can be applied to dynamic estimation.

- Weighted Least Squares [Grainger and Stevenson 1996]. Some data are weighted differently than others depending on the error and the accuracy of measuring instruments; requires of a system model. It is valid for dynamic estimation and in the same cases as least squares.

- Hibrid Estimator [Heydt 1991]. Combination of normal and weighted least squares and physical circuit laws. Requires of a system model, applied in dynamic estimation, it is used in harmonic estimation in power networks.

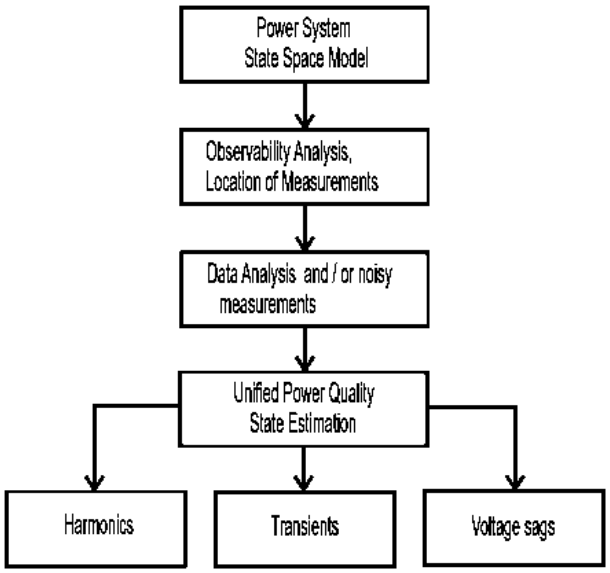

Figure 2.2 Unified Power Quality State Estimation.

- Kalman Filter [Kennedy *et al.* 2003]. It is based on the error of least squares or weighted least squares, which is dynamically minimized, requires of a model. Dynamic estimation is applied for protection relays, load forecasting, supervisory control and data acquisition, harmonic estimation, transients and voltage depressions. Several versions are used based on the Kalman filter, such as the extended and unscented Kalman filters; for nonlinear models and networks, and versions using parallel processing (parallel Kalman filter) [Huang *et al.* 2011].

- Neural Networks [Heydt 1991]. Develops a nonlinear network, the network parameters are identified by the least squares approach, does not require of a system model. This technique can be applied to dynamic estimation; its implementation is experimental.

- Genetic Algorithms [Arabkhaburi et al., 2006]. These algorithms are inspired by biological evolution and molecular-genetic basis and are included as part of the evolutionary algorithms. A genetic algorithm is a directed search method based on probability that can be used to solve search and optimization problems, it can be applied in the state estimation and the optimal location of measurements.

Table 2.1 shows a summary of the state estimation solution methods.

2.2.1 Periodic Steady State Estimation

The purpose of this periodic steady state estimation is to determine the nodal voltages, line and load currents in the power system starting with the system and measurements models in an over, normal or under-determined condition when system is in the periodic steady state and the initial transient period has finished. The measurements can be contaminated with noise. The measurements can be optimally distributed in the

system or have an arbitrary distribution being necessary in this case apply the observability analysis to determine the system observable areas.

Table 2.1 State estimation solution methods

State Estimation Solution Methods
Leat Squares
Weighted Least Squares
Weighted Least Absolute Value
Singular Value Decomposition
Kalman Filter
Extended Kalman Filter
Unscented Kalman Filter
Neural networks
Genetic Algorithms

2.2.1.1 Least Squares State Estimation

It is based on the difference between the estimated values of the states $\hat{\mathbf{x}}$, and correct or actual value $\mathbf{x}$, this error is minimized by the least squares method; i.e., minimizing $|\mathbf{x}_{estimated}-\mathbf{x}|^2$.

A variation is the method of weighted least squares, in which a weighting factor is applied to the elements representing the square of the errors for each measurement according to their accuracy and reliability [Monticelli 2000].

Since the vector $\mathbf{z}$ contains the measurements from the system, and $\mathbf{x}$ is the state vector, they are related by:

$$\mathbf{z} = \mathbf{h}(\mathbf{x}) + \mathbf{e} \tag{2.1}$$

Where $\mathbf{e}$ represents the errors in the measurements, their values depend on the measurement noise that can result in the adjustment, calibration and resolution of the instruments, the measurement is not the indicated, or communication interference and erroneous measurements. The objective is to minimize the square error *J*:

$$J = \mathbf{e}^T \mathbf{e} \tag{2.2}$$

To minimize *J*, it is assigned:

$$\frac{dJ}{d\mathbf{x}} = 0 \tag{2.3}$$

The derivative depends on the measurement model. For the case of a linear model:

$$\mathbf{z} = \mathbf{H}\mathbf{x} + \mathbf{e} \tag{2.4}$$

Therefore:

$$\frac{dJ}{d\mathbf{x}} = \frac{d}{d\mathbf{x}}((\mathbf{z}-\mathbf{H}\mathbf{x})^T(\mathbf{z}-\mathbf{H}\mathbf{x})) = 2\mathbf{H}^T(\mathbf{z}-\mathbf{H}\mathbf{x}) = 0$$

$$\mathbf{x} = (\mathbf{H}^T\mathbf{H})^{-1}\mathbf{H}^T\mathbf{z} = \mathbf{H}^+\mathbf{z} \tag{2.5}$$

Where $\mathbf{H}^+$ is the pseudo-inverse of $\mathbf{H}$, being $\mathbf{H}^T\mathbf{H}$ a no singular matrix.

For the weighted least squares estimator, the sum of the squares of the errors is:

$$J_w = \sum_{i=1}^{n} \mathbf{r}_i\mathbf{e}_i^2 = \mathbf{e}^T\mathbf{R}\mathbf{e} \tag{2.6}$$

Elements r are the weighting factors, which form the diagonal matrix **R**, which is called the weight matrix. Comparing Equations (2.2) and (2.6), it is concluded that:

$$\mathbf{x} = (\mathbf{H}^T\mathbf{R}\mathbf{H})^{-1}\mathbf{H}^T\mathbf{R}\mathbf{z} \tag{2.7}$$

When **R=I** where **I** is the unit matrix, this is the un-weighted case. If the measurements model is nonlinear, it can be decomposed into Taylor series, to be linearized and analyzed by the above method. The Taylor series expansion of **z** around $\mathbf{x}_0$ is:

$$\mathbf{z} = \mathbf{h}(\mathbf{x}_0) + \left.\frac{d\mathbf{h}(\mathbf{x})}{d\mathbf{x}}\right|_{\mathbf{x}=\mathbf{x}_0}(\mathbf{x}-\mathbf{x}_0) + \frac{1}{2}\left.\frac{d^2\mathbf{h}(\mathbf{x})}{d\mathbf{x}^2}\right|_{\mathbf{x}=\mathbf{x}_0}(\mathbf{x}-\mathbf{x}_0) + \ldots \tag{2.8}$$

The linear term is represented as $\mathbf{H}(\mathbf{x}-\mathbf{x}_0)$ truncating the series at the linear term, the estimate for **x** is:

$$\mathbf{x} = \mathbf{x}_0 - (\mathbf{H}^T\mathbf{R}\mathbf{H})^{-1}\mathbf{H}^T\mathbf{R}(\mathbf{x}_0 - \mathbf{z}) \tag{2.9}$$

The solution **x** depends on the linearization point $\mathbf{x}_0$; usually an iterative process is applied. It defines an initial point, the matrix **H** is calculated at the initial value of **x**, then an estimated state **x** is obtained, the point of linearization moves to the calculated state. This process is repeated until a specified tolerance is met, using the following iterative formula:

$$\mathbf{x}_k = \mathbf{x}_{k-1} - (\mathbf{H}_{k-1}^T\mathbf{R}\mathbf{H}_{k-1})^{-1}\mathbf{H}_{k-1}^T\mathbf{R}(\mathbf{h}(\mathbf{x}_{k-1}) - \mathbf{z}_{k-1}) \tag{2.10}$$

Being $|\mathbf{x}_k - \mathbf{x}_{k-1}|$ small enough.

For the case of linear model, if the statistics of measurement error **e** are known, the statistics of *J* can be calculated. In the event that **e** is Gaussian, the distribution of *J* is chi-square [Grainger and Stevenson 1996]. For this special case, it is possible to assess the quality of the estimate by reviewing the statistics of the chi-square distribution. For the nonlinear case, the process is more complicated than for cases with lower levels of measurement error or with Gaussian distribution, where the index *J* has about a chi-square distribution.

An alternative method of solving systems of linear equations (2.5), under or over-determined, which can be applied recursively to solve the state estimation in the time domain is the QR decomposition.

2.2.2 Kalman Filter

The term filter usually refers to filter circuits which suppress or enhance signals, depending on the application. However, in systems theory this term is used in a different context, being a device that processes certain specific inputs to obtain determined outputs [Grewal and Andrews 2001]. The most common filter of this type is the state estimator, which processes measurements so that estimates the quantities that are not monitored in other parts of the system. These parts can have measurements but cannot be taken into account, e.g., the measurement with errors or excessive noise or the measurement point physically does not exist, as in the case of synchronous generator internal voltage or in other cases where the measuring equipment can be prohibitively expensive [Kalman 1960], [Blood *et al.* 2008].

The Kalman filter uses the least squares approach; it is applied to dynamic systems. Let us consider a system with the discretized state equation:

$$\mathbf{x}_{k+1} = \boldsymbol{\varphi}_k \mathbf{x}_k + \mathbf{v}_k \tag{2.11}$$

$\mathbf{x}$ is the state vector, $\boldsymbol{\varphi}$ the state transition matrix and $\mathbf{v}$ the process noise. The discretized measurement equation can be written as,

$$\mathbf{z}_k = \mathbf{H}_k \mathbf{x}_k + \mathbf{w}_k \tag{2.12}$$

$\mathbf{z}$ represents the measurements, which may contain noise, assigned to $\mathbf{w}$, $\mathbf{H}$ is the measurement matrix. $\mathbf{x}$, $\mathbf{z}$, $\mathbf{v}$ and $\mathbf{w}$ are vectors of appropriate dimension. Assigning to noises $\mathbf{v}$ and $\mathbf{w}$, a zero mean and covariance matrices $\mathbf{Q}_k$ and $\mathbf{R}_k$ at time k respectively, according to the dynamics of the system, and the initial estimate $\bar{\mathbf{x}}_k$ of vector $\mathbf{x}_k$.

The Kalman filter algorithm is based on minimizing the sum of squared errors:

$$J = E((\mathbf{x}_k - \mathbf{x}_{k-1})^T (\mathbf{x}_k - \mathbf{x}_{k-1})) \tag{2.13}$$

The Equation (2.13) uses the expected value or mean as related vectors are stochastic; the parameter J is the index to be minimized. To illustrate the algorithm, initially a nonlinear or linear function $\boldsymbol{\varphi}(\mathbf{x})$ representing the system model can be considered and in case of nonlinear model, this model must be linearized. The Kalman filter algorithm consists of the iterative process described next:

For the specific HSE formulation, the dynamic version of (2.4) can be expressed in discrete form with (2.12). The solution using the recursive Kalman filter consists on updates of time and measurement [Zhang J. *et al.* 2011]. Time updating comprises the following steps:

1.- Project the state

$$\hat{\mathbf{x}}_k^- = \boldsymbol{\varphi}_k \hat{\mathbf{x}}_{k-1} \tag{2.14}$$

2.- Project the error covariance matrix

$$\mathbf{P}_k^- = \boldsymbol{\varphi}_k \mathbf{P}_{k-1} \boldsymbol{\varphi}_k^T + \mathbf{Q}_k \tag{2.15}$$

Where $\hat{\mathbf{x}}_k^-$ is the initial estimate of $\hat{\mathbf{x}}_k$ and $\mathbf{P}_k^-$ the initial estimate of error covariance $\mathbf{P}_k$, initially can be the unitary matrix, $\mathbf{Q}_k$ is the covariance matrix of $\mathbf{v}$. The measurement update consists of the following steps:

1.- Update the Kalman gain

$$\mathbf{G}_k = \mathbf{P}_k^- \mathbf{H}_k^T (\mathbf{H}_k \mathbf{P}_k^- \mathbf{H}_k^T + \mathbf{R}_k)^{-1} \tag{2.16}$$

2.- Update state estimate

$$\hat{\mathbf{x}}_k = \mathbf{x}_k^- + \mathbf{G}_k (\mathbf{z}_k - \mathbf{H}_k \hat{\mathbf{x}}_k^-) \tag{2.17}$$

3.- Update the error covariance matrix

$$\mathbf{P}_k = (\mathbf{I} - \mathbf{G}_k \mathbf{H}_k) \mathbf{P}_k^- \tag{2.18}$$

The process continues when new measurements are received, the estimated state $\hat{\mathbf{x}}$, represents the state estimation response. The estimated state variables, KF gain and error covariance matrices are evaluated at each time step. Figure 2.3 illustrates this algorithm [Grewal and Andrews 2001].

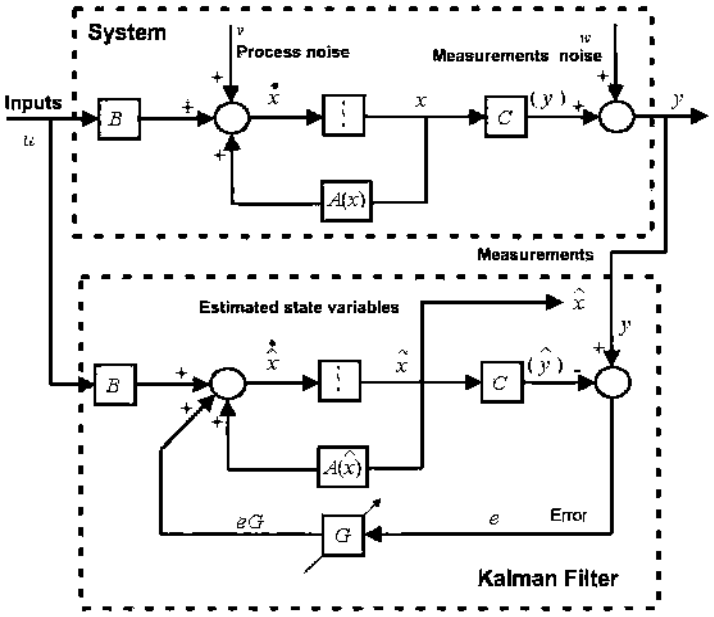

Figure 2.3 KF diagram

The Kalman filter has been proposed to estimate the levels of harmonics in the power system. The discretized measurements during the period of study of certain voltages and currents are used as inputs to the Kalman filter to dynamically estimate the harmonic levels [Kennedy *et al.* 2003]. If there are nonlinear loads, the corresponding measurements of the nodal voltages and line currents originate the Kalman filter answers to changes in the levels of harmonics, being possible to compute the THD. Though if the network configuration instantaneously changes, for example, switching lines and loads on the system, the estimator can give erroneous results initially. Also, regularly the switching of large loads occurs gradually, thus allowing the Kalman filter to respond properly to changes in the estimation. Figure 2.4 shows the flowchart for the discrete Kalman filter.

The discrete Fourier transform (DFT) can be applied to measured and estimated signals to obtain their harmonic spectrum, thus transforming the data into the time domain to the frequency domain [Arrillaga *et al.* 2000], [Brigham 1988].

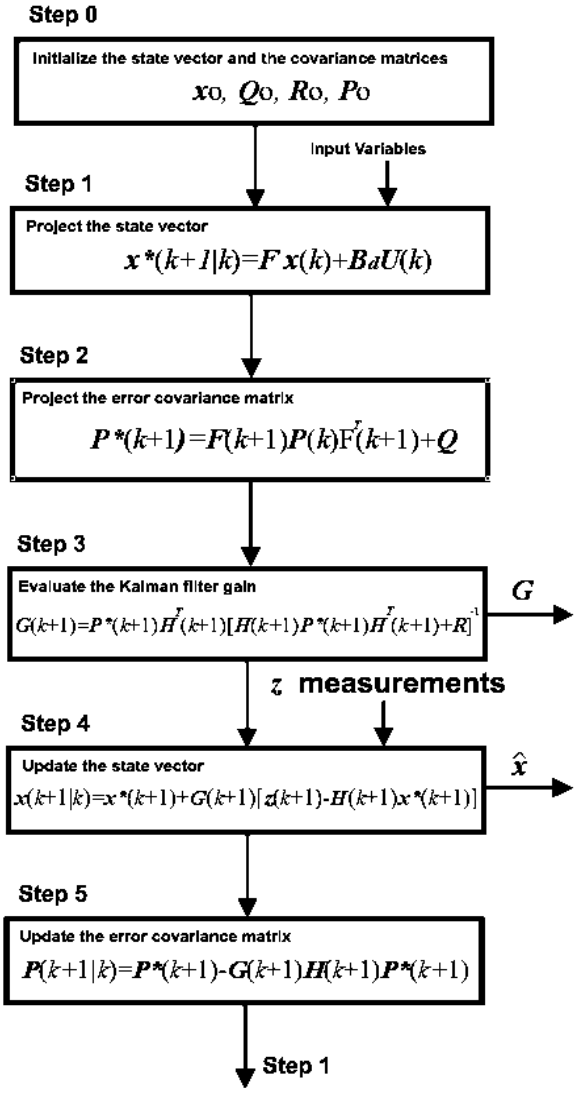

Figure 2.4 Flowchart of the discrete Kalman filter

2.2.2.1 Time-varying Harmonics

The electrical load in the power system changes constantly and the generator output changes to meet demand. This causes time variant harmonic levels, so that the HSE has been extended to analyze these variations using the Kalman filter [Beides and Heydt 1991], [Yu *et al.* 2005a]. The Kalman filter uses the method of least squares in a dynamic sense to analyze this variation in time.

The measurement equation in the time domain state estimation is related with the output equation of the state space model, adapted after the available measurements from the system; the model is solved taking into account these measurements.

A different approach to the HSE solution is the Artificial Neural Networks (ANN). With this method, parallel connection provides high-speed solution. The main disadvantage is the difficulty of ANN training and verification. This requires large data sets, which are not generally available [Heydt 1991].

2.2.3 Extended Kalman Filter

The extended Kalman filter is an alternative to the Kalman filter when the system is nonlinear and the linearization process is made by means of Jacobians included in the filter formulation [Kuang-Rong and Shyh-Jier 2002].

The extended Kalman filter (EKF) can be applied to nonlinear systems. Assuming a nonlinear model and the corresponding nonlinear measurement equation,

$$\dot{\mathbf{x}} = \mathbf{f}(\mathbf{x}, \mathbf{u}, \mathbf{v}) \tag{2.19}$$

$$\mathbf{y} = \mathbf{h}(\mathbf{x}, \mathbf{u}, \mathbf{w}) \tag{2.20}$$

v is the process noise vector, **w** is the measurement noise vector, **f** is the nonlinear function modeling the system, **h** is the nonlinear output function, **y** is the output vector, the measurement vector is formed selecting variables form this output vector.

An iterative process can be defined for the nonlinear discrete-time case by converting the model from continuous to discrete time, approximating the differential equations to difference equations [Grewal and Andrews 2001], initially the time derivative of **x**, is ,

$$\dot{\mathbf{x}} = (\mathbf{x}(k) - \mathbf{x}(k-1)) / \Delta t \tag{2.21}$$

Solving for $\mathbf{x}(k)$,

$$\mathbf{x}(k) = \Delta t \dot{\mathbf{x}} + \mathbf{x}(k-1) = \Delta t \mathbf{f}(\mathbf{x}(k\text{-}1), \mathbf{u}(k\text{-}1), \mathbf{v}(k\text{-}1)) + \mathbf{x}(k-1) \tag{2.22}$$

Discrete measurements equation is,

$$\mathbf{y}(k) = \mathbf{h}(\mathbf{x}(k), \mathbf{u}(k), \mathbf{w}(k)) \tag{2.23}$$

The time step is represent by *k*. The noise process **v** and the measurement noise **w** are assumed stationary, zero mean, and with normal distribution without correlation between them,

$$E[\mathbf{w}_k] = 0 \tag{2.24}$$

$$\mathbf{E}[\mathbf{w}_k \mathbf{w}_k^T] = \mathbf{R}_k \tag{2.25}$$

$$\mathbf{w}_k \sim \mathrm{N}(0, \mathbf{R}_k) \tag{2.26}$$

$$E[\mathbf{v}_k] = 0 \tag{2.27}$$

$$E[\mathbf{v}_k \mathbf{v}_k^T] = \mathbf{Q}_k \tag{2.28}$$

$$\mathbf{v}_k \sim \mathrm{N}(0, \mathbf{Q}_k) \tag{2.29}$$

Q $n \times n$ order and **R** $m \times m$ order are the covariance matrices for **v** and **w**, respectively, with *n* states and *m* measurements.

The EKF is based on a system model and partial measurements to estimate the state vector. It uses the Equation (2.22) and the measurements Equation (2.23), to estimate the system dynamics in the time domain and to evaluate the state and output variables in the study interval. The sources and levels of harmonics in a power system vary with time and can be evaluated with this algorithm [Ghahremani and Kamwa 2011], [Charalampidis and Papavassilopoulos 2011].

The EKF algorithm is illustrated in Figure 2.5 , the main steps are the projection and updating, which are evaluated at each time step.

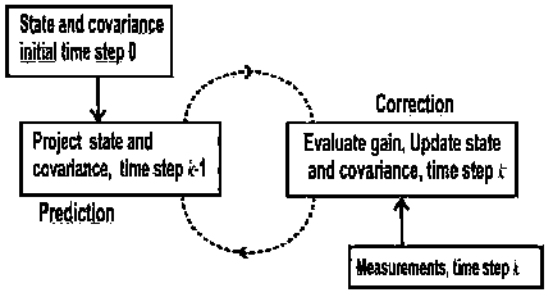

Figure 2.5 Extended Kalman Filter, Prediction-Correction State Estimator

The waveforms of the measured variables in the **y** vector are sampled from the power system in discrete form. With these data, the EKF algorithm can be recursively applied.

The algorithm has two stages [Grewal and Andrews 2001], i.e.,

1. Initialization
2. Update time and measurement

The initialization computes:

$$\hat{\mathbf{x}}_0^+ = \mathbf{E}(\mathbf{x}_0) \tag{2.30}$$

$$\mathbf{P}_0^+ = \mathbf{E}[(\mathbf{x}_0 - \hat{\mathbf{x}}_0^+)(\mathbf{x}_0 - \hat{\mathbf{x}}_0^+)^T] \tag{2.31}$$

E is the expected value, **P** is the error covariance matrix, + indicates update estimate and – indicates project estimate. The subscripts k and k-1 denote the time instants $t=k\Delta t$ and $t=(k\text{-}1)\Delta t$, respectively.

Time and measurement updating has four steps, [Ghahremani and Kamwa 2011]:

2.1) Compute the partial derivative matrices:

$$\mathbf{F}_{k\text{-}1} = \partial \mathbf{f}_{k-1} / \partial \mathbf{x}\big|_{\hat{\mathbf{x}}_{k\text{-}1}^+} \tag{2.32}$$

$$\mathbf{L}_{k\text{-}1} = \partial \mathbf{f}_{k-1} / \partial \mathbf{v}\big|_{\hat{\mathbf{x}}_{k\text{-}1}^+} \tag{2.33}$$

The **F** and **L** matrices are of $n \times n$ order.

2.2). Projection of the state estimate and error covariance matrix:

$$\mathbf{P}_k^- = \mathbf{F}_{k\text{-}1}\mathbf{P}_{k\text{-}1}^+\mathbf{F}_{k\text{-}1}^T + \mathbf{L}_{k\text{-}1}\mathbf{Q}_{k\text{-}1}\mathbf{L}_{k\text{-}1}^T \tag{2.34}$$

$$\hat{\mathbf{x}}_k^- = \mathbf{f}_{k\text{-}1}(\hat{\mathbf{x}}_{k\text{-}1}^+, \mathbf{u}_{k\text{-}1}, \mathbf{v}_{k\text{-}1}) \tag{2.35}$$

2.3). Compute the partial derivative matrices:

$$\mathbf{H}_k = \partial \mathbf{h}_k / \partial \mathbf{x}\big|_{\hat{\mathbf{x}}_k^-} \tag{2.36}$$

$$\mathbf{M}_k = \partial \mathbf{h}_k / \partial \mathbf{w}\big|_{\hat{\mathbf{x}}_{k\text{-}1}^+} \tag{2.37}$$

H is of $m \times n$ order and **M** of $m \times m$ order.

2.4). Compute the EKF gain, update the state estimate and error covariance matrix as:

$$\mathbf{K}_k = \mathbf{P}_k^-\mathbf{H}_k^T(\mathbf{H}_k\mathbf{P}_k^-\mathbf{H}_k^T + \mathbf{M}_k\mathbf{R}_k\mathbf{M}_k^T)^{-1} \tag{2.38}$$

$$\hat{\mathbf{x}}_k^+ = \hat{\mathbf{x}}_k^- + \mathbf{K}_k[\mathbf{y}_k - \mathbf{h}_k(\hat{\mathbf{x}}_k^-, \mathbf{u}_k, \mathbf{w}_k)] \tag{2.39}$$

$$\mathbf{P}_k^+ = (\mathbf{I} - \mathbf{K}_k\mathbf{H}_k)\mathbf{P}_k^- \tag{2.40}$$

The EKF gain provides an estimate of the state variables and decreases the influence of measurement noise; this gain is a time-varying quantity (2.38). The state vector is updated taking into account the vector **y**, which represents the measurements from the system, Equation (2.39).

P is the error covariance matrix, (2.40) represents the **P** dynamics since there is a recursive relationship between expressions (2.34) and (2.40). This recursive formulation can be applied to follow the variations of harmonic levels in a power system [Beides and Heydt 1991], [Kennedy *et al.* 2003]. The estimate state $\hat{\mathbf{x}}$ and error covariance matrices are evaluated each time step.

2.2.4 Unscented Kalman Filter

The unscented transformation (UT) has been applied to the state estimation; this transformation is based on the spread of the mean and covariance via a nonlinear transformation. The unscented Kalman filter (UKF) does not use the derivative, thus avoiding analytical or numerical derivative solutions [Elnady and Salama 2005], [Julier and Uhlmann 2004]. Assuming nonlinear models for the system and measurements, represented as,

$$\dot{\mathbf{x}} = \mathbf{f}(\mathbf{x}, \mathbf{u}, \mathbf{v}) \tag{2.41}$$

$$\mathbf{y} = \mathbf{h}(\mathbf{x}, \mathbf{u}, \mathbf{w}) \tag{2.42}$$

The UKF uses a deterministic approach to calculate the mean and the covariance. $2n$ +1 sigma points are defined by using a square root decomposition of the previous covariance. The spread of these points through model (2.41) is performed to obtain a weighted mean and covariance. W_i represents the defined scalar weights as,

$$W_0^{(m)} = \lambda / (n + \lambda) \tag{2.43}$$

$$W_0^{(c)} = \lambda / (n + \lambda) + (1 + \alpha^2 + \beta) \tag{2.44}$$

$$W_i^{(m)} = W_i^{(c)} = 1 / (2(n + \lambda)) \quad i = 1, ..., 2n \tag{2.45}$$

$$\lambda = \alpha^2 (n + \kappa) - n \tag{2.46}$$

$$\gamma = \sqrt{(n+\lambda)} \tag{2.47}$$

Where n is the number of states, λ and γ are scale parameters. α and κ determine the sigma points dispersity degree; β is associated with the distribution of **x**, if this is Gaussian β=2 is an optimal value; α=10^{-3} and κ=0 are typical normal values [Julier and Uhlmann 1997].

UT takes the sigma points with their associated mean and covariance, and these points are transformed by applying the nonlinear function **f**, then the mean and covariance are computed for transformed points. Each point is assigned a weight W_i [Valderde *et al.* 2011]. UKF assumes a discrete time nonlinear system denoted by,

$$\mathbf{x}_{k+1} = \mathbf{f}(\mathbf{x}_k, \mathbf{u}_k, \mathbf{v}_k, t_k) \tag{2.48}$$

$$\mathbf{y}_k = \mathbf{h}(\mathbf{x}_k, \mathbf{u}_k, \mathbf{w}_k, t_k) \tag{2.49}$$

$$\mathbf{w}_k \sim \mathrm{N}(0, \mathbf{R}_k) \tag{2.50}$$

$$\mathbf{v}_k \sim \mathrm{N}(0, \mathbf{Q}_k) \tag{2.51}$$

The process noise **v** and the measurements noise **w** are assumed stationary, with zero mean and uncorrelated, **Q** $n \times n$ y **R** $m \times m$ are the covariance matrices for **v** and **w**, respectively.

The algorithm has the following steps [Van der Merwe and Wan 2001]:

1. Initialization, k=0.

$$\hat{\mathbf{x}}_0^+ = \mathbf{E}(\mathbf{x}_0) \tag{2.52}$$

$$\mathbf{P}_0^+ = \mathbf{E}[(\mathbf{x}_0 - \hat{\mathbf{x}}_0^+)(\mathbf{x}_0 - \hat{\mathbf{x}}_0^+)^T] \tag{2.53}$$

E is the expected value, **P** is the error covariance matrix, + indicates an update estimate and – a project estimate. The subscripts *k* and *k*-1 denote the time intervals $t=k\Delta t$ and $t=(k\text{-}1)\Delta t$, respectively.

2. Sigma points evaluation.

$$\boldsymbol{\chi}_{k-1} = [\hat{\mathbf{x}}_{k-1} \quad \hat{\mathbf{x}}_{k-1} + \gamma\sqrt{\mathbf{P}_{k-1}} \quad \hat{\mathbf{x}}_{k-1} - \gamma\sqrt{\mathbf{P}_{k-1}}] \tag{2.54}$$

3. Update the time step from *k* to *k*-1.

$$\boldsymbol{\chi}^*_{k|k-1} = \mathbf{f}[\boldsymbol{\chi}_{k-1}, \mathbf{u}_{k-1}] \tag{2.55}$$

$$\hat{\mathbf{x}}_k^- = \sum_{i=0}^{2n} W_i^{(m)} \boldsymbol{\chi}^*_{i,k|k-1} \tag{2.56}$$

$$\mathbf{P}_k^- = \sum_{i=0}^{2n} W_i^{(c)} [\boldsymbol{\chi}^*_{i,k|k-1} - \hat{\mathbf{x}}_k^-][\boldsymbol{\chi}^*_{i,k|k-1} - \hat{\mathbf{x}}_k^-]^T + \mathbf{Q}_k \tag{2.57}$$

$$\boldsymbol{\chi}_{k|k-1} = [\hat{\mathbf{x}}_k^- \quad \hat{\mathbf{x}}_k^- + \gamma\sqrt{\mathbf{P}_k^-} \quad \hat{\mathbf{x}}_k^- - \gamma\sqrt{\mathbf{P}_k^-}] \tag{2.58}$$

$$\mathbf{y}^*_{k|k-1} = \mathbf{h}[\boldsymbol{\chi}_{k|k-1}] \tag{2.59}$$

$$\hat{\mathbf{y}}_k^- = \sum_{i=0}^{2n} W_i^{(m)} \mathbf{y}^*_{i,k|k-1} \tag{2.60}$$

4. Evaluate the error covariance matrices as,

$$\mathbf{P}_{\hat{y}k\hat{y}k} = \sum_{i=0}^{2n} W_i^{(c)} [\mathbf{y}^*_{i,k|k-1} - \hat{\mathbf{y}}_k^-][\mathbf{y}^*_{i,k|k-1} - \hat{\mathbf{y}}_k^-]^T + \mathbf{R}_k \tag{2.61}$$

$$\mathbf{P}_{xkyk} = \sum_{i=0}^{2n} W_i^{(c)} [\boldsymbol{\chi}_{i,k|k-1} - \hat{\mathbf{x}}_k^-][\mathbf{y}^*_{i,k|k-1} - \hat{\mathbf{y}}_k^-]^T \tag{2.62}$$

5. The KF equations are used to evaluate the filter gain, the estimate state and the error covariance matrix as,

$$\mathbf{K}_k = \mathbf{P}_{xkyk} \mathbf{P}^{-1}_{\hat{y}k\hat{y}k} \tag{2.63}$$

$$\hat{\mathbf{x}}_k^+ = \hat{\mathbf{x}}_k^- + \mathbf{K}_k (\mathbf{y}_k - \hat{\mathbf{y}}_k^-) \tag{2.64}$$

$$\mathbf{P}_k^+ = \mathbf{P}_k^- + \mathbf{K}_k \mathbf{P}_{\hat{y}k\hat{y}k} \mathbf{K}_k^T \tag{2.65}$$

The first four steps are equivalent to the prediction stage, Equations (2.54)-(2.62) and the last step, Equations (2.63)-(2.65) represent the KF update stage [Van der Merwe and Wan 2001].

The UKF can be used to estimate the nodal voltage waveform, obtaining these waveforms at unmonitored nodes in order to identify voltage depressions.

The *rms* voltage value can be determined by processing the discrete values for the voltage waveform according to the sampling frequency. The *rms* voltage, V_{rms}, for a discrete voltage signal can be calculated as,

$$V_{rms}(iN) = \sqrt{\frac{1}{N}\sum_{j=(i-1)N+1}^{iN} V_j^2} \qquad i \geq 1 \tag{2.66}$$

Where V_j is the voltage sample j and N is the number of samples per cycle, i is the sampled cycle. This expression can be applied to discrete waveforms of voltage and current [Albu and Heydt 2003], [Moreno *et al.* 2009].

The measured waveforms may be contaminated with noise, **Q** and **R** covariance matrices are considered with constant values, this is only valid when the noise characteristics are constant, such as standard deviation and variance. If the noise is not constant **Q** and **R** must be computed each time step and an adaptive Kalman filter formulation is required. The KF can estimate a system with time-varying noise by calculating online **Q** and **R** [Gao and Wang 2010].

The system modeling should take into account important details, such as disturbances, electrical load variations in the network or element values not determined exactly, which are intensified by the size of the network; the existence of phenomena such as thermal electrical noise of components and the accuracy of the system parameters. These effects can be taken into account by a statistical term that is the process noise, represented by **v**. Measuring instruments can present errors and noise; and these can be taken into account by other statistical term represented by **w** [Gao and Wang 2010].

2.2.5 Singular Value Decomposition

The singular value decomposition (SVD) is a technique to solve singular matrices or near to be singular; this method indicates the singular values and obtains a numerical solution; this decomposition can be applied to square and no square matrices. Considering **z=Hx**, the measurement equation, **x** is the state vector of *n* order and **z** is the measurement vector of *m* order. The *rank* of **H** matrix is the dimension of the range space. The null space is limited by the vectors which satisfy the equation **Hx**=0; its dimension is equal to the *nullity*; *rank* plus *nullity* is equal to *n* [Press *et al.* 2007], [Lobos *et al.* 1998].

When the system is over determined ($m>n$), the solution can be calculated using the normal Equation (2.5) by least squares or by SVD. The solution minimizes the length or norm of **x**. The existence of a solution depends on whether the column vectors span the vector space with dimension *m*. Under this condition, the *rank* of **H** is *m*, or if the columns are linearly independent, the *rank* of **H** is *n*; this is only true when $m \geq n$ [Strang 1988].

The measurement equation solution using the SVD can be only one when the system is over or normally determined ($m > n$ or $m = n$), but when the system is under determined ($m < n$) there is an infinite number of solutions [Arrillaga *et al.* 2000], but the SVD can find a solution with minimum norm and defines

the system observability. Observable states can be estimated and unobservable areas of the system can be delimited [Strang 1988]; in these areas the state variables cannot be estimated. SVD can be used to verify the system observability before or during the state estimation [Yu *et al.* 2004], [Hajian *et al.* 1989].

The number of nonzero singular values equals the *rank* of matrix **H**, and therefore a matrix has many zero singular values as *n-rank*(**H**). The singular values are the positive square roots of the eigenvalues of the matrix $\mathbf{H}^T\mathbf{H}$. The singular values inspection provides information about the observability of the system. The SVD is able to estimate state variables when a system is partially observable, especially when the system is under determined [Yu *et al.* 2004]. In this case, there are an infinite number of solutions for the measurement equation. The SVD obtains a particular solution $\mathbf{x}_p$ and when the null space vector $\mathbf{x}_{nsi}$ is added to this particular solution, we obtain a valid solution. Possible solutions are expressed as,

$$\mathbf{x} = \mathbf{x}_p + \sum_{i=1}^{N} (k_i \mathbf{x}_{ns_i}) \tag{2.67}$$

The number of null space vectors N equals the number of zero singular values (*n-rank*(**H**)), k_i is an arbitrary constant and $\mathbf{x}_{nsi}$ is a null space vector. Observability can be defined by inspecting the position of zero entries in the null space vectors. If all i-th elements of all null space vectors are zero then adding null space vectors to a particular solution does not change the i-th element of this particular solution, therefore, the system is observable for that element [Arrillaga *et al.* 2000]. These variables correspond to zeros in all null space vectors; they do not change, and are fully specified by the particular solution and correspond to the estimation in observable areas. The state variables corresponding to the nonzero elements in the null space vectors are unobservable parts, so these variables cannot be uniquely determined. From the above, it follows that the observability of a system model can be determined through analysis of null space vectors. SVD can be used to verify the observability of the system before or during the state estimation [Yu *et al.* 2004].

The SVD factorizes the measurement matrix **H** as,

$$\mathbf{H} = \mathbf{U}\mathbf{W}\mathbf{V}^T \tag{2.68}$$

The smaller sized SVD is $\mathbf{H}_{mn}=\mathbf{U}_{mn}\mathbf{W}_{nn}\mathbf{V}^T_{nn}$, normal sized is $\mathbf{H}_{mn}=\mathbf{U}_{mm}\mathbf{W}_{mn}\mathbf{V}^T_{nn}$, with m measurements and n state variables.

In smaller size systems, **W** is a diagonal matrix n order with positive or equal to zero elements, which are the singular values of **H.** **U** and **V** are orthogonal, **U** is an orthogonal column matrix of order $m \times n$, **V** is an orthogonal row matrix ($\mathbf{U}^T\mathbf{U}=\mathbf{V}^T\mathbf{V}=\mathbf{I}$ y $\mathbf{HV}=\mathbf{UW}$). **U** is the matrix of eigenvectors of $\mathbf{H}\mathbf{H}^T$, **V** is the matrix of eigenvectors of $\mathbf{H}^T\mathbf{H}$ y $\mathbf{W}\mathbf{W}^T$ is a diagonal matrix of eigenvalues.

The measurement equation solution using SVD is [Press *et al.* 2007],

$$\mathbf{x} = \mathbf{V}\mathbf{W}^{-1}\mathbf{U}^T\mathbf{z} \tag{2.69}$$

The condition number of a matrix is the division of its largest singular value to the smallest. A singularity is considered close to zero when its value is close to or less than the largest singular value multiplied by the number of machine precision used (10^{-6} for single precision and 10^{-12} for double precision)

[Strang 1988]. The condition number is a measure of how close is a matrix to become singular. If a matrix is singular, it has at least one singular value equal to zero and its condition number is undefined or infinite. A matrix with a large condition number is said to be ill-conditioned. Using a normal size for SVD, if a single value is zero or close to zero, a zero is placed in the corresponding diagonal element of $\mathbf{W}^{-1}$ instead of $1/w$, then if,

$$\mathbf{W} = \begin{bmatrix} \mathbf{S} & 0 \\ 0 & 0 \end{bmatrix} \tag{2.70}$$

The **W** pseudo-inverse is defined as,

$$\mathbf{W}^{+} = \begin{bmatrix} \mathbf{S}^{-1} & 0 \\ 0 & 0 \end{bmatrix} \tag{2.71}$$

The **H** pseudo-inverse is,

$$\mathbf{H}^{+} = \mathbf{V}\mathbf{W}^{+}\mathbf{U}^{T} \tag{2.72}$$

The solution using the pseudo-inverse is,

$$\mathbf{x}^{+} = \mathbf{H}^{+}\mathbf{z} = \mathbf{V}\mathbf{W}^{+}\mathbf{U}^{T}\mathbf{z} \tag{2.73}$$

The pseudo-inverse solution calculates the minimum square error, if there are multiple solutions, the pseudo-inverse computes the minimum norm solution [Press *et al.* 2007], [Strang 1988].

2.2.6 Pseudo and Virtual Measurements

The observability can be improved using different types of information: pseudo and virtual measurements. The pseudo measurements are estimated based on historical data. Virtual measurements require no measurement. For example, the zero current injection in a switching substation where no load is directly connected.

HSE divides the nodes in suspects (with nonlinear loads) and not suspects being those nodes where there are no known nonlinear loads (for example, between the generator and transformer or in switching substations).

This produces the partition of the measurement equation,

$$\begin{bmatrix} \mathbf{h}_{11} & \mathbf{h}_{12} \\ \mathbf{h}_{21} & \mathbf{h}_{22} \end{bmatrix} \begin{bmatrix} \mathbf{v}_1 \\ \mathbf{v}_2 \end{bmatrix} = \begin{bmatrix} \mathbf{i}_1 \\ 0 \end{bmatrix} \tag{2.74}$$

Where:

$\mathbf{v}_1$ voltage vector of suspect nodes

$\mathbf{v}_2$ voltage vector of non suspect nodes

$\mathbf{i}_1$ injected harmonic current vector in nodes or line currents in suspect nodes.

From Equation (2.74):

$$\mathbf{v}_2 = [-\mathbf{h}_{22}^{-1}\mathbf{h}_{21}]\mathbf{v}_1 \tag{2.75}$$

To reduce the number of unknowns, (2.75) is used in (2.74) to eliminate voltages in non-suspect nodes,

$$[\mathbf{h}_{11} - \mathbf{h}_{12}\mathbf{h}_{22}^{-1}\mathbf{h}_{21}]\mathbf{v}_1 = \mathbf{i}_1 \tag{2.76}$$

Although this reduces the number of unknowns, it has the disadvantage of removing the possibility of using harmonic voltage measurements at not suspect nodes. The preferred option is not to partition the nodes and instead add a measure to the measurements equation, called virtual measurement (for each not suspect node). This process is illustrated for phasors although can also be applied to instantaneous quantities.

Not only the focus is on the harmonics but also for inter-harmonics and sub-harmonics, which are produced by loads such as cyclo-converters and arc furnaces. Estimation techniques can be applied to inter and sub-harmonics in the same way as for HSE [Pham *et al.* 2000].

2.3 Optimal Location of Meters

Meter optimal installation involves finding the optimal number of measurements and the best position in the system, to identify the location and magnitude of the harmonics, voltage and power transients by estimating the state. One approach to solve this problem has been the use of the minimum condition number of the measurement matrix as the criterion together with the sequential removal [Madtharad *et al.* 2005].

The observability is important to compute the state estimation, the system must be observable. If the system is not observable, determine which state variables are not observable or not susceptible to be estimated likewise establish the observable variables. For the case of power systems, it can be established which areas of the system that are observable and which are not. In addition to the observability using the available measurements should be treated the optimal location of measurements and the possible reduction of their number to ensure the system observable condition. Observability must be determined before and during the state estimation; a method that has been used is the SVD, which by analysis of the resulting matrices from the decomposition makes possible to identify the degree of observability, when the system has an under-determined condition, even if during the estimation, changes take place in network topology or there are fewer measurements due to failures in communication or measuring systems. The SVD is able to determine the degree of observability of the system, its observable and unobservable areas, thus enabling the evaluation of the estimation. The SVD is an effective method to analyze the observability [Madtharad *et al.* 2005].

2.3.1 Algorithm for optimal location of meters

The number of meters that an operator can install on the system is economically limited. The more sensors connected to the system adequately distributed, the more accurate the state estimation, but the cost can be very high [Madtharad *et al.* 2005]. A methodology is required to select the optimal locations to install measuring devices.

The minimum condition number of the measurement matrix **H** based on a sequential removal can be used as a criterion for this problem. The condition number of a matrix is the ratio of the largest singular value

to the smallest. A matrix is singular if its condition number is infinite, and would be considered ill-conditioned if its condition number is large, that is, if the reciprocal of this number approaches the floating point precision of the machine in use.

A brute force method can be used to calculate a comparative measure of all possible combinations for the location of meters [Farach *et al.* 1993]. The procedure examines all possibilities and provides a solution. For a system with N nodes, M possible locations with P meters to install, the possible combinations must be computed to determine the best measurement locations, namely $\binom{M}{P}$ combinations.

For example for a system with 27 nodes, 141 possible locations and 9 meters, the possible combinations are $\binom{141}{9}$ i.e., $4.68X10^{13}$. Usually the number of possibilities is very large.

The simulations with power system models indicate that the location process may be performed in a sequential manner. The sequential elimination method finds the M+1 best locations containing the M best locations. This method has been proven to be valid in many cases as it is possible to find near optimal locations.

There is a reduction in the number of possible combinations with the sequential method. This process need not to be repeated from the beginning when increasing or decreasing the number of meters. The sequential method only needs to compute $P(2M+1-P)/2$ combinations to determine the best location, or the location closest to the optimum. The computational effort required by the sequential method is minor, compared to the full enumeration method for a real system.

For the same system of 27 nodes, 141 locations with 9 meters, the sequential method requires to compute 1233 combinations instead of the $4.68X10^{13}$ combinations required for the full enumeration approach.

The meter installation is usually assumed symmetrical. This restriction limits the search for the optimum location in asymmetric power systems.

Figure 2.6 shows the flowchart of the algorithm for the optimum measuring location. Of all possible locations, the objective is to minimize the condition number of the measurement matrix.

The number of meters is always limited due to high cost, so the number represented by P must be minimized. However, to improve the redundancy in the measurements, what is important for the identification of erroneous measurements, virtual measurements and pseudo-measurements should be included in the measurement matrix. Virtual measurements provide information that do not need to be measured and are determined by the topology, configuration or system operation. Pseudo-measurement are based on historical data.

The system should normally be observable to obtain a unique solution, the minimum required number of measurements must be equal to the number of state variables. As a result, for n state variables to minimize P, M must also be minimized [Madtharad *et al.* 2005].

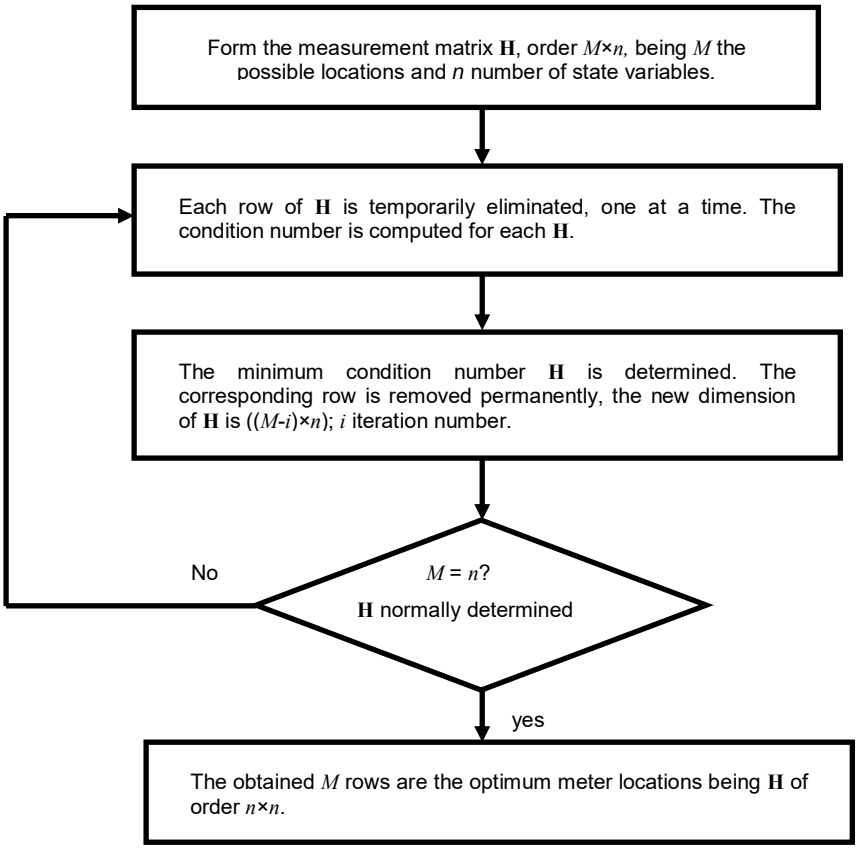

Figure 2.6 Flowchart of the sequential method to determine the optimal location of meters

The algorithm needs to iterate until $M=n$ to ensure a normally observable system, this means that the number of cycles are M-n iterations. On each iteration every possible location is temporarily removed, then computes the condition number of the measurements matrix, the location having the smallest condition number is eliminated, reducing the number of rows in M, and to obtain $M=n$. At this point the condition number of **H** measurement matrix is minimal, the ill-conditioning of this matrix will be minimal too.

As a result, the measurement matrix of the proposed algorithm is not singular, which ensures the system solution. In this case, all the state variables can be obtained, that is, when all of the singular values of the measurement matrix **H** are different from zero. The number of possible locations is reduced from M to n by sequentially removing remaining locations. This condition will have the optimum locations for the meters or the closest to the optimum.

2.4 Data Errors and Noise

Incorrect measurements can be present during the state estimation process. They can be generated by lack of calibration and/or meter wrong connection, meter failures, incorrect system model parameters or wrong network topology when estimating, e.g. switching on transmission lines.

The presence of erroneous data degrades the state estimation accuracy, the problem is solved by the detection, identification and elimination of erroneous data. In this case, it is important to mention that by

reducing the number of measurements, the measurement model can be moved from an over-determined to a normal or even under-determined condition; this change must be considered in the algorithm to solve the state estimation [Wu *et al.* 1988]. For the purpose of this work the error detection is not performed.

2.5 Conclusions

The power quality state estimation should be evaluated at both steady and transient state applications in real time or as close as possible to real time during the operation of power systems.

The steady state estimation has been traditionally computed in the frequency domain. For the application on power quality it should also be evaluated in the time domain, since determining the waveforms implicitly contain a wide harmonic spectrum, especially in case of time-variant harmonics or a description of a time function in the case of transients.

The time domain state estimation can be recursively applied each time step using the evaluation methods in the frequency domain, such as the method of weighted and normal least squares, with appropriate memory and computational power.

The most applied method in the time domain is the Kalman filter, this method can be easily adapted to different system and measurements models.

The SVD allows the state estimation in cases where the measurement equation is in an under-determined condition, which is the most common case in the power quality state estimation. Traditional state estimation in the frequency domain usually deals with an over-determined condition.

Virtual or pseudo measurements improve the condition and the observability of the system. They add equations to the measurement model, virtual measurements are set according to the operating system condition and the pseudo measurements use past historic data in the power system.

The optimal location of meters can be determined using the sequential elimination algorithm to obtain a normally determined measurement equation.

Chapter 3

Power Quality State Estimation and Computational Techniques

3.1 Introduction

Due to the diversity of electric loads, the importance of power quality problems has been increasing, example of this is the proliferation of electronic devices that are sensitive to changes in voltage, such as computers, electronic equipment, diagnostic systems in hospitals or in automated production lines with controllers and industrial robots. In some industrial systems, an interruption or voltage depression of 30% lasting hundredths of a second can reset the controllers and stop a production line and can take several hours to restart the line. Therefore, the power quality is a very important aspect in the supply of electricity and is indicative of the competitiveness of utilities [Short *et al.* 2003].

The power quality problems are manifested in voltage variations, which can be in form of transients due to load switching, depressions, over-voltages, complete interruption or harmonic distortion caused by nonlinear loads [Domijan *et al.* 1993].

With the connection of renewable energy sources or distributed generation, the power system must take into account that the power quality of such sources influences the power quality of the entire system as a whole, so it must fulfill the requirements for quality by the power system operation. The quality is fundamentally altered due to variability of the primary source of energy and its influence on the generated wind power, which can change in the short-term.

The switching components of power electronics to integrate renewable sources greatly influence the power quality. Among these devices are rectifiers and inverters; therefore, it is required that these converters are designed to transform energy with acceptable quality with low distortion AC power delivered to the system. The IEC 61400-21 standard [IEC 2008] includes recommendations for connecting the renewable sources relating the network power quality.

The planning and operation of generation must take into account the power quality, the quality parameters are related to:

1) The variability of the power source.
2) The power factor (reactive power demand).
3) Harmonic distortion (harmonic emissions).
4) Voltage fluctuations.
5) Variations in frequency.

Ideal power quality means that the continuous voltage is sinusoidal with a constant frequency and magnitude; it is described in terms of voltage, frequency and interruption [Dugan *et al.* 2002]. Voltage quality must meet requirements of national and international standards. Under these rules, voltage disturbances are divided into

voltage variations, flicker, transient and harmonic distortion, Figure 3.1 shows the classification of the different phenomena of power quality.

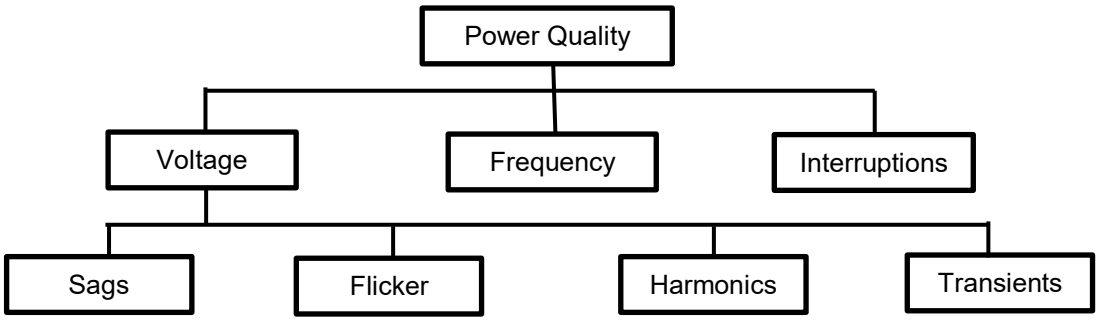

Figure 3.1 Power quality phenomena.

The power quality is the set of electrical characteristics limits which allow systems to operate normally, and for which they were designed without a significant loss in performance or life. The term is used to describe the electrical power consumed by an electric load with the ability to function properly. Without the proper power, an electrical device may malfunction, fail prematurely or not operate. There are many ways in which electrical power may have a low quality and many reasons for this low quality.

The power industry includes electricity generation, power transmission and distribution to consumers, until the electricity is transformed into the load. The complexity of the system to carry electricity from generation to the point of consumption, combined with climate variations, operation, demand and other factors provide adverse conditions that compromise the power quality.

The power quality depends mainly on the voltage and less on power or current. Power is simply the flow of energy or current demanded by load; it can present variations which can be very large or have a very low controllability.

The power quality can be described by a set of values in certain parameters, such as:

- Service continuity
- Voltage magnitude variation
- Transient voltages and currents
- Harmonic content in waveforms

The power quality can be seen as a problem of compatibility, i.e. to analyze whether the equipment connected to the network supports events in the network, and if the power delivered, including the events, is compatible with the equipment or connected load. Compatibility problems have at least two solutions: increase the quality of energy and therefore power or fabricate and install equipment more resistant to the adverse effects of poor power quality.

The tolerance of data processing equipment to voltage variation is characterized by CBEMA [Bollen 2000], which defines the duration and magnitude of voltage variations that can be tolerated by a particular computer or equipment.

Ideally, voltage is supplied with sine waveform taking a magnitude and frequency defined by the standards in each country, however, in practice the power source is not ideal and generally may deviate at least in some of the following ways [Heydt 1991]:

• Fluctuations in the voltage peak or *rms* value.

• A surge or swell occurs when the *rms* voltage exceeds its nominal value by 10 or even 80% for 0.5 cycles to one minute.

• A voltage depression or sag is when the voltage *rms* value decays of its nominal value by 10-90% by 0.5 cycles to one minute.

• Repetitive or random fluctuations in the voltage *rms* value between 90 and 110% of nominal value can produce the phenomenon known as flicker in the lighting equipment. The flicker is presented as rapid variations and visible in the illumination level.

• Abrupt but brief increases in voltage, called spikes, pulses, or shocks, usually caused by inductive loads subject to switching, or more severely by lightning.

• Low voltages occur when the nominal voltage drops down from 90% for over a minute. The term medium voltage or brownout is used to describe the phenomenon when the voltage drops between full power, bright lights and a blackout. It occurs when incandescent lights reduce their luminosity; it is used to describe a reduction in voltage by the control center to reduce demand or increase operating margins.

• The over-voltage occurs when the rated voltage is increased above 110% for more than a minute.

• Frequency variations.

• Waveform distortion described by harmonics.

• Impedance at low nonzero frequency (occurs when a load demands greater power and the voltage decreases).

• High frequency impedance nonzero (occurs when a load demands a large amount of current, suddenly shuts demanding much less current suddenly, then a voltage sag or a spike is present due to the line inductances of the power source).

These power quality problems have different causes. Some problems are due to shared infrastructure and common connections. For example, a network failure can result in voltage sags, which affect some consumers; the greater the failure, the greater the number of consumers affected. A problem in a consumer installation can cause a transient that affects all consumers of the same subsystem. Problems, such as harmonics, can increase within the facility itself and can spread within the network and affect other consumers. Harmonic problems can be solved with a combination of good design practice, testing, modifying, restricting and reducing the equipment causing harmonics. Appendix A details the power quality phenomena.

3.2 State Space Representation

Electrical systems can be represented by a differential algebraic equation (DAE) system that may be transformed to state space by obtaining a system of ordinary differential equations (ODE); these equations can be expressed with the vector-matrix notation [Kundur 1994]. The matrix representation simplifies the

mathematical modeling of systems. Besides, the increment of states, inputs or outputs, do not increase the complexity of the equations [Ogata 2002].

Notation to model a non-autonomous system dependent of time t is represented by (3.1) and (3.2):

$$\dot{\mathbf{x}} = \mathbf{f}(\mathbf{x}, \mathbf{u}, t) \tag{3.1}$$

$$\mathbf{y} = \mathbf{g}(\mathbf{x}, \mathbf{u}, t) \tag{3.2}$$

Where **f** is the vector containing the n first order differential equations, **x** is the state vector n order, **u** is the input vector, **g** is the algebraic equation vector, **y** is the output vector and t is the time variable.

The expression for $d\mathbf{x}/dt$ is the state equation and the expression for **y** is the output equation; if vector functions **f** and **g** are functions of time, the system is called time-variant.

If the state and output equations are linearized or are linear, they can be expressed by:

$$\dot{\mathbf{x}}(t) = \mathbf{A}(t)\mathbf{x}(t) + \mathbf{B}(t)\mathbf{u}(t) \tag{3.3}$$

$$\mathbf{y}(t) = \mathbf{C}(t)\mathbf{x}(t) + \mathbf{D}(t)\mathbf{u}(t) \tag{3.4}$$

Where $\mathbf{A}(t)$ is the state matrix, $\mathbf{B}(t)$ is the input matrix, $\mathbf{C}(t)$ is the output matrix and $\mathbf{D}(t)$ is the direct transmission matrix. A system is said to be linear if it obeys the superposition principle.

With an integration time step Δt, the solution of (3.3) at time t can be expressed in terms of the solution at t-Δt:

$$\mathbf{x}(t) = \mathbf{x}(t - \Delta t) + \int_{t-\Delta t}^{t} [\mathbf{A}(\zeta)\mathbf{x}(\zeta) + \mathbf{B}(\zeta)\mathbf{u}(\zeta)]d\zeta \tag{3.5}$$

Where ζ is the integration variable.

If **f** and **g** do not depend of time, the system is called time-invariant; in this case, the above equations are simplified to the following:

$$\dot{\mathbf{x}}(t) = \mathbf{A}\mathbf{x}(t) + \mathbf{B}\mathbf{u}(t) \tag{3.6}$$

$$\mathbf{y}(t) = \mathbf{C}\mathbf{x}(t) + \mathbf{D}\mathbf{u}(t) \tag{3.7}$$

The ODE solution can be numerically computed by applying the conventional trapezoidal rule [Zill 2002], [Kundur 1994], as,

$$\mathbf{x}_{k+1} = \mathbf{x}_k + \frac{1}{2}h[\mathbf{f}(t_k, \mathbf{x}_k) + \mathbf{f}(t_{k+1}, \mathbf{x}_{k+1})] \tag{3.8}$$

Where h is the integration step, t is the independent variable. This is an implicit method, having the general form:

$$\mathbf{x}_{k+1}^{(i+1)} = \mathbf{x}_k + \frac{1}{2}h[\mathbf{f}(t_k, \mathbf{x}_k) + \mathbf{f}(t_{k+1}, \mathbf{x}_{k+1}^{(i)})] \tag{3.9}$$

A good initial estimate for $\mathbf{x}_{k+1}^{(0)}$ can be obtained from the formula:

$$\mathbf{x}_{k+1}^{(0)} = \mathbf{x}_k + h\mathbf{f}(\mathbf{x}_k, \mathbf{y}_k) \tag{3.10}$$

This process is known as predictor-corrector method, the process concludes when a given tolerance of the absolute difference between the last two iterations is satisfied, which meets a certain number of iterations, or a time interval of study has been met.

3.2.1 Sources Identification, Components and Nonlinear Loads

Normally the sources are represented with linear models but can have a nonlinear representation according to the complexity of the model to use or the study that has to be performed. When the sources are represented as nonlinear formulation consequently the algorithms to use must be applied properly to achieve a solution to the problem that is being analyzed generally this is more complicated than if it is taken the linear form.

For state estimation, these characteristics of the sources are analyzed within the system model identification to form a model representing the physical network, while maintaining a balance between complexity and accuracy. If a model is very complex near to the real system, its solution will be complicated, but if a model is very simple, its solution will be simpler, its response may be far from practical reality. This is particularly important within the state estimators because if the system to estimate is not properly represented the state estimation solution can be away from the solution or the real situation.

The main components of a power system are generators, transmission lines, transformers, capacitors banks and electric loads. These components can be approximately represented by linear models, but usually can be adopted a more accurate representation taking into account nonlinear effects.

Within the nonlinear components used in the modeling of electric power systems there are magnetizing branches, nonlinear models of the transformer, electric arc furnaces, FACTS devices such as thyristor-controlled reactor (TCR), controlled series compensator thyristor (CSCT), the STATCOM static compensator, the static var compensator (SVC), converters and rectifiers, among others. According to the study that is to be done using single or three phase models, thus generating a number of ODE's for the mathematical modeling, which are to be solved to find the dynamic response of the power system under given operating conditions.

For state estimators, the more accurately represent a system through the model, the state estimation is also more accurate using this model, but the solution logically involves higher complexity of algorithms to be used to compute the response and the state estimation.

3.2.2 Load Identification

A nonlinear load can be represented by a Norton equivalent circuit having a parallel admittance to a current source. Even if the load is passive (no harmonic current source), the HSE gives the harmonic current injection due to the current in the linear component (admittance). Figure 3.2 shows a general electrical load

representation. The purpose of load identification is to determine if the harmonic current of the load ($I_{Load}(h)$) is due to the distortion of the voltage at the terminals of the load (flowing into the Norton admittance) and the magnitude of the active harmonic current injection (current source Norton $I_N(h)$). Examining the results for a determined number of harmonic frequencies, the types of nonlinear load connected to a node can be estimated. At present, load identification ignores the complexity of the coupling between harmonic frequencies [Du *et al.* 1999].

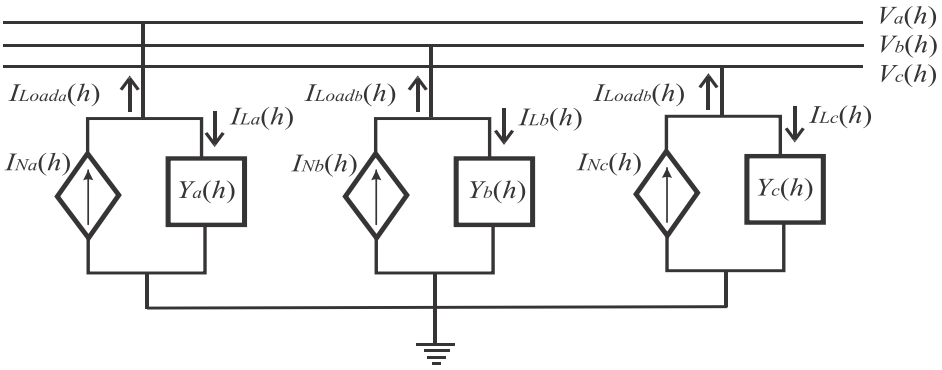

Figure 3.2 Norton equivalent of a three-phase load

3.3 Methods of analysis

The electrical network model mathematically expressed by a set of differential and algebraic equations describing the system can dynamically use three types of analysis, i.e. time domain, frequency domain, and hybrid time and frequency domain. Each method has its field of application in the analysis of power systems, depending on the studies that are required [Ramos 2006]. In this work, the power quality state estimation and its methodology are analyzed with an approach on the time domain.

In the time domain, the periodic behavior of the network is determined by integrating the set of differential equations (ODE's) describing the dynamics of the system. The representation of nonlinear components, time-varying, or loads, is performed in this domain through ODE's. The set of ODE's is solved either by explicit numerical integration methods explicit, or implicit predictor-corrector methods. The main advantage of this analysis in the time domain is that in the solution, an unlimited and implicit number of harmonics in the waveforms of the state variables representing the dynamic behavior of the system are obtained. The main disadvantages of this analysis are: obtaining the set of ODE's, modeling of the system, particularly in systems with a considerable amount of components. The devices with low damping, including the transformers, the synchronous machine or switching devices, can cause a considerable number of integration periods to reach the periodic steady state [Medina *et al.* 2003], [Medina and Ramos-Paz 2005].

An advantage of the analysis in the frequency domain is the straight forward procedure to obtain the set of equations that model the power system. Nonlinear and time varying components are represented by Norton equivalents [Arrillaga *et al.* 1995]. The disadvantages of this method are the memory requirements to represent the entire power network and the computational effort to solve the system of equations, which

requires the inversion or factorization of large order sparse matrix of coefficients and a high degree of dispersity. Another disadvantage is that the number of harmonics to be analyzed is limited and directly influences the accuracy of the method, as well as the involved computational effort.

In the hybrid analysis the linear part of the network is analyzed in the frequency domain while the nonlinear part is analyzed in the time domain. [Semlyen and Medina 1995] proposes a hybrid analysis method, where the linear elements dependent of frequency are analyzed in the frequency domain, and nonlinear and time-varying elements in the time domain. Appendix B presents the ODE solution methods.

3.4 Periodic Steady State Evaluation

The periodic steady state of a power network can be obtained by the brute force (BF) method, which is the integration of the set of ODE's, dynamic model of the system, over a period of the fundamental frequency from a vector of initial conditions. Once the integration is evaluated in this period of time, the maximum error is determined between the vector of initial conditions of the states and the state vector obtained at the end of the integration period. If the maximum error is greater than the convergence criterion, the vector of initial conditions is replaced by the state vector and integration is repeated periodically to meet the convergence criterion for the periodic steady state of a grid.

3.4.1 Newton Techniques and Extrapolation to Limit Cycle

The determination of periodic steady state is one of the most important problems in the analysis of electrical networks, since in practice its components are nonlinear and time-varying. In [Chua and Ushida 1981] methods of rapid approach to the periodic steady state are classified as brute force, perturbation, harmonic balance and shooting.

The BF method integrates the set of ODE dynamic model of the system to reach the periodic steady state. This integration is performed by implicit, explicit or predictor-corrector methods. The disadvantage of this method is to use a considerable number of integration periods particularly when the system is under damped, the transient component takes considerable time to disappear [Ramos 2006].

The perturbation method is based on an iterative process, which begins with the determination of an initial solution. This initial solution is obtained by the linearization of equations which are the dynamic model of the system.

In the harmonic balance method each state variable is represented by a Fourier series, which satisfies the requirement of periodicity. Then, apply an optimization algorithm to adjust coefficients of the Fourier series, so that the equations are satisfied with the minimum error. Although this algorithm avoids the use of a numerical integration process of the ODE set modeling the system dynamics, its main disadvantage is the large number of variables to be optimized by the algorithm, which is reflected in an increased computational effort and in the use of computational resources. For example, if a system contains n variables and each requires $2m+1$ Fourier coefficients, then there will be $n(2m+1)$ variables to be adjusted by the optimization algorithm. This makes the algorithm impractical, particularly for large electrical networks [Ramos 2006].

One of the techniques used for the determination of periodic steady state of electrical circuits are the shooting methods, such as those proposed by [Aprille and Trick 1972], [Semlyen and Medina 1995]. The objective of these methods is to find a vector of initial conditions $\mathbf{x}(0)$, so that when integrating the system of equations $d\mathbf{x}/dt=\mathbf{f}(\mathbf{x},\mathbf{u},t)$, over a complete period of time T, from the determined initial condition $\mathbf{x}(0)$ the equality of final and initial conditions, $\mathbf{x}(t)=\mathbf{x}(0)$ under a defined tolerance, is obtained, indicating that the periodic steady state has been reached.

The Numerical Differentiation (ND) is a Newton-type method of extrapolation to the limit cycle proposed in [Semlyen and Medina 1995], based on the concept of Poincaré map. The methods used in this investigation to determine the periodic steady state are the ND and Enhanced Numerical Differentiation (END) [Segundo and Medina 2010].

3.4.2 Fast Approach to Periodic Steady State

There are several methods to quickly reach the periodic steady state of ODE's that represent the dynamic behavior of physical systems, including electrical systems. In this thesis, the ND and END methods are used to achieve a rapid convergence to periodic steady state.

If the excitation for the ODE's set is periodic, then $\mathbf{f}(.,t)$ is a T-periodic vector. Steady state solution $\mathbf{x}(t)$ is also periodic and can be represented by the limit cycle for $\mathbf{x}$.

In the process of convergence to the limit cycle, the cycles of a transient orbit are close to the limit cycle. Its position is described by its representation on the Poincaré map ρ. A simple cycle maps its starting point $\mathbf{x}^i$ to its end point $\mathbf{x}^{i+1}$ and maps a perturbation segment $\Delta\mathbf{x}^i$ from a base cycle [Semlyen and Medina 1995] to $\Delta\mathbf{x}^{i+1}$. The mappings near a limit cycle are quasi-linear so the Newton method or its approximation can be used to obtain a point near the limit cycle $\mathbf{x}^{\infty}$.

To take advantage of the linearity in the vicinity of a base cycle, $d\mathbf{x}/dt=\mathbf{f}(\mathbf{x},t)$ can be linearized around a solution from t_i until t_i+T. This results in the variational problem:

$$\Delta\dot{\mathbf{x}} = \Delta\mathbf{f}(\mathbf{x}(t),t) = D_x\mathbf{f}(\mathbf{x}_t,t)\Delta\mathbf{x} = \mathbf{J}(t)\Delta\mathbf{x} \tag{3.11}$$

Where $\mathbf{J}(t)$ is the Jacobian matrix (T-periodic). The initial condition is:

$$\Delta\mathbf{x}(t_i) = \Delta\mathbf{x}^i \tag{3.12}$$

Equation (3.12) is an ODE, linear and time-varying, with solution of form:

$$\Delta\mathbf{x}(t) = \exp\left(\int_{t_i}^{t}\mathbf{J}(t)dt\right)\Delta\mathbf{x}^i \tag{3.13}$$

This equation satisfies $d\mathbf{x}/dt=\mathbf{f}(\mathbf{x},t)$. For $t=t^i+T$, in (3.13),

$$\Delta\mathbf{x}^{i+1} = \mathbf{\Phi}\Delta\mathbf{x}^i \tag{3.14}$$

Being:

$$\mathbf{\Phi} = \exp\left(\int_{t_i}^{t_{i+T}} \mathbf{J}(t)dt\right) \tag{3.15}$$

$\mathbf{\Phi}$ is almost the same for any t_i so that mapping near the limit cycle is nearly linear.

Equation (3.13) shows the input segments are mapped to correspond to the output segments by means of the matrix $\mathbf{\Phi}$. The matrix $\mathbf{C}$ is identified and defined in [Semlyen and Medina 1995], must be $\Delta\mathbf{x}^i = \mathbf{x}^\infty - \mathbf{x}^i$, so $\Delta\mathbf{x}^{i+1} = \mathbf{x}^\infty - \mathbf{x}^{i+1}$. Substituting in (3.14) and solving for $\mathbf{x}^\infty$ gives,

$$\mathbf{x}^\infty = \mathbf{x}^i + \mathbf{C}(\mathbf{x}^{i+1} - \mathbf{x}^i) \tag{3.16}$$

Being an estimation of the limit cycle with:

$$\mathbf{C} = (\mathbf{I} - \mathbf{\Phi})^{-1} \tag{3.17}$$

Equation (3.16) leads to a Newton process if $\mathbf{\Phi}$ and $\mathbf{C}$ are updated each iteration using (3.15) and (3.17). This process is linearly convergent if $\mathbf{C}$ is kept constant or updated at any stage of the iterative process after its first evaluation.

The main problem of efficiently finding the limit cycle is the identification of $\mathbf{\Phi}$ matrix. The following section describes the numerical differentiation method, where $\mathbf{\Phi}$ is identified. This method requires to evaluate the base cycle $\mathbf{x}(t)$ over a period T, starting from $\mathbf{x}^i$.

3.4.3 Numerical Differentiation Method

The numerical differentiation method (ND) efficiently computes the periodic steady state of a system in the time domain. If a set of first-order ODE mathematically models a dynamic system and this has in turn a periodic steady-state solution, this can be calculated using the Poincaré map and extrapolating to the limit cycle the state variables through Newton methods [Parker and Chua 1989]. The ODE model is represented by $d\mathbf{x}/dt=\mathbf{f}(\mathbf{x},t)$.

The state variables in the limit cycle $\mathbf{x}^\infty$ can be evaluated as indicated in [Semlyen and Medina 1995], using (3.16) and (3.17).

The ND is applied to accelerate the convergence of the state variables to the limit cycle and thus quickly reaches a solution for the power system periodic steady state. The method is summarized as follows: a base cycle $\mathbf{x}(t)$ is computed, after evaluating the state variables in the time domain for a certain number of cycles. By state variable perturbation at the start of the base cycle, the difference between the last two values at the end of the cycle are calculated to obtain $\Delta\mathbf{x}^{i+1}$, which allows to identify $\mathbf{\Phi}$ matrix by columns, then the $\mathbf{C}$ matrix is obtained to compute $\mathbf{x}^\infty$. This vector represents an estimate of the state variables in the limit cycle. This process ends when the difference between two succesive evaluations of $\mathbf{x}^\infty$ meets a convergence criterion, e.g., 10^{-6}.

3.4.4 Enhanced Numerical Differentiation

The enhanced numerical differentiation (END) uses the half-wave symmetry of the excitation signals in the system, such as the waveform of voltage sources [Segundo and Medina 2010].

This methodology consists in evaluating **Φ**, approximating **x**(t+T) by extrapolation of **x**(t+T/2). With this approach, the integration of d**x**/dt=**f**(**x**,t) to compute **x**(t+T) is not required to be performed over a full period, but only about half period, this increases the computational efficiency of the numerical differentiation method because it is only processed half cycle.

There are multiple conditions in the power system operation. One is when the network is balanced and free from harmonic distortion, in this case, the dc signals have only a dc component in the harmonic spectrum, and the ac components only have the fundamental frequency component. The periodic steady state of this system is calculated using phasors [Segundo 2010].

A different case is when the network is balanced and there are harmonic sources in the network; the dc component and ac signals have different harmonic components. Harmonic flows are generated according to the network topology, assuming nonlinear components and loads connected to the system.

A more realistic case is when the source voltage, load, and the power system are unbalanced and have harmonic flows. Then the ac signals on the limit cycle satisfy the following equality:

$$\mathbf{x}_i(t+T) = -\mathbf{x}_i(t+T/2) \tag{3.18}$$

The signals with a dc component can not satisfy (3.18), because these signals contain only even harmonics in periodic systems and therefore can be set if a signal that satisfies (3.18), this signal has no dc component. Furthermore, signals with dc component in the limit cycle satisfy the following equation:

$$\mathbf{x}_i(t+T) = \mathbf{x}_i(t+T/2) \tag{3.19}$$

If a signal satisfies (3.19) in the limit cycle, it is concluded that this is a signal with a dc component and this signal satisfies,

$$\frac{d\mathbf{x}_i(t)}{dt}\frac{d\mathbf{x}_i(t+T/2)}{dt} > 0 \tag{3.20}$$

The END is based on the following steps:

1) Integrate d**x**/dt=**f**(**x**,t) from t to t+T/2.

2) Evaluate (3.20) using finite differences to calculate the derivatives.

This operation is only performed twice during the solution process. To evaluate (3.20) it takes a very simple operation that does not consume time. If Equation (3.20) is not satisfied, the ODE set d**x**/dt=**f**(**x**,t) is integrated from t+T/2 to t+T using the conventional numerical differentiation. If (3.20) is satisfied, the dc component and ac variables are identified stating that close to the limit cycle, ac variables satisfy (3.18) and dc-component variables satisfy (3.19).

This method only requires integrating half period T/2, instead of a complete cycle T, as in the numerical differentiation method. It has been reported that the computer efficiency of this method is up to 100% higher than the associated with the ND method [Segundo and Medina 2010].

3.5 Parallel Processing Techniques

The parallel processing techniques have been applied to solve different problems in the modeling and analysis of power systems, such as the assessment of transients, the power flow solution, the periodic steady state evaluation, time and frequency domain response of electrical networks [Peng *et al.* 2011]. In this investigation, these techniques are applied to solve the time domain state estimation using a parallel algorithm for the KF.

The advantages of parallel processing are the execution time reduction and the size of systems to be solved, making possible real time implementations and more in detail modeling. The parallel processing has been possible due to the development of the very large scale of integration technology (VLSI) and the need of solution of big and complex problems. There are two parallel architectures widely used; i.e., multiprocessor and multicomputer [Owens *et al* 2008]. The multiprocessor architecture connects processors sharing a common memory, the communication and synchronization use shared variables. The multicomputer connects computers using a high speed communication network; these computers do not share memory and the communication uses messages [El-Rewini and Abd-El-Barr 2005]. A configuration CPU-GPU is a multiprocessor architecture.

The execution time is not the most convenient measure to evaluate a sequential or parallel algorithm, as this time varies with the size of the problem, the efficiency or speed-up is a more convenient way to assess a parallel algorithm, this is defined as the ratio of the time execution with one processing element to the time execution with multiple processing elements,

$$E_{relative} = \frac{t_1}{t_p} \tag{3.21}$$

t_1 execution time of one process element.

t_p execution time of p process elements.

Parallel processing can reduce the order of complexity of algorithms, the execution time and computational effort depending on the instructions or functions that are part of the algorithm, the problem size and number of processors used in parallel processing, this type of processing can decrease the computational requirements for real-time implementations.

3.5.1 GPU Parallel Processing

Graphics Processing Units (GPU) began as graphics processors with a specific function but subsequently increased their computational power and programmability. Between the years 1990-2000, multidisciplinary scientific research began using GPUs to simulate and experience in a wide range of scientific applications [Nvidia Cuda API 2012]. The parallel processing has been applied to obtain the periodic steady state of power systems with nonlinear loads [Medina *et al.* 2003a].

Applications achieve better results, in some cases hundreds of times, compared with the CPU; sequential code, the challenge was that GPUs required the use of graphics programming, application program

interfaces (API) such as OpenGL and Cg to program the GPU. This limited the accessibility of scientific applications to GPUs.

The GPUs potential was established, so the effort was into make completely programmable GPUs, with a programming similar to C, C++ and Fortran.

The main objective in parallel processing is to use the GPU along with the CPU to accelerate scientific and engineering applications. The use of GPU has become one of the standards for parallel computing [Owens et al 2008].

The GPU can be applied to perform intensive computational effort in parallel, while the remaining sequential code runs on the CPU. From the point of view of the user, the applications run significantly faster.

A CPU and GPU combination is very convenient because the CPU consist of cores optimized for sequential processing in series, while the GPU cores consist of thousands of smaller but more efficient processors designed for parallel processing. Sequential instructions run in series in the CPU while the parts in parallel run in the GPU, as shown in Figure 3.3.

GPUs have evolved to the point where many practical applications have been implemented by taking advantage of GPUs and run significantly faster than on multi-core systems. Future computing architectures will be hybrid systems with parallel-core GPUs working in tandem with multi-core CPUs [Owens et al 2008].

GPUs are essentially parallel processors, and their efficiency depends on the degree of parallelism in the problems to solve.

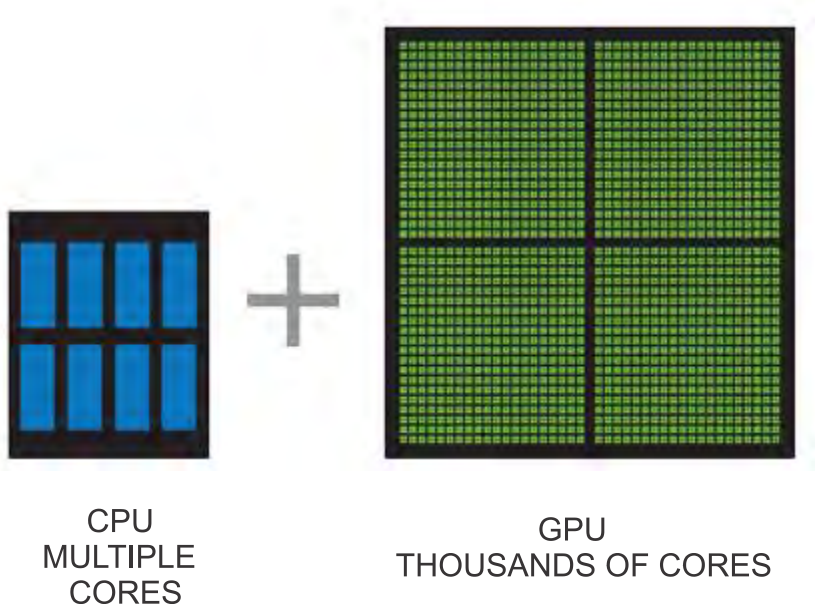

Figure 3.3 CPU and GPU sequential and parallel processing

The Compute Unified Device Architecture (CUDA) [Nvidia Cuda API 2012] is a parallel computing platform and programming model that enables the use of a GPU to perform parallel processing. The programming is very similar to that of C, C++, or Fortran, since incorporates extensions of these languages in

the form of basic instructions, to make, parallel programming of the GPU simpler, easier to program and debug.

These instructions allow to run on massive form the parallelism in a process or algorithm and direct the compiler to the corresponding application on the GPU execution. This is the hybrid computing model where CPUs and GPUs work together to solve problems requiring a solution of otherwise considerable computational effort.

CUDA is based on the combination of hardware and software that enables GPUs to run programs written in C, C++, Fortran, and other languages [NVIDIA CUDA C 2012]. A CUDA program runs parallel functions called kernels which run through many threads in parallel. The programmer or compiler arranges these threads in blocks, and blocks in grids, as shown in Figure 3.4.

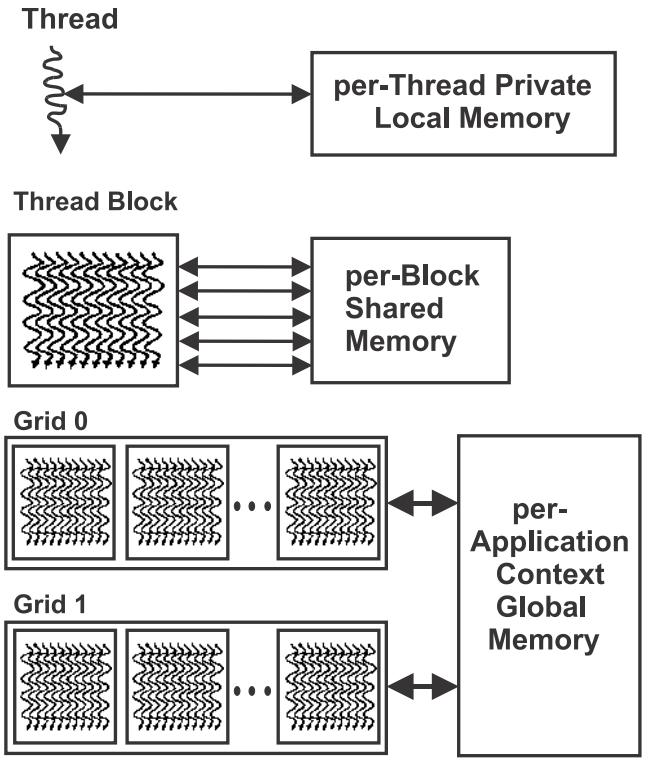

Figure 3.4 CUDA hierarchy, thread, blocks and grids, corresponding to the private memory space per thread, shared memory and global memory block by application.

Each thread within each block runs and refers to a kernel. Each thread also has a thread identifier and block within its thread block and its grid, a program counter, registers, private memory for each thread, data inputs, and output results.

A thread block is a set of concurrently executing threads that can cooperate with each other through their synchronization and a shared memory. A thread block has its block identifier within the grid. A grid is an array of thread blocks that execute the same kernel, reads inputs from global memory, writes results to global memory, and synchronizes between the dependent kernel calls. In the CUDA parallel programming model, each thread has a private memory space used by each thread to thread communication, data sharing,

and shared results in parallel algorithms. Grids of blocks of threads share results in global memory space after kernel global synchronization.

The CUDA execution in hardware is made using CUDA hierarchy threads, which maps to a hierarchy of processors in the GPU; a GPU executes one or more kernels, a multiprocessor executes one or more blocks of threads, and the cores of CUDA and other execution units execute instructions of thread. The threads run in groups of threads called warps. Programmers can ignore the execution of warps to run a correct functionality and can focus on individual thread programming; consequently, they can greatly improve the performance of threads and having warps running in the same path of code and memory access with close directions [Nvidia Cuda API 2012]. Figure 3.5 shows the parallel processing flow on CUDA.

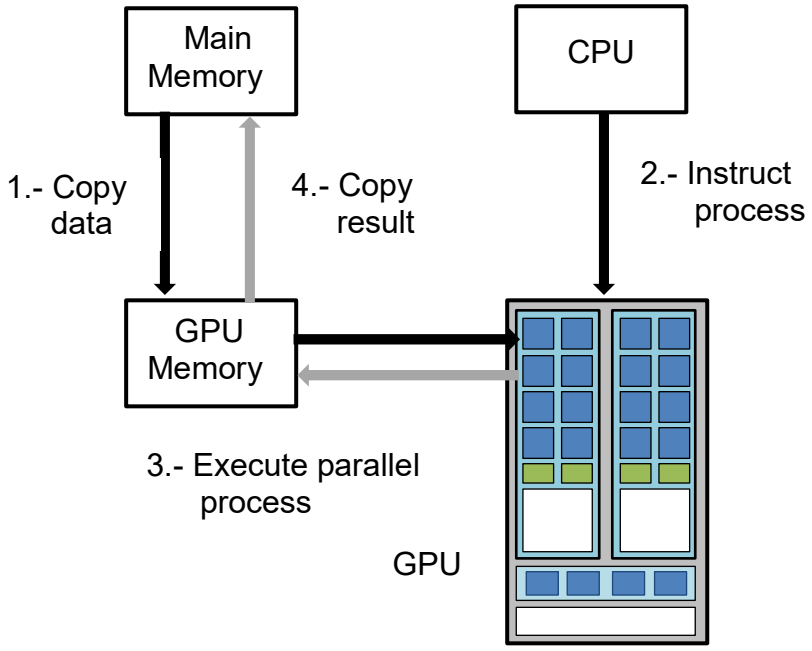

Figure 3.5 Parallel processing flow on CUDA

In the CUDA programming, applications are implemented to exploit the parallelism of GPUs, thus allowing the generation of a large number of threads which run simultaneously [Owens *et al* 2008]. The threads run in the GPU, which acts as coprocessor of the host or CPU running the main program. CUDA has instructions to reserve, copy and free memory data between CPU and GPU memory in both directions. The execution sequence can be alternatively sequential code-parallel kernel code.

3.5.2 CUBLAS Library and Kalman Filter

CUDA can use the CUBLAS library that is a parallel equivalent of the Basic Linear Algebra Subprograms (BLAS). This library can be used to solve linear algebra problems in parallel using the GPU, such as the evaluation of vector and matrix operations, which are used in many applications, such as the state estimation in electric power systems and power quality.

The CUBLAS functions that are required to evaluate the steps for the Kalman filter algorithm are Daxpy for vector addition, Dgemv for matrix-vector multiplication, Dgeam for matrix addition, Dgemm for matrix multiplication. These functions are implemented in the CUBLAS library for parallel execution in the GPU [Nvidia Cublas 2012]. The inverse matrix on the same algorithm can be evaluated by the LU decomposition and forward and backward substitutions, CUBLAS functions to implement LU decomposition are Dscal and Dger. These functions evaluate the Crout reduction algorithm and function Dtrsm implements the forward and backward substitutions [Nvidia Cublas 2012], in step 3 to evaluate the Kalman filter gain. The matrix inversion uses most of the execution time for the Kalman filter algorithm and in the state estimation is calculated at each time step [Huang *et al.* 2011]. Table 3.1 indicates the Cublas functions used to execute the Kalman filter steps.

Table 3.1 CUBLAS functions for the Kalman filter

Kalman filter step	**CUBLAS functions**
1) Project state	Dgemv, Daxpy
2) Project error covariance	Dgemm, Dgeam
3) KF gain	Dgemm, Dgeam, Dger, Dscal, Dtrsm
4) Update state	Dgemv, Daxpy
5) Update error covariance	Dgemm, Dgeam

3.6 Conclusions

The different phenomena related to power quality especially harmonics, transients and voltage depressions can be estimated in the time domain using a unified methodology of estimation based on an algorithm, this algorithm depends on the type of system model and measurements, for example if they are linear or nonlinear models.

The identification system is important for state estimation to balance accuracy and complexity of the solution. This identification includes sources, components and loads in the power system.

Newton techniques and extrapolation to limit cycle can be used to obtain the periodic steady state. The normal and enhanced version of the numerical differentiation can be applied in case studies of the power quality state estimation to obtain adequate initial condition for state variables or to evaluate the state estimation under the periodic steady state.

The state estimation should be evaluated by efficient algorithms and adequate computational techniques, in order to be implemented in real time or quasi real time, one of such technique which can be applied to the estimation is parallel processing, since by this technique, the execution time can be reduced in the numerical process of the state estimation, especially when networks of large scale are considered, as is the actual case in most practical power systems. One of the multiprocessor parallel platforms is the CPU-GPU configuration which is used in this investigation.

Chapter 4

Harmonic State Estimation

4.1 Introduction

The harmonic state estimation (HSE) main objective is to estimate the harmonic levels in the power network using a limited number of measured harmonic data [Yu *et al.* 2004]; however, these data can be contaminated with noise and gross errors. The choice of measurement points and quantities to be measured are important aspects to be taken into account [Madtharad *et al.* 2005]. The discretized waveforms of a limited number of voltages and currents in a time interval are the input data to the HSE; the solution is based on a time sequence of the system measurements [Kennedy *et al.* 2003], [Yu *et al.* 2005a].

In the open literature, different important contributions on HSE in the harmonic frequency domain are available, e. g., [Arrillaga *et al.* 2000], [Kennedy *et al.* 2003], [Cheng *et al.* 2010]. In this work, the HSE is efficiently solved in the time domain through a Kalman Filter (KF) algorithm [Kennedy *et al.* 2003], [Beides and Heydt 1991].

The HSE follows variations in the waveforms and harmonics by means of a KF approach using the criterion of minimizing the sum of the square errors between the measured and estimated values [Du *et al.* 1996]; these errors indicate the estimated values accuracy and dynamically reflect the changes with time in the state variables [Tan *et al.* 2005]. The system model is a set of ODE's in the time domain, which can be expressed in the state space [Watson & Arrillaga 2007].

The time domain HSE solution is based on the application of the Kalman filter (KF), Poincaré map and extrapolation to the limit cycle using a numerical differentiation (ND) procedure. The noisy state variables measurements to be used for HSE are taken from a simulation of the network harmonics propagation. The estimated harmonic magnitudes are obtained applying the Discrete Fourier Transform (DFT), [Brigham 1988].

The results obtained with the proposed Time Domain Harmonic State Estimation (TDHSE) formulation are compared and validated against the actual system response, which is the mathematical model solution, and against the solution obtained with the PSCAD/EMTDC simulator.

This investigation considers the linear time invariant case to mainly demonstrate the KF algorithm performance, in association with the ND method to solve the HSE. For the case of nonlinear time invariant or variant systems, it is necessary to adapt the methodology to use the adaptive or extended KF algorithms [Yu *et al.* 2005a]. Figure 4.1 shows the HSE flowchart.

4.2 Kalman Filter Formulation

The advantage of the time domain approach over the frequency domain is in cases where the system has non stationary voltage and current signals, time-varying harmonic sources or transient load conditions [Grewal and Andrews 2001].

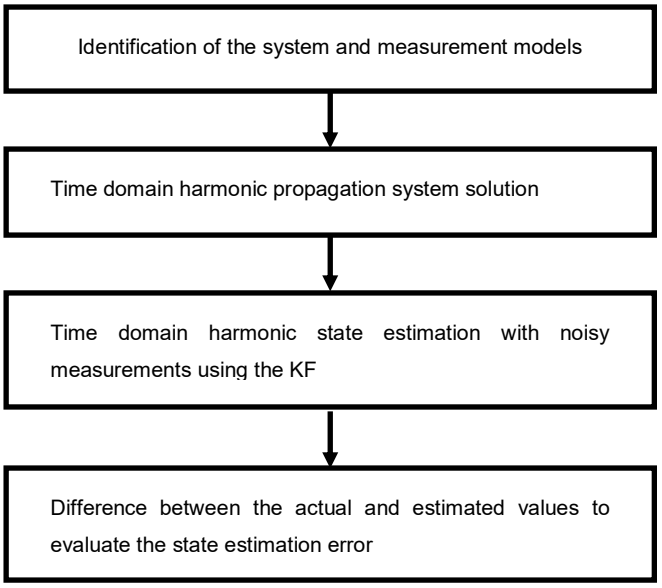

Figure 4.1 HSE flowchart

Initially a state space model and the output equation for the system are identified to represent system dynamics. The measurement equation (**z**=**Hx**) is related with the output equation, all or some output variables can be chosen as measurement variables to form the measurement equation [Grewal and Andrews 2001], i.e.,

$$\dot{\mathbf{x}} = \mathbf{A}\mathbf{x} + \mathbf{B}\mathbf{u} + \mathbf{v} \tag{4.1}$$

$$\mathbf{y} = \mathbf{C}\mathbf{x} + \mathbf{D}\mathbf{u} + \mathbf{w} \tag{4.2}$$

v and **w** are the process and measurement noises respectively. They are considered white, stationary, and Gaussian noises, with zero average and with no correlation among them.

The expressions (4.1) and (4.2) are related to the dynamics of the system. For the case of nonlinear system elements or loads, the state matrices may result to be time dependent and they have to be evaluated each time step. If they are nonlinear, it is convenient to apply the extended Kalman filter based on the Taylor series decomposition and the Kalman filter [Grewal and Andrews 2001], [Mahmoud *et al.* 2000].

The linear measurement equation is,

$$\mathbf{z} = \mathbf{H}\mathbf{x} + \mathbf{e} \tag{4.3}$$

z is the measurement vector, **H** the measurement matrix, **x** the state vector, and **e** the error vector.

4.2.1 Kalman Filter

The KF [Arrillaga *et al.* 2000], uses the state space matrices (4.1), (4.2) and the measurement Equation (4.3), to follow the dynamics of the system in the time domain and to evaluate the state and output variables in the time interval under study. Sources and harmonic levels in a power system vary with time and can be followed with this algorithm. Section 2.2.2 describes the KF algorithm; a detailed explanation of the KF algorithm is given in [Grewal and Andrews 2001].

The Kalman filter takes the discretized state equation of a system:

$$\mathbf{x}_{k+1} = \boldsymbol{\varphi}_k \mathbf{x}_k + \mathbf{v}_k \tag{4.4}$$

$\boldsymbol{\varphi}$ is the state transition matrix related with state matrix. The discrete measurement equation is:

$$\mathbf{z}_k = \mathbf{H}_k \mathbf{x}_k + \mathbf{w}_k \tag{4.5}$$

The measurements may be contaminated with noise represented by vector **w**.

The Kalman filter consists on time update and measurement update [Zhang J. *et al.* 2011]. Time update comprises the following steps:

Project the state vector:

$$\hat{\mathbf{x}}_k^- = \boldsymbol{\varphi}_k \hat{\mathbf{x}}_{k-1} \tag{4.6}$$

Project the error covariance matrix

$$\mathbf{P}_k^- = \boldsymbol{\varphi}_k \mathbf{P}_{k-1} \boldsymbol{\varphi}_k^T + \mathbf{Q}_k \tag{4.7}$$

Where $\hat{\mathbf{x}}_k^-$ is the project estimate of $\hat{\mathbf{x}}_k$ and $\mathbf{P}_k^-$ the project estimate of the error covariance matrix $\mathbf{P}_k$; $\mathbf{Q}_k$ is the covariance matrix of **v**.

The measurement update stage is:

Evaluate the Kalman gain:

$$\mathbf{G}_k = \mathbf{P}_k^- \mathbf{H}_k^T (\mathbf{H}_k \mathbf{P}_k^- \mathbf{H}_k^T + \mathbf{R}_k)^{-1} \tag{4.8}$$

Update state estimate:

$$\hat{\mathbf{x}}_k = \mathbf{x}_k^- + \mathbf{G}_k (\mathbf{z}_k - \mathbf{H}_k \hat{\mathbf{x}}_k^-) \tag{4.9}$$

Update the error covariance matrix

$$\mathbf{P}_k = (\mathbf{I} - \mathbf{G}_k \mathbf{H}_k) \mathbf{P}_k^- \tag{4.10}$$

$\hat{\mathbf{x}}$ vector represents the state estimate of the system.

The recursive KF formulation can be applied to follow the harmonic level variations in a power system [Kennedy *et al.* 2003]. The estimate $\hat{\mathbf{x}}$, the KF gain and the error covariance matrices are evaluated at each time step.

The discrete Fourier transform (DFT) is applied to process the measured and estimated waveforms to obtain their harmonic spectrum, i.e., to transform time-domain data into frequency-domain data [Arrillaga *et al.* 2000a], [Brigham 1988].

4.2.2 Numerical Differentiation Method

This numerical technique can be used to calculate the periodic steady state of nonlinear power networks and circuits in the presence of harmonics [Segundo and Medina 2008], [Segundo 2010]. This result can be used together with the KF algorithm to speed-up the HSE evaluation in a power network. The ND method quickly obtains a periodic steady state system condition after the initial transient, then the KF takes measurements added with noise and evaluates the HSE under slower state variable fluctuations, to obtain a more accurate state estimation and consequently with a smaller estimation error. The ND method reduces the execution time needed to obtain the HSE solution, due to the reduction of cycles to process, as can be observed from the case studies, mainly when the system is under damped.

4.3 Case Studies

The proposed algorithm is applied for the analysis of the test system shown in the Figure 4.2; power network data are reported in [Arrillaga *et al.* 2000], [Watson & Arrillaga 2007]. Generators are connected to M220 and R220 busbars. The generators are individually represented by a voltage source model behind a phase impedance. The power transformers are represented by a two-winding three-phase model and the power lines with a pi-model with length-dependent parameters, which in addition accounts for conductor and geometry configuration. The loads of 2.6, 0.75 and 0.5 MW are connected at T220, I220 and R220 buses, respectively, which is a part of the rated load. This light load condition is used to better appreciate the harmonic magnitudes. The case studies were implemented in Matlab script with an Intel Core Duo CPU T5870, 2 Ghz, 4 GB RAM system.

For a three-phase analysis, a 45 ODE set is to be solved; for the HSE solution, 27 state variables are taken as measurements and the rest, 18 state variables, are taken as estimated variables; for the measured state variables, 12 are the nodal voltages and 15 are line currents. This definition gives an over-determined measurement state estimation equation with an observable system condition, $\mathbf{z}=\mathbf{H}\mathbf{x}$, where $\mathbf{z}$ is a 27×1 vector, $\mathbf{H}$ is a 27×18 matrix and $\mathbf{x}$ is a 18×1 vector. This equation, related with expression (4.3), is solved for $\mathbf{x}$ to obtain the estimated state variables using the KF algorithm, Equations (4.6)-(4.10).

A three-phase harmonic current source is simulated as a current injection at the T220 busbar. The harmonic current components are given in Table 4.1; simulating the harmonic injection at the T220 busbar by a six pulse rectifier, which can be a part of a HVDC link. The resulting ODE set is efficiently solved with the ND method using the trapezoidal rule of integration, with a step size of 0.039 ms (512 points per period) to obtain the periodic steady state solution of the system. In all cases, the ND method is applied at 0.04 seconds of simulation. The initial conditions for the state variables are set to zero.

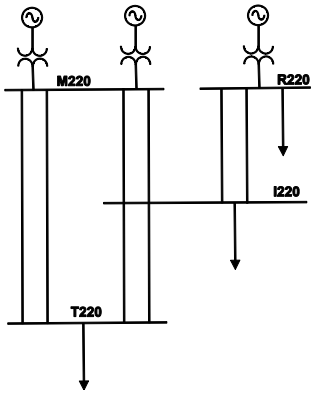

Figure 4.2 Test system

Table 4.1 Harmonic Injections

Harmonic	Peak Value (Amps)	Phase Sequence
5	4	-
7	2	+
11	1	-
13	0.5	+

The periodic steady state solution is given in terms of nodal voltage and line current waveforms. The ODE model was implemented in Matlab and was validated against the results obtained with the PSCAD/EMTDC simulator [Pscad 2005]. The selected measurement set is taken from this harmonic propagation simulation. Besides, the measurements are assumed to be without gross errors, but with the process noise **v** and the measurements noise **w**, added to **x** and **z**, respectively, as shown in (4.1) and (4.2). These noises can be generated during the simulation by means of stochastic numbers; **v** and **w** are Gaussian and uncorrelated. The **Q** and **R** noise covariance matrices are taken as 0.0001 and 0.1 diagonal matrices respectively, the standard deviations are the square root of variance, giving values of 0.01 and 0.3 for **v** and **w** noises; this shows the condition with a low process noise but noisy measurements. The KF algorithm takes the system model and the noisy measurements and evaluates the HSE according to Equations (4.6)-(4.10). Three case studies are presented: balanced harmonic source at the T220 busbar, balanced harmonic sources at the T220 and I220 busbars and an unbalanced harmonic source at the T220 busbar.

4.3.1 Balanced Harmonic Source connected at the T220 Busbar

Figure 4.3 shows the actual and estimated state variables and their differences for the estimated line currents. The actual values are taken from the propagated harmonic simulation. As mentioned before, the estimated values are calculated taking the selected measurement variables **z** and the **H** matrix into the KF algorithm, Equations (4.6)-(4.10). A close agreement is obtained between the actual/real and the proposed TDHSE method responses; the maximum difference is around 10 Amps or 4% for state variables 16-18; the difference is negligible for state variables 25-45. When the estimated state variables are known, other variables currents and voltages can be calculated to evaluate all the variables in the system.

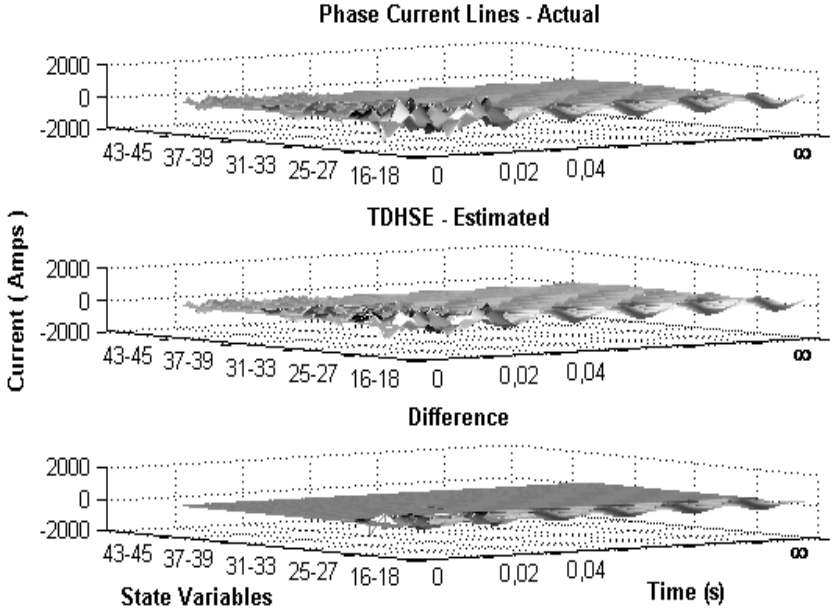

Figure 4.3 Actual, Time Domain Harmonic State Estimation with Kalman filter and difference between actual and estimated values, for line currents. The ND is applied at 0.04 s, ∞ represents the limit cycle with a tolerance of 10^{-6}.

Figure 4.4 shows the voltage waveforms at the T220 busbar (phases A, B and C) state variables 1-3. The voltage waveform presents a small distortion due to harmonic injection in this busbar, as indicated in Table 4.1. The fast periodic steady state solution obtained once the ND method is applied. These nodal voltages are part of the measurement set.

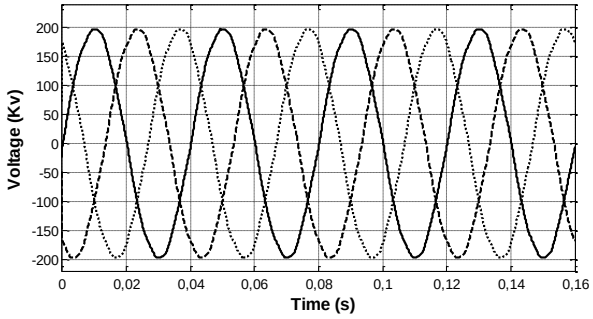

Figure 4.4 Actual voltage, T220 busbar, phases A, B and C, limit cycle tolerance of 10^{-6}.

Figure 4.5 describes the phase current waveform for the I220-T220 line, state variable 37, this is the most distorted line current in the system. Figure 4.5(a) shows the actual waveform for this current, the measurement and the added noise are illustrated. The noise is stationary, Gaussian and with a standard deviation of 0.3. The TDHSE algorithm takes as data the noisy measurements and evaluates the state estimation response. Figure 4.5(b) illustrates this response; a close agreement is obtained between the actual, the proposed TDHSE method based on the KF algorithm and the PSCAD/EMTDC responses.

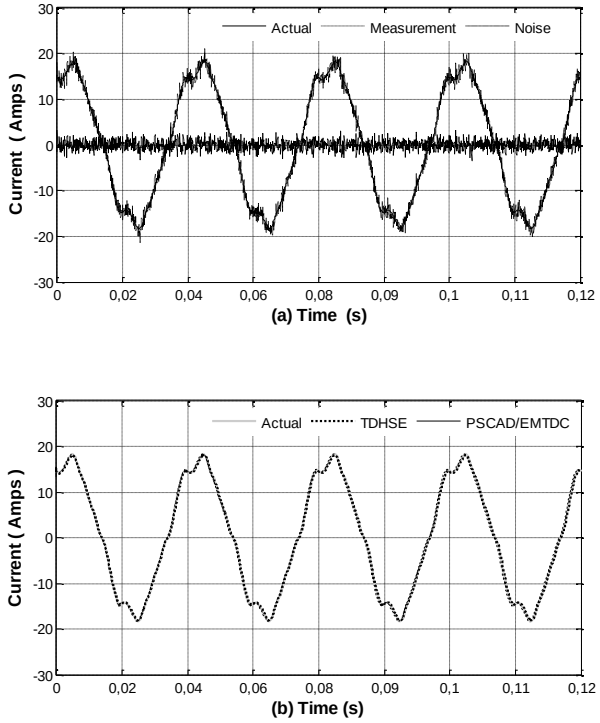

Figure 4.5 Phase current, I220-T220 line, state variable 37. (a) Noisy measurement and noise, (b) Actual, TDHSE with KF, PSCAD/EMTDC responses; limit cycle tolerance of 10^{-6}.

The periodic steady state is obtained after four applications of the ND method with a tolerance of 10^{-6}. Table 4.2 shows the numerical convergence process, $\mathbf{\Phi}$ was identified once and kept constant for subsequent ND method applications. For this case, 189 full cycles (NC) were required by the Brute Force (BF) method [Parker and Chua 1989], while 52 were needed by the ND method, or just 27.5% of NC calculated with the BF method; this percentage varies for each case and depends on the system damping. However, with the ND application the TDHSE is swiftly evaluated, and more accurately, due to the reduction in the processed cycles and with less state variables fluctuations during the simulation time.

Table 4.2 Convergence Process BF and ND Methods

NC	BF	ND
1	3.278430e+05	3.278430e+05
2	3.059034e+05	3.059034e+05
⋮	⋮	⋮
3	2.206703e+05	2.206703e+05
49	1.477264e+02	6.731162e+01
50	5.995236e+01	1.481480e-02
51	1.056377e+02	4.588714e-06
52	6.878134e+01	1.775334e-09
⋮	⋮	
189	9.309442e-07	

Figure 4.6 shows the harmonic content for the current I220-T220 line. The harmonics were obtained through a DFT application to the current waveform. A close agreement is observed between the actual, TDHSE method and PSCAD/EMTDC responses. The detected harmonics are of the same order as those injected at the T220 busbar. The maximum difference is of the order of 0.1% for the 7th harmonic. The slight difference observed with PSCAD/EMTDC response is due to the numerical difference between the applied numerical integration methods.

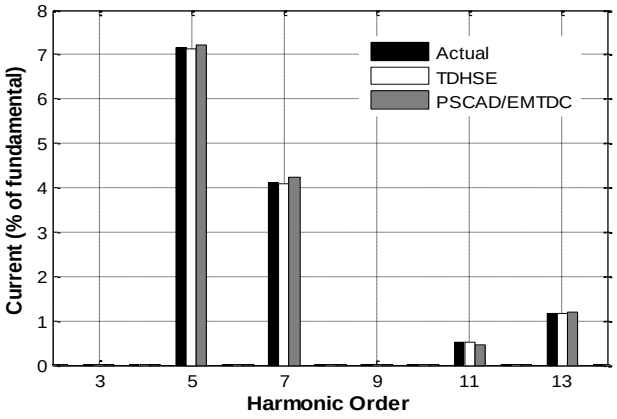

Figure 4.6 Phase current harmonic spectrum, I220-T220 line, state variable 37, harmonic source at T220 busbar.

4.3.2 Balanced Harmonic Sources connected at the T220 and I220 Busbars

Figures 4.7 and 4.8 show the results obtained with the connection of equal harmonic sources at the T220 and I220 busbars. The injected harmonic content is illustrated in Table 4.1. The harmonic spectrum shown in Figure 4.7 changes with respect to that shown in Figure 4.6, mainly due to the change in the voltage distortion at the I220 and T220 busbars, under the connection of harmonic sources to these busbars, and due to the I220-T220 line characteristic impedance.

The TDHSE can appropriately follow the harmonic variation. Figure 4.7(a) shows that the average difference between the actual and the estimated response is negligible. It shows again a close agreement between the actual, TDHSE method and PSCAD/EMTDC responses. Figure 4.7(b) shows the harmonic spectrum for the phase current I220-T220 line, state variable 37. For the case of phase current M220-T220 line, state variable 25 shown in Figure 4.8, the actual, estimated TDHSE method and PSCAD/EMTDC responses practically overlap.

Table 4.3 shows the detail of Brute Force (BF) and ND methods convergence, in terms of cycles and maximum convergence error. For this case of harmonic sources at the T220 and I220 busbars, the ND method requires 51 NC or 26.9% of the 189 NC required by the BF method, with a tolerance of 10^{-6}. Again, the ND reduced the number of cycles needed to evaluate the HSE.

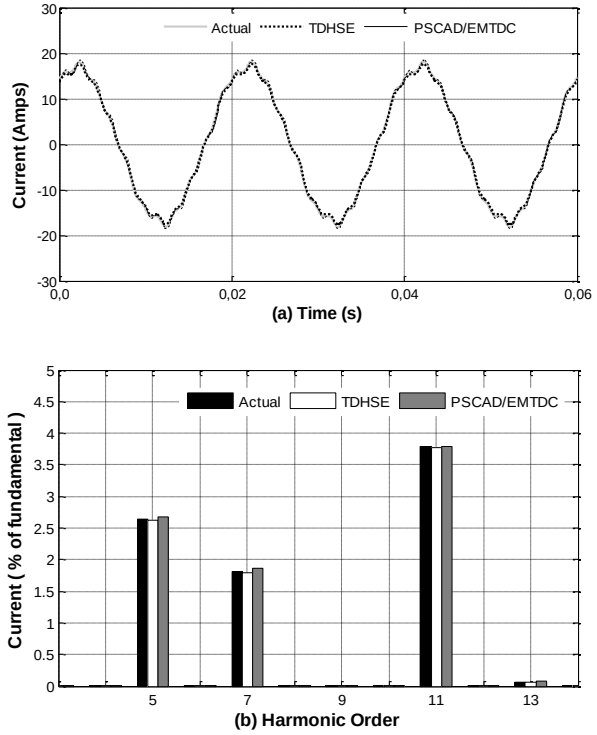

Figure 4.7 Phase current, I220-T220 line, (a) Harmonic sources at the T220 and I220 busbars, (b) Harmonic spectrum.

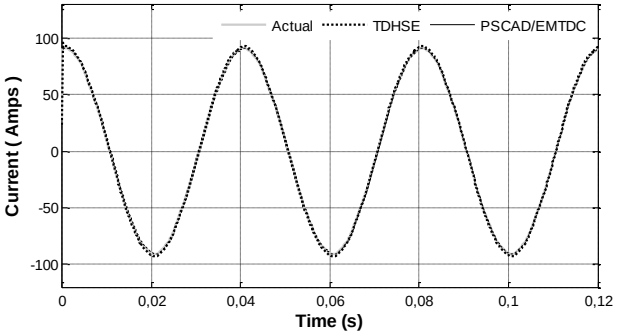

Figure 4.8 Phase current M220-T220 line, state variable 25, harmonic sources at the T220 and I220 busbars; limit cycle tolerance of 10^{-6}.

Table 4.3 Convergence Process BF and ND methods with two harmonic sources

NC	BF	ND
1	3.276234e+05	3.276234e+05
2	3.057082e+05	3.057082e+05
⋮	⋮	⋮
3	2.205417e+05	2.205417e+05
49	1.476383e+02	5.870963e+01
50	5.995984e+01	4.985083e-03
51	1.055846e+02	7.047202e-07
⋮	⋮	
189	9.323121e-07	

4.3.3 Unbalanced Harmonic Source connected at the T220 Busbar

An unbalanced harmonic condition can be present when a 3-phase nonlinear load demands an unbalanced current; this type of loads can be arc furnaces, smelters or electric welders among others. The unbalanced load condition can be due to a transient load, a loss of phase connection, a temporary 3-phase unbalanced converters or 1-phase converters operation [Heydt 1991]. Figure 4.9(a) illustrates the response for phase current I220-T220 line, state variables 37-39, with an unbalanced harmonic source connected at the T220 busbar. Phases A, B and C have a harmonic injection equal to 100%, 50% and 25%, respectively, of that shown in Table 4.1. The actual and estimated TDHSE responses are again validated against the PSCAD/EMTDC simulation. A close agreement is achieved. Figure 4.9(b) shows the unbalanced phase current harmonic spectrum. For this particular case, the 5th, 7th, 11th and 13th harmonics are present, according to the injected harmonic content at the T220 busbar, being the 5th harmonic in phase A the largest in magnitude, i.e., around 7%.

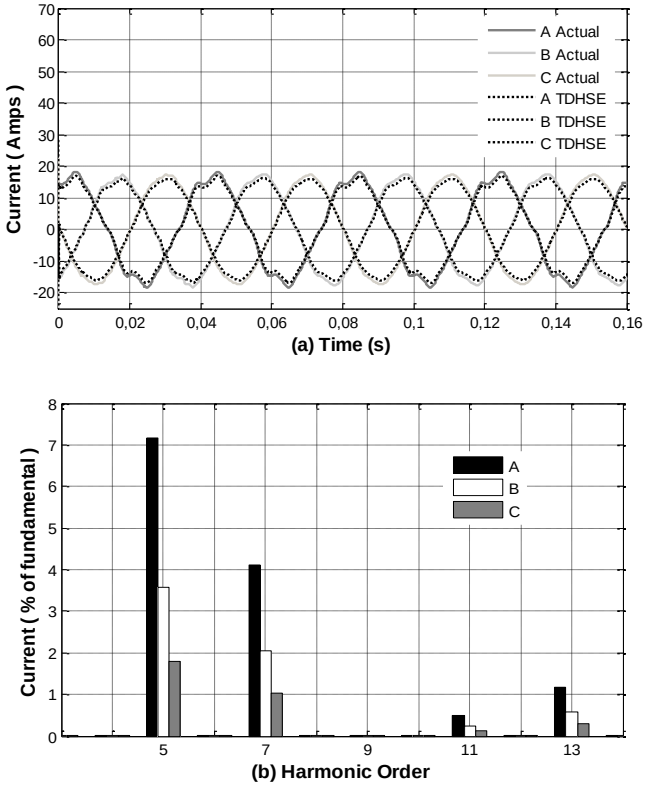

Figure 4.9 Phase current, I220-T220 line, state variables 37-39. (a) Unbalanced harmonic source at the T220 busbar, (b) harmonic spectrum.

4.4 Harmonic State Estimation using the Extended Kalman Filter

The extended Kalman filter (EKF) can be applied to assess the HSE in case of nonlinear systems. Section 2.2.5 presents an introduction to EKF algorithm, considering discrete models and the covariance matrices. Let us assume a nonlinear model and the corresponding measurement equation,

$$\dot{\mathbf{x}} = \mathbf{f}(\mathbf{x}, \mathbf{u}, \mathbf{v}) \tag{4.11}$$

$$\mathbf{y} = \mathbf{h}(\mathbf{x}, \mathbf{u}, \mathbf{w}) \tag{4.12}$$

v is the process noise, **w** is the measurement noise, **f** is the nonlinear function modeling the system, **h** is the nonlinear output function, **y** is the output vector. The EKF has two stages [Ghahremani and Kamwa 2011]:

1) Initialization defines the state vector and the error covariance matrix,

$$\hat{\mathbf{x}}_0^+ = \mathbf{E}(\mathbf{x}_0) \tag{4.13}$$

$$\mathbf{P}_0^+ = \mathbf{E}[(\mathbf{x}_0 - \hat{\mathbf{x}}_0^+)(\mathbf{x}_0 - \hat{\mathbf{x}}_0^+)^T] \tag{4.14}$$

E is the expected value, + indicates update estimate and – project estimate. The subscripts k and k-1 denote time instants $t=k\Delta t$ and $t=(k\text{-}1)\Delta t$, respectively.

2) Update time and measurement has four steps:

2.1). Evaluate the partial derivative matrices **F** and **L** of $n\times n$ order:

$$\mathbf{F}_{k\text{-}1} = \partial \mathbf{f}_{k-1} / \partial \mathbf{x}\big|_{\hat{\mathbf{x}}_{k\text{-}1}^+} \tag{4.15}$$

$$\mathbf{L}_{k\text{-}1} = \partial \mathbf{f}_{k-1} / \partial \mathbf{v}\big|_{\hat{\mathbf{x}}_{k\text{-}1}^+} \tag{4.16}$$

2.2). Project the error covariance matrix and state estimate:

$$\mathbf{P}_k^- = \mathbf{F}_{k\text{-}1}\mathbf{P}_{k\text{-}1}^+\mathbf{F}_{k\text{-}1}^T + \mathbf{L}_{k\text{-}1}\mathbf{Q}_{k\text{-}1}\mathbf{L}_{k\text{-}1}^T \tag{4.17}$$

$$\hat{\mathbf{x}}_k^- = \mathbf{f}_{k\text{-}1}(\hat{\mathbf{x}}_{k\text{-}1}^+, \mathbf{u}_{k\text{-}1}, \mathbf{v}_{k\text{-}1}) \tag{4.18}$$

2.3). Evaluate the partial derivative matrices **H** ($m\times n$ order) and **M** ($m\times m$ order):

$$\mathbf{H}_k = \partial \mathbf{h}_k / \partial \mathbf{x}\big|_{\hat{\mathbf{x}}_k^-} \tag{4.19}$$

$$\mathbf{M}_k = \partial \mathbf{h}_k / \partial \mathbf{w}\big|_{\hat{\mathbf{x}}_{k\text{-}1}^+} \tag{4.20}$$

2.4). Evaluate the EKF gain, update the state estimate and the error covariance matrix:

$$\mathbf{K}_k = \mathbf{P}_k^-\mathbf{H}_k^T(\mathbf{H}_k\mathbf{P}_k^-\mathbf{H}_k^T + \mathbf{M}_k\mathbf{R}_k\mathbf{M}_k^T)^{-1} \tag{4.21}$$

$$\hat{\mathbf{x}}_k^+ = \hat{\mathbf{x}}_k^- + \mathbf{K}_k[\mathbf{y}_k - \mathbf{h}_k(\hat{\mathbf{x}}_k^-, \mathbf{u}_k, \mathbf{w}_k)] \tag{4.22}$$

$$\mathbf{P}_k^+ = (\mathbf{I} - \mathbf{K}_k\mathbf{H}_k)\mathbf{P}_k^- \tag{4.23}$$

The EKF is a prediction-correction process, the prediction step is a time update using (4.18), w hich predicts the state variables based on the prior estimated state variables obtained in the previous step, error covariance matrix is also predicted. The correction step evaluates the filter gain to obtain the corrected state variables (4.22) The filter gain, the state estimate vector $\hat{\mathbf{x}}$, and the error covariance matrices (**P**) are evaluated each time step. The jacobians are evaluated with current predicted states, the EKF uses these jacobians instead of the linear system matrices in the case of KF; the inverse matrix in (4.21) takes most of the execution time. The prior formulation is applied to case studies in the next Section.

4.4.1 Case Studies

Figure 4.10 shows the modified IEEE 14 bus test system, used in the next case studies, considering a base power of 100 MVA and a base voltage of 132 kV. Lines 1-2, 1-5, 2-3, 2-4, 2-5, 3-4 and 4-5 are represented by a *pi* model and by a series impedance the rest of lines; the transformers 4-9, 5-6, 4-8-9, are represented by a leakage reactance, according to the IEEE 14 bus test system [IEEE 2013]. The generators are individually represented by a sinusoidal voltage source model behind a phase impedance.

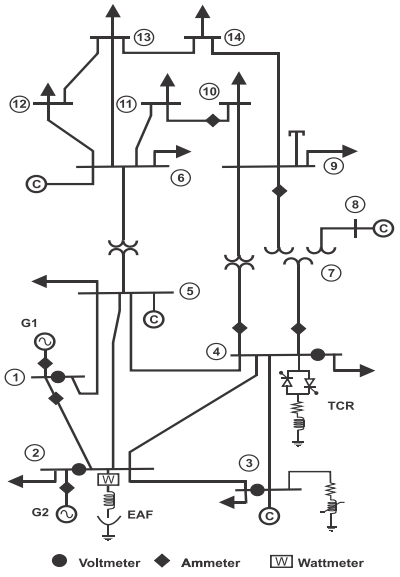

Figure 4.10 Modified IEEE 14 bus test system with nonlinear loads

Nonlinear loads are connected to nodes 2 (electric arc furnace EAF), 3 (nonlinear inductance) and 4 (thyristor controlled reactor TCR). These loads inject harmonic currents; under this load condition the HSE can be evaluated using the EKF algorithm. Appendix E presents a measurement system configuration.

For single-phase analysis, a set of 51 differential equations is to be solved representing (4.11). To obtain the HSE, 12 measurements are taken from the system to form the output state estimation Equation (4.12). As indicated in Figure 4.10; these are 7 line currents, 4 nodal voltages and the EAF real power. Table 4.4 shows the state variables and Table 4.5 shows the output variables to be measured.

Table 4.4 State variables

Description	State Variable
Line current	1-20
Nodal voltage	21-34
Generator current	35-36
Nodal load current	37-47
Nonlinear inductance flux	48
EAF current and radius	49-50
TCR current	51

Table 4.5 Output measurement variables

Description	Variable
Line current	1, 8, 9, 15, 18
Nodal voltage	21, 22, 23, 24
Generator current	35, 36
EAF real power	49, 50

The HSE is evaluated with 512 points per cycle, the system fundamental frequency is 60 Hz, the initial condition is set to zero, except for the electric arc furnace radius that is set to 0.1 pu; the initial state covariance matrix $\mathbf{P}_0$ is a diagonal matrix with elements equal to 10^2; the process and measurement noise are defined with normal distribution, zero mean and a standard deviation of 0.01. The process and measurement covariance **Q** and **R** matrices are diagonal with 0.01^2 elements; **L** and **M** are assumed to be identity matrices, being n=51 the number of state variables and m=12 the number of measurements.

Figure 4.11 shows the actual and estimate state variables and their differences for the line currents. A close agreement is obtained between the actual and EKF method responses; the maximum difference is of 7% at the initial transient, after this, the difference is less than 1%. When the estimate state variables are known, other variables can be calculated to know the system state. The actual values are obtained from the harmonic propagation solution using the set of differential equations modeling the system and the fourth order Runge-Kutta method to compare the EKF estimation. A small-scale test system has been used to illustrate the application of the proposed dynamic state estimation methodology. However, it can be applied to the practical dynamic state estimation assessment of larger scale power networks. The extended Kalman filter method can appropriately account for the presence of high frequency effects by using the adequate step size during the time domain solution, which can have an implicit harmonic content of low and high order.

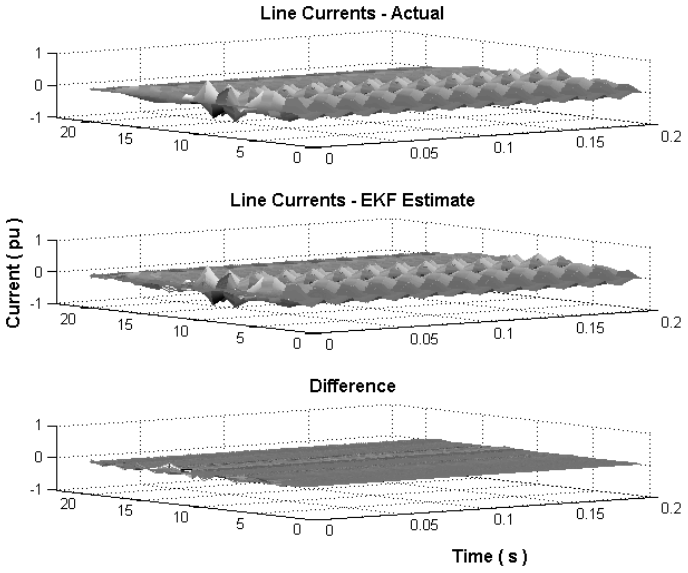

Figure 4.11 Actual, EKF estimate and difference for line currents

Figure 4.12 shows the line 3-4 current waveform. This is one of the most distorted currents, a close agreement is observed between the actual and the EKF method which present a total harmonic distortion (THD) of 56%; the small differences observed are mainly due to the noisy condition in the measurements. The harmonic distortion is due to harmonic injection originated by the nonlinear loads connected at nodes 3 and 4, the nonlinear inductance at node 3 and the TCR at node 4, as illustrated in Figure 4.10.

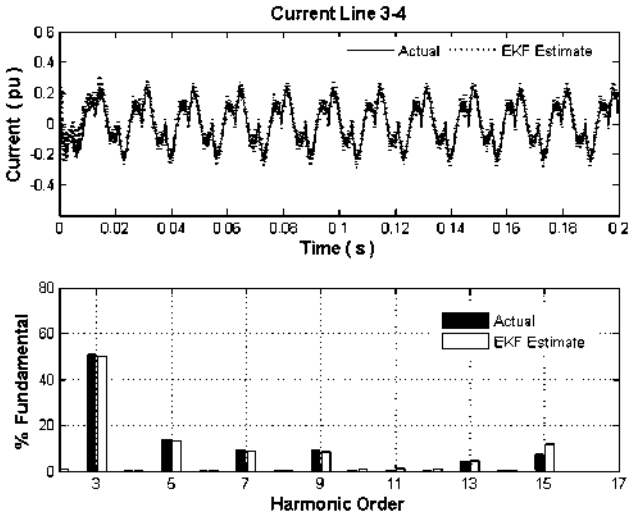

Figure 4.12 Actual and estimate current line 3-4, harmonic spectrum

The nonlinear inductance current is shown in Figure 4.13; the response obtained with the EKF method closely follows the actual current waveform; they only differ during the initial transient in the first cycle. The total harmonic distortion THD is 7.2%.

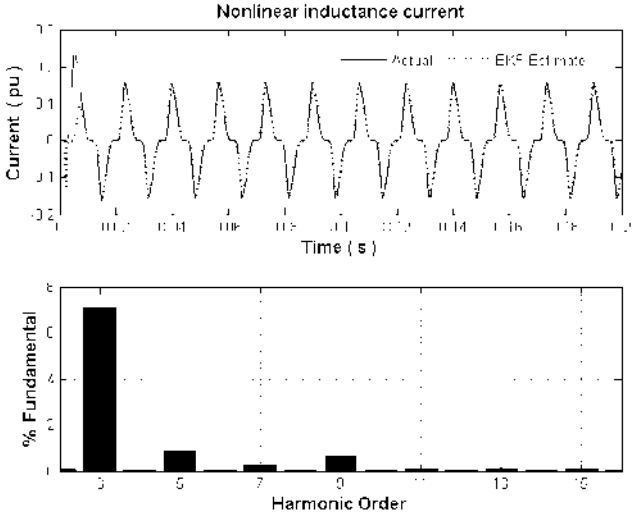

Figure 4.13 Actual and estimate nonlinear inductance current, harmonic spectrum

The TCR current is shown in Figure 4.14, the harmonic content illustrates the harmonics injected by the TCR; the THD is 45.1% for both waveforms. The TCR firing angle is 100 degrees.

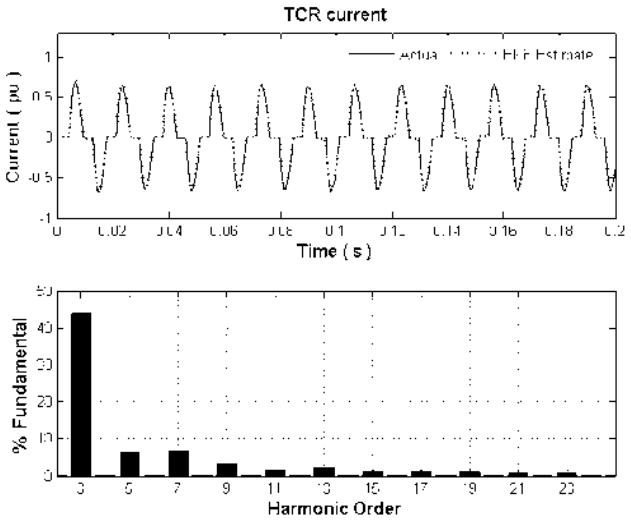

Figure 4.14 Actual and estimate TCR current, harmonic spectrum

Figure 4.15 shows the EAF current, radius and real power; actual and EKF estimate for the initial transient of 12 cycles; the EAF current has a dc component due to the EAF initial period. The radius and real power have high frequency components, which eventually disappear in steady state, but can be present according to the EAF operation, originating harmonic currents. By definition, the real power is an output measured variable but it is not a state variable.

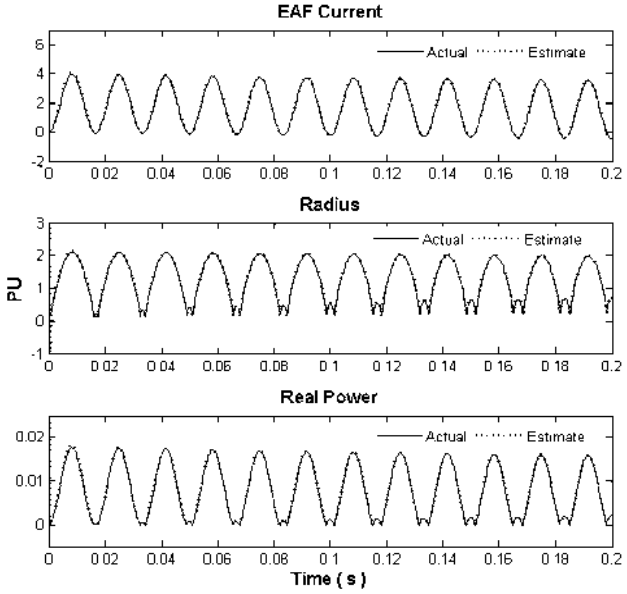

Figure 4.15 EAF current, radius and real power, actual and estimate

The EKF gain during the study interval is shown in Figure 4.16. This gain shows a quick convergence to a stable value with fluctuations during the TCR thyristor switching, which originates numerical oscillations in the EKF algorithm. These oscillations are damped in the next time steps of the

numerical solution process. The EKF gain corresponds to the state variable 36, being the current generator at node 2.

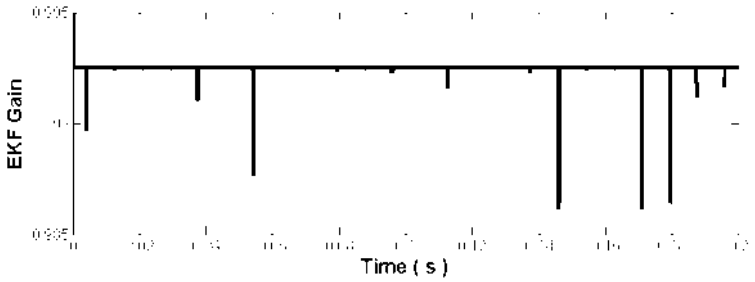

Figure 4.16 EKF gain for the state variable 36 current generator node 2

4.5 Harmonic State Estimation using the Parallel Kalman Filter

HSE can be evaluated using parallel processing techniques by adapting the Kalman filter algorithm to be parallel processed. A parallel Kalman filter (PKF) is implemented using the CUDA platform and CUBLAS library on a GPU to estimate varying harmonics and inter-harmonics. Figure 4.17 shows the HSE-PKF flowchart.

An important fact in parallel programming using a GPU is the necessary exchange of data between the CPU and the GPU. To decrease the execution time, the flow of data between the CPU and the GPU is minimized allocating first the necessary data to execute the KF algorithm, then these data are numerically processed and the results are saved back to the CPU, when the estimation is completed, the GPU memory is cleared [Nvidia Cublas 2012].

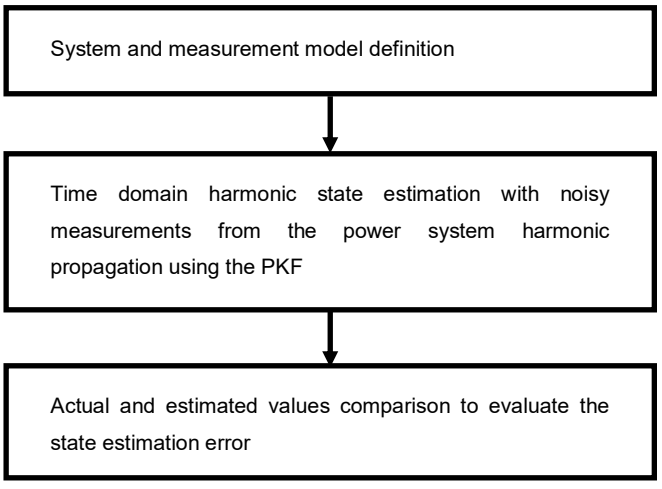

Figure 4.17 HSE using the PKF flowchart

The PKF method to evaluate the HSE is,

1) Data allocation in GPU memory.

2) PKF execution on GPU.
3) The HSE result is saved in CPU memory.
4) The GPU memory is free when the study interval ends.

The PKF computes the matrix operations as inverse, multiplication, addition and subtraction in the algorithm each time step in parallel form. The necessary matrices and vectors are allocated and set with initial values, then the recursive KF algorithm is executed on the GPU using the CUBLAS library, the result of the state estimation is sent from the GPU to CPU.

The CUBLAS functions evaluate the KF steps, these are indicated in Table 4.6. They assess vector-vector sum (Daxpy), matrix-vector multiplication (Dgemv), matrix-matrix sum (Dgeam), matrix-matrix multiplication (Dgemm), among others; these functions are implemented in the CUBLAS library to be executed in parallel form on the GPU [Nvidia Cublas 2012].

The inverse matrix in the KF algorithm is computed with the LU decomposition and backwards-forwards substitutions, the CUBLAS functions used to implement this decomposition are Dscal and Dger. These functions evaluate the Crout's reduction algorithm and the Dtrsm function implements the backwards and forwards substitutions. This step consumes most of the time execution of the KF algorithm and is calculated each time-step of the state estimation [Volkov and Demmel 2008].

Table 4.6 Matrix Operations and CUBLAS functions for the parallel Kalman filter

STEP	Cublas Fun.	ORDER	OPERATION	
1).- Project state				
1.1).- Project state	Dgemv	*n*x1	multiply matrix-vector	$\hat{\mathbf{x}}_k = \mathbf{F}\mathbf{x}_{k-1}$
1.2).- Add	Daxpy	*n*x1	add vectors	$\hat{\mathbf{x}}_k = \mathbf{F}\mathbf{x}_{k-1} + \mathbf{B}\mathbf{u}_k$
1.3).- Transpose		*n*x*n*	transpose	$\mathbf{F}^T$
1.4).- Multiply	Dgemm	*n*x*n*	multiply matrices	$\mathbf{F}\mathbf{P}_{k-1}$
1.5).- Multiply	Dgemm	*n*x*n*	multiply matrices	$\mathbf{F}\mathbf{P}_{k-1}\mathbf{F}^T$
1.6).- Add	Dgeam	*n*x*n*	add matrices	$\mathbf{P}_k^- = \mathbf{F}\mathbf{P}_{k-1}\mathbf{F}^T + \mathbf{Q}$
2).- Update state				
2.1).- Transpose		*m*x*n*	transpose	$\mathbf{H}^T$
2.2).- Multiply	Dgemm	*n*x*n*	multiply matrices	$\mathbf{P}_k^-\mathbf{H}^T$
2.3).- Multiply	Dgemm	*m*x*m*	multiply matrices	$\mathbf{H}\mathbf{P}_k^-\mathbf{H}^T$
2.4).- Add	Dgeam	*m*x*m*	add matrices	$\mathbf{H}\mathbf{P}_k^-\mathbf{H}^T + \mathbf{R}$
2.4).- Inverse				
2.4.1).- LU Decomp.				
2.4.1.1).- LU	Dscal	*m*x*m*	multiply vector by scalar	

2.4.1.2).- LU	Dger	*m*x*m*	add matrix with product of vectors	
2.4.2).- Substitutions				
2.4.2.1).- Backwards	Dtrsm	*m*x*m*	backwards substitution	
2.4.2.1).- Forwards	Dtrsm	*m*x*m*	forwards substitution	$[\mathbf{H}\mathbf{P}_k^{-}\mathbf{H}^T + \mathbf{R}]^{-1}$
2.5).- KF gain	Dgemm	*n*x*m*	multiply matrices	$\mathbf{K} = \mathbf{P}_k^{-}\mathbf{H}^T[\mathbf{H}\mathbf{P}_k^{-}\mathbf{H}^T + \mathbf{R}]^{-1}$
2.6).- Multiply	Dgemv	*m*x1	multiply matrix-vector	$\mathbf{H}\hat{\mathbf{x}}_k$
2.7).- Subtract	Daxpy	*m*x1	subtract vectors	$\mathbf{z} - \mathbf{H}\hat{\mathbf{x}}_k$
2.8).- Multiply	Dgemv	*n*x1	multiply matrix-vector	$\mathbf{K}[\mathbf{z} - \mathbf{H}\hat{\mathbf{x}}_k]$
2.9).- Add	Daxpy	*n*x1	add vectors	$\mathbf{x}_k = \hat{\mathbf{x}}_k + \mathbf{K}[\mathbf{z} - \mathbf{H}\hat{\mathbf{x}}_k]$
2.10).- Multiply	Dgemm	*n*x*n*	multiply matrices	$\mathbf{KH}$
2.11).- Subtract	Daxpy	*n*x*n*	subtract matrices	$\mathbf{I} - \mathbf{KH}$
2.12).- Multiply	Dgemm	*n*x*n*	multiply matrices	$\mathbf{P}_k = [\mathbf{I} - \mathbf{KH}]\mathbf{P}_k^{-}$
				n states, *m* measurements

4.5.1 HSE using PKF case studies

The IEEE 14 bus test system is used in the following case studies. The test system is modified including harmonic sources connected to nodes 5 and 13 to represent nonlinear loads that inject harmonic currents; under this condition the HSE can be evaluated using the PKF algorithm [Chang *et al.* 2004].

A set of 43 first-order differential equations representing the system is solved to obtain the time-domain harmonic propagation using the RK4 method with a time-step of 512 points per cyle or 32.55 μs. Table 4.7 shows the state variables and the output variables to be measured.

The HSE is evaluated taking the observation or measurement equation **z**=**Hx** into the PKF algorithm. The measurement vector **z** takes 38 measurements shown in Table 4.7, 15 line currents, 11 load currents and 12 nodal voltages. With this set of measurements the observation equation is under-determined, 38 states are observable while 5 are partially observable. The PKF estimates the state variables in a minimum mean squared error sense between the actual and estimated values.

Table 4.7 State and measured variables

Description	**State Variables**	**Measured Variables**
Line current	1-20	1-15
Nodal voltage	21-32	21-32
Load current	33-43	33-43

4.5.1.1 HSE with harmonic sources at nodes 5 and 13

Table 4.8 shows the harmonic injections, which can be present during the normal operation of the power system when nonlinear loads are connected, e.g., an AC/DC converter, a HVDC link or an uninterruptible power supply [Dugan *et al.* 2002].

Table 4.8 Harmonic injections nodes 5 and 13

Node	**5**				**13**			
Harmonic	5	7	11	13	5	7	11	13
Peak Value A	6	3	1.5	0.75	3	1.5	0.75	0.37

The PKF is able to estimate the state variables using the first-order ODE model of the system and the available measurements, which are added with a stationary and Gaussian noise having a 2% signal-to-noise ratio (SNR).

The actual and proposed PKF responses are compared; the maximum difference is approximately of 2% due to the noisy measurements used in the PKF algorithm. Figure 4.18 shows the actual and estimated state variables and their difference for the line currents. The actual values were obtained from the harmonic propagation simulation.

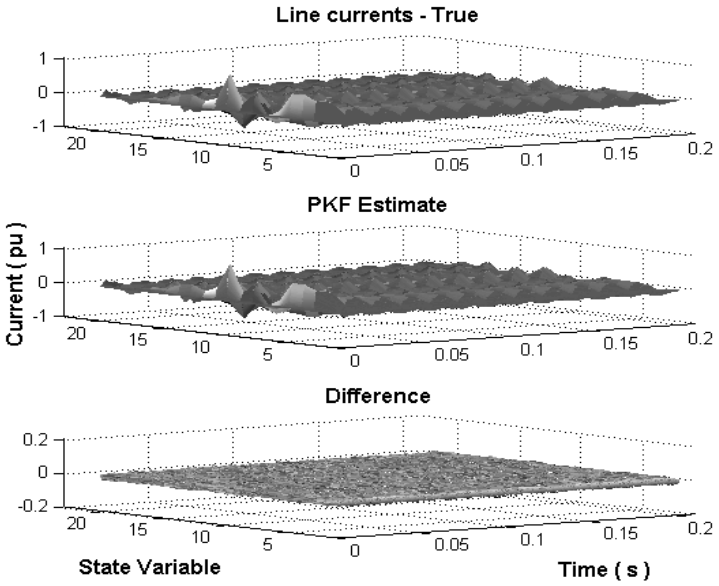

Figure 4.18 Actual, PKF estimate, and difference for line currents

The generator currents at nodes 1 and 2 are calculated using the estimates for the line currents and applying the KCL to evaluate the total harmonic distortion (THD). Figure 4.19 shows these currents; actual and estimate waveforms are represented and validated by direct comparison against the PSCAD/EMTDC response, a window size of 12 cycles is used. Figure 4.20 illustrates the harmonic content for the generator

currents obtained by applying the discrete Fourier transform (DFT). The THD is of 7.33% and 3.57% for generators nodes 1 and 2 respectively. This harmonic distortion is originated due to the harmonic currents injected in nodes 5 and 13; they flow through the lines and reach the generators and loads, affecting adversely their operation.

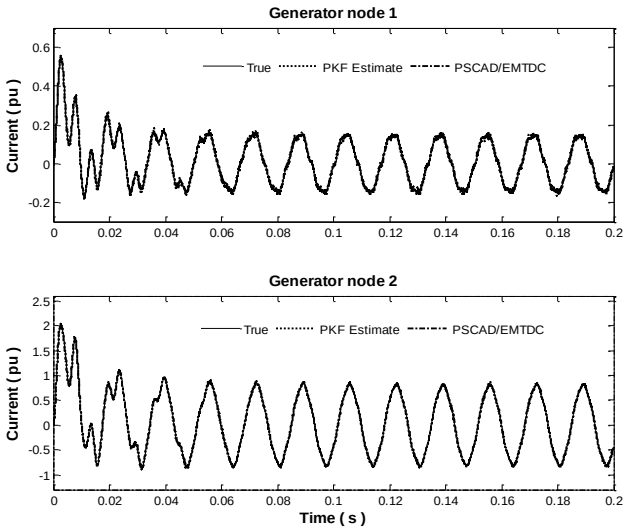

Figure 4.19 Actual, PKF estimate, and PSCAD/EMTDC response generator currents nodes 1-2

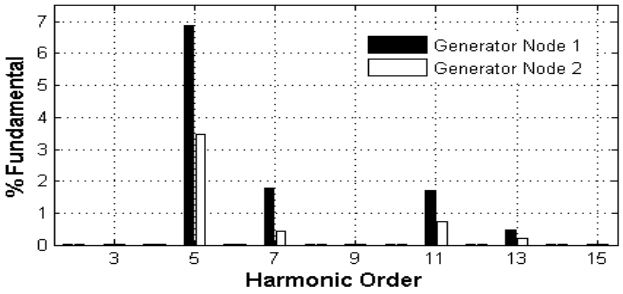

Figure 4.20 Harmonic spectrum, generator currents nodes 1-2

4.5.1.2 HSE with time varying harmonics

Time varying harmonic currents are present during the operation of an electrical system, e.g., a transient condition of a nonlinear component [Watson & Arrillaga 2007]. The injected harmonics of the previous case are increased during the last six cycles, to simulate and estimate this time varying harmonic condition.

The harmonic magnitude is increased two times of their initial values in nodes 5 and 13. This condition verifies the use of the PKF to estimate the variant harmonics.

Figure 4.21 presents the waveforms for currents in lines 2-5 and 5-6; these lines are connected to node 5 where the variant harmonic current is present. The harmonic distortion changes according to the new

injection of harmonics. The fluctuation starts at cycle 6 or 0.1 s, and the PKF estimates the harmonic variable condition; the estimated currents agree with the actual values.

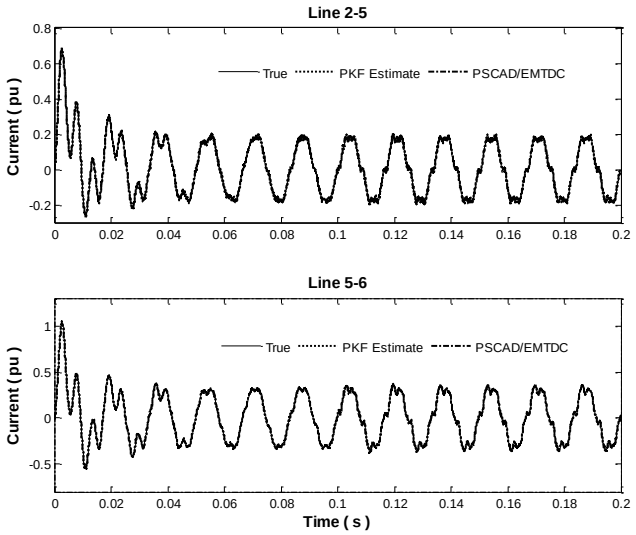

Figure 4.21 Actual, PKF estimate, and PSCAD/EMTDC response for time varying harmonics in line currents 2-5 and 5-6

Figure 4.22 shows the waveforms for the generator currents under the time-varying harmonic condition; the actual and estimate values closely agree. The harmonic content is obtained by applying the DFT as shown in Figure 4.23; the generator node 1 THD changes from 7.95% to 14.73% and for generator node 2 the THD changes from 4.26% to 7.22%.

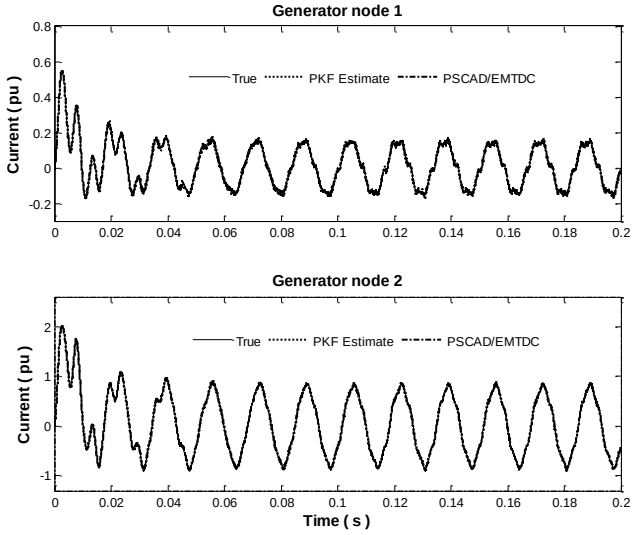

Figure 4.22 Actual, PKF estimate, and PSCAD/EMTDC response for time varying harmonics in generator currents nodes 1-2

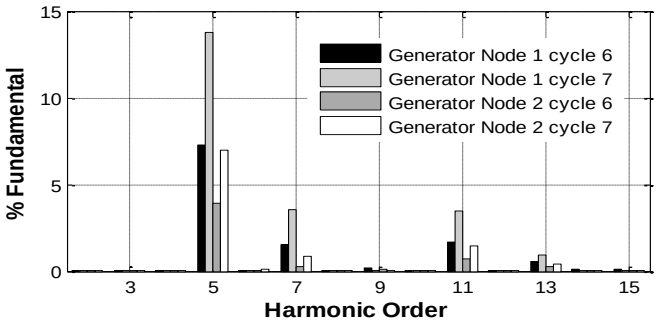

Figure 4.23 Harmonic spectrum for time varying harmonics in generator currents nodes 1-2

4.5.1.3 HSE including inter-harmonics

The inter-harmonics are components of a waveform between the harmonics of the fundamental frequency, which can be discrete frequencies or have a wide spectrum. They have an adverse effect on the power quality originating heating, flicker, interference and saturation [Testa *et al.* 2007]. The inter-harmonics are generated by nonlinear loads such as frequency converters, cyclo-converters, speed drives and arc furnaces [Gunther 2001].

The injected harmonics in nodes 5 and 13 are modified to include a sub-harmonic of 30 Hz with a magnitude of 50 A. Also an inter-harmonic of 90 Hz and 25 A of magnitude is injected to analyze the effect on the line currents using the PKF-HSE methodology. Figure 4.24 shows the actual, PKF estimate and PSCAD/EMTDC waveforms for generator current in nodes 1-2.

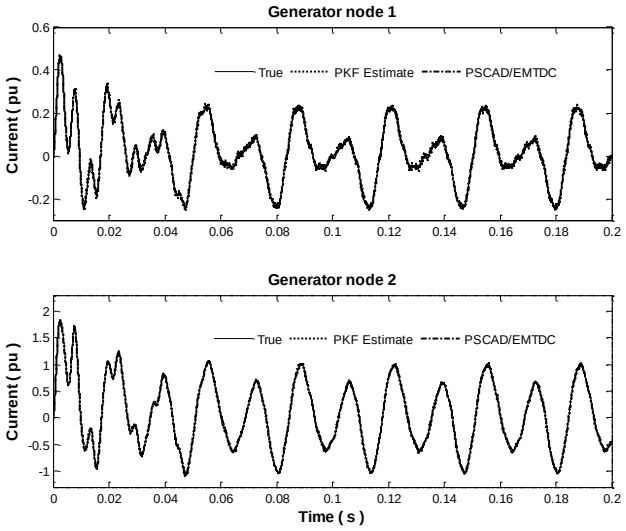

Figure 4.24 Actual, PKF estimate, PSCAD/EMTDC response during subharmonics and inter-harmonics generator currents nodes 1-2

The harmonic distortion is high due to the inter-harmonics injection. Actual and estimated waveforms agree. The DFT is applied again to obtain the harmonic content. Generator node 1 presents a THD

of 24.98%, and the generator node 2 of 11.47%. In Figure 4.25 the magnitude of the fundamental harmonic is 1.0 pu, and the waveforms have a dc component with even harmonics present, which is due to the inter-harmonic condition.

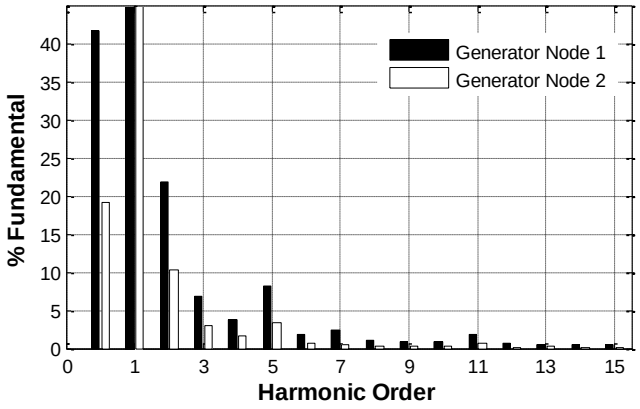

Figure 4.25 Harmonic spectrum, sub-harmonics and inter-harmonics, generator currents nodes 1-2

4.5.2 CPU-GPU Specification and execution time

The HSE case studies were implemented on an Intel Core TM i7-3770 CPU, 3.4 GHz, 16.0 GB RAM with a NVIDIA GeForce GTX 680 GPU. The GPU characteristics are given in Table 4.9.

Table 4.9 Nvidia GeForce GTX 680 GPU card data

Processor Cores	1536
GPU Clock rate	1.08 GHz
Memory	2.0 GB
Memory Clock rate	3.0 GHz
Memory Bus Width	256-bit

The power system model was replicated three times to create larger systems, and the execution time was measured, Table 4.10 presents the results on the execution time. The speed-up increases with the size of model as is expected using the parallel processing CPU-GPU and CUBLAS, compared against the sequential CPU C++ code.

Table 4.10 Execution time (s)

Models	CPU C++ code	CPU-GPU CUBLAS	Speed-up
1	36.29	22.5	1.61
2	434.72	52.24	8.32
3	1965.01	79.13	24.83

4.6 Harmonic State Estimation using the Enhanced Numerical Differentiation

The enhanced numerical differentiation (END) Section 3.4.4 can be applied to assess the HSE together with the KF based on the next steps:

1) State variable waveform test of half wave symmetry.

2) END obtains the periodic steady state for the power system providing an adequate initial condition to the KF.

3) The KF solves the state estimation with a smaller error using a network model and a partial set of measurements from the power system.

4) The state estimation result is used to evaluate all the variables in the power system, e.g., nodal voltages, the line, generator and load currents. Figure 4.26 shows END-KF method.

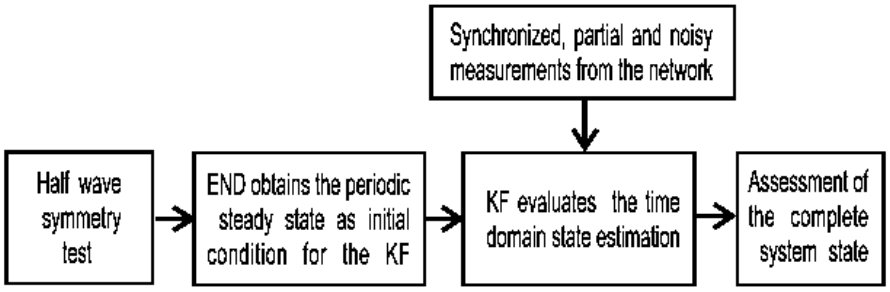

Figure 4.26 END-KF method

The IEEE 14 bus test system is modified with harmonic current injections at nodes 5 and 14 to simulate nonlinear loads and evaluate the HSE by the END-KF method. These harmonics current sources are variable inputs and can be used to represent nonlinear electrical loads, e.g. converters or rectifiers; they are part of $\boldsymbol{u}$ input vector, and excite the test system generating harmonic distortion in the line currents and nodal voltages [Dugan *et al.* 2002]. Table 4.11 presents the harmonic content of these harmonics sources, the base current is 355 amps; and the state space model of the system is solved numerically using the fourth order Runge-Kutta method (RK4) to obtain the harmonic propagation.

Table 4.11 Harmonic Injections

Harmonic	Peak value (pu) Node 5	Peak value (pu) Node 14
5	0.0159	0.008
7	0.008	0.004
11	0.004	0.002
13	0.002	0.001

The KF is used to estimate the harmonic flows in the lines and the distortion in nodal voltages. The END method abbreviates the initial transient, first two cycles, and quickly obtains the periodic steady state under an established tolerance. After this, the KF is applied to estimate the state under the load and the

injected harmonics condition, cycles 3 to 6 of simulation, making possible to obtain the harmonics propagation in the system considering its model and noisy and partial measurements. The measurements are taken from the harmonic propagation and are added with randomly generated noise.

Table 4.12 shows the convergence process to the limit cycle for the brute force (BF), the ND and the END methods. It is shown in terms of the number of cycles (NC) required to obtain the periodic steady state and the involved absolute error during the numerical solution with a time step of 32.55 μs, two base cycles are evaluated to apply the ND and END methods.

Table 4.12 Convergence Process BF, ND and END Methods

NC	BF	ND	END
1	0.3901535	0.3901535	0.3901535
2	0.1610222	0.1610222	0.1610222
⋮	⋮	⋮	⋮
24	6.665175-06	⋮	2.4831e-09
47	5.335378e-06	2.472597e-09	1.6306e-15
92	3.625146e-06	1.665335e-15	
137	2.463121e-06		
⋮	⋮		
1315	9.946260e-11		

The BF method takes 1315 cycles to reach the periodic steady state, for a tolerance of 10^{-10}, the ND method takes 92 cycles while the END method needs 47 cycles to satisfy the same tolerance, representing the 3.5% of the total number of cycles used by the BF method. This percentage changes for each case depending on the damping degree of the system.

Figure 4.27 shows the actual, the KF estimate and their difference for line currents. The actual values are taken from the propagated harmonic solution obtained with the END method and represent the periodic steady state solution. With the END application the state estimation is smoothly and accurately evaluated, due to the reduction of cycles numerically processed with less variation during the state estimation interval. The state estimation is obtained taking the measurement equation (**z=Hx**) into the KF algorithm, the **z** vector takes 20 line currents and their derivatives as measurements, the discrete model takes the same variables as states, i.e., **H** is an identity matrix, the system is normally determined and observable. The KF estimates the states in a least mean squared error sense between the actual and estimated values. The measurement noise is assumed stationary, Gaussian and of 2% signal to noise ratio (SNR). The maximum difference is around 1% between the actual and the proposed KF estimate.

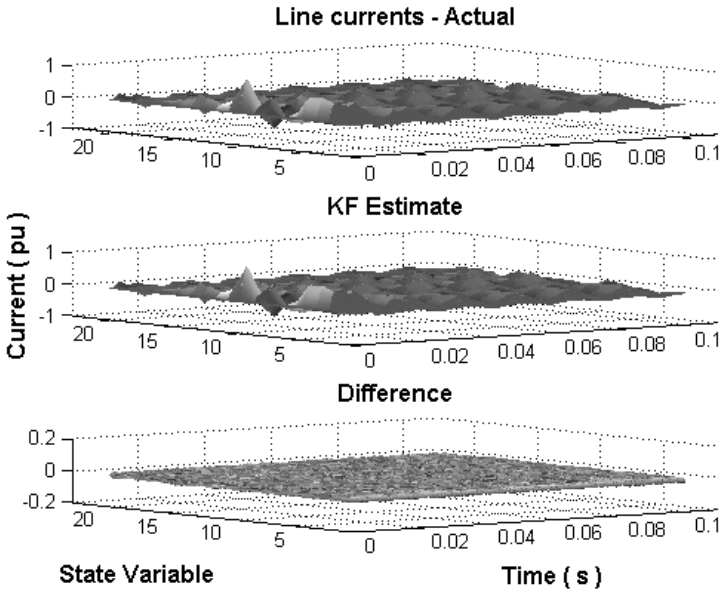

Figure 4.27 Actual, KF estimate and difference, HSE line currents

The generator currents at nodes 1-2 are obtained with the line current estimates and applying the KCL to these nodes. Figure 4.28 shows the generator currents, actual and KF estimate; they are compared against the PSCAD/EMTDC response. The KF is applied under the periodic steady state determined by the END method.

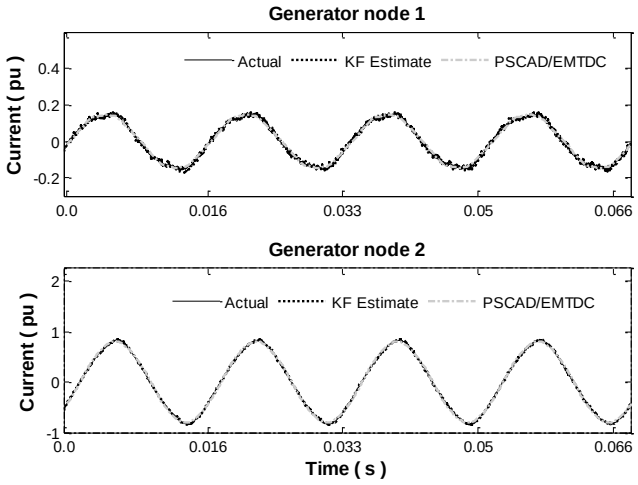

Figure 4.28 Actual, KF estimate, PSCAD/EMTDC response, current generators nodes 1-2

Figure 4.29 illustrates the harmonic spectrum for the current in the generators, obtained with the application of the DFT. The total current harmonic distortion THD*i* is 7.27% and 4.32% for generators nodes 1-2, respectively. This harmonic distortion is due to the harmonic currents injected in nodes 5 and 14.

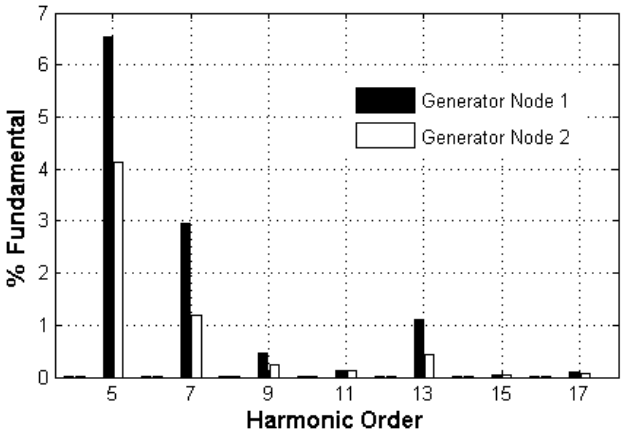

Figure 4.29 Harmonic spectrum, current generators nodes 1-2.

4.6.1 Time-Varying Harmonics Propagation

The power system presents a variable condition in the harmonic flows during normal operation [Baggini 2008]. In order to account for this effect, the injected harmonics of previous case study are increased during the last two cycles of simulation. The harmonics magnitude is changed to 5 times of their initial value in node 5 shown in Table 4.11, to illustrate the use of the KF to follow the time-varying harmonics. The signal to noise ratio SNR for measurements remains constant and equal to 2%.

Figure 4.30 presents the current waveform in lines 2-5 and 5-6, these lines are connected to node 5, where the variable harmonic current is present.

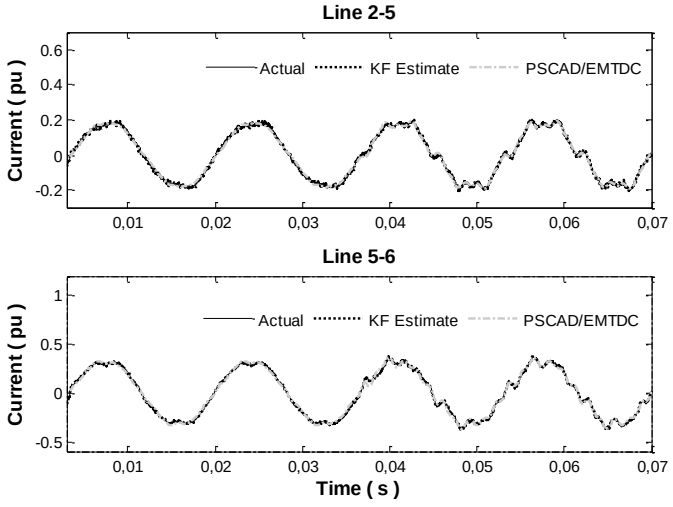

Figure 4.30 Actual, KF estimate, PSCAD/EMTDC, current lines 2-5 and 5-6, with varying harmonics.

The harmonic distortion changes with the new harmonics injection, the KF estimates the harmonic variable condition. The estimated currents agree with the actual value, this estimation is evaluated after the periodic steady state is obtained with the END method.

Figure 4.31 illustrates the current harmonic spectrum lines 2-5 and 5-6, for cycles 4 and 5, with the assumed variable harmonic condition. The THD*i* in line 2-5 changes from 7.42% to 15.16% and for current in line 5-6 varies from 7.56% to 14.8%. The even harmonics are due to the random generated noise added to the measurements.

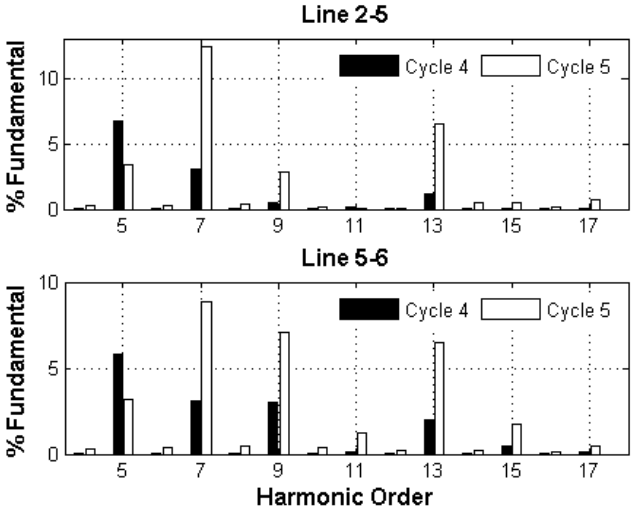

Figure 4.31 Harmonic spectrum, current lines 2-5 and 5-6, variable harmonic condition node 5.

4.7 Conclusions

A time domain harmonic state estimator, using the KF formulation and a Newton method based on Poincaré map, ND and END processes and extrapolation to the limit cycle has been presented.

The results obtained with the proposed methodology have been successfully compared against the actual system response and that obtained with the PSCAD/EMTDC simulator. The results agree even in the presence of measurement noise. The periodic steady state solution for the full system has been efficiently obtained with the application of the ND method, thus, allowing an efficient harmonic state estimation assessment in the time domain to be achieved by the reduction of the number of cycles to be processed numerically.

The power system has been represented by a first order ODE set; the time domain solution has been based on the application of numerical integration and the ND method to achieve a periodic steady state solution. The harmonic flow in the system depends on the sources, their placement in the system, network topology and loads. Balanced and unbalanced case studies have been analyzed, the estimated state variables waveforms were obtained with the proposed methodology and their harmonic content evaluated with the application of DFT. These results can be used, for instance, to find the harmonic sources, to locate and design the installation of filters and to determine the harmonic flows.

A time domain harmonic state estimator based on the application of the EKF has been proposed for the nonlinear power system case. The EKF results have been compared against the power system harmonic response, obtaining a close agreement. The power system has been represented by a set of nonlinear differential equations.

The proposed HSE method using the EKF requires of a model and a set of synchronized output measurements from the system, to estimate the states, then the estimate output vector can be calculated to compare with the measured output variables and finally obtain the error or residual in the state estimation.

A time domain harmonic state estimator based on the application of the PKF implemented using the CUDA platform and the CUBLAS library on a GPU has been proposed. The results obtained with the PKF methodology have been successfully compared against the actual system response and the PSCAD/EMTDC simulation. The system model was replicated increasing the speed-up with the size of model as expected using the parallel processing.

The HSE method using the PKF requires a system model and a set of synchronized output measurements from the system to estimate the state variables; the estimate output variables are in turn calculated to be compared with the measured output variables. The HSE with PKF has been evaluated for computational efficiency on the GPU to demonstrate speed-up in comparison with the sequential execution.

The END exploits the half wave symmetry of the voltage and current waveforms in the power system and gives a convenient initial value for the state estimation, thus avoiding the possible divergence problems in the application of the KF associated with a model, noisy and partial measurements from the system, and providing a fast state estimation assessment. The KF estimates the electrical system state, with reduced state variable fluctuations and with a smaller estimation error. A close agreement was obtained between the responses in all cases.

Chapter 5
Transient State Estimation

5.1 Introduction

This chapter presents a methodology to evaluate the Transient State Estimation (TSE) based on the Singular Value Decomposition (SVD) using the normal and enhanced numerical differentiation method in time domain of a power system. Transient phenomena such as faults, sags and load changes can be estimated with the TSE, covering over, normal and under-determined cases, according to the number of measurements and state variables related through the measurement state estimation equation; proposed as being a function of measurements and their derivatives. The system observability can be determined by means of SVD. If the system is unobservable, the SVD can determine which parts of the network are observable. The TSE takes partial measurements, calculates the best estimated state variables and completely determines the system state representing a transient condition. The periodic steady state following a transient condition can be obtained through a Newton method based on a Numerical Differentiation (ND) process, Poincaré map and extrapolation to the limit cycle; this method is applied before and after the simulated transient. The TSE results are validated through direct comparison against those obtained with the Power Systems Computer Aided Design/Electromagnetic Transients Program including Direct Current (PSCAD/EMTDC) simulator. The TSE can be classified as part of the PQSE [Heydt 1991], [Dugan *et al.* 2002].

Widely accepted methods to solve the time domain TSE are the recursive normal and weighted least squares, least mean squares [Dash *et al.* 2012], SVD [Yu and Watson 2007], Kalman filter [Kumar *et al.* 2006], optimization methods [Rakpenthai *et al.* 2010] and neural networks [Heydt 1991]. Some practical limitations are associated with the above methods, i.e., the least square methods have disadvantage to solve the state estimation mainly in under-determined cases or ill conditioned matrices; the Kalman filter requires the initial previous state and the covariance matrices; the optimization methods and neural networks demand a high computational effort when are applied in the time domain. A method based on the SVD is shown to solve the TSE, in association with the ND method to obtain the periodic steady state of the power system. Identified advantages of the SVD method are in the solution of ill conditioned matrices and under-determined cases, in addition to the intrinsic observability analysis during the state estimation [Arefi *et al.* 2011].

The choice of measurement points and quantities to measure are important to consider as this modifies the system observability [Saha *et al.* 2012] and if the measurement equation is over, normal or under-determined [Yu and Watson 2007], [Madtharad *et al.* 2005].

TSE estimates fluctuations in the waveforms; one approach is to use the criterion of minimizing the squared error sum between the measured and estimated values (least square estimation LSE). This error indicates the state estimation accuracy [Monticelli 1999], [Abur and Exposito 2004]. The state space formulation matrices are used to follow the system dynamics in the time domain and to evaluate the state and output variables; with these variables and the equilibrium laws of the system, all related variables in the system can be calculated [Tan *et al.* 2005].

In TSE, the measurement equation is linear, and a direct solution is performed. In state estimation a useful criterion is the weighted least squares; this can be used with the normal equation to solve the estimation, but this formulation fails when the measurement matrix is ill conditioned; under this condition an alternative to use is the SVD [Tan *et al.* 2005].

A Newton method based on numerical differentiation (ND), Poincaré Map and extrapolation to the limit cycle can be used to calculate the periodic steady state before and after the transient state, the TSE can be solved under this periodic steady state to ensure that only one transient is present in the network; the ND method reduces the execution time and the computational effort with the transient simulation mainly when considering a system with long time constants or the system is under-damped, this is possible due to the reduction of the cycles to be processed numerically [Bay 1999], [Segundo and Medina 2008]. Figure 5.1 shows the TSE flowchart.

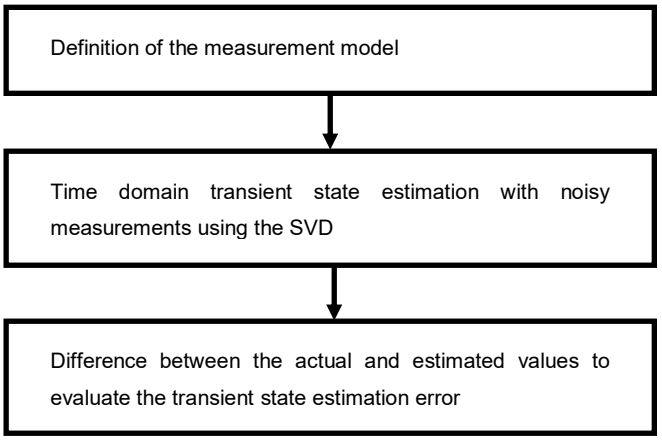

Figure 5.1 TSE flowchart

5.2 Transient State Estimation Formulation

The methodology includes the next four steps to solve the time domain TSE using the SVD and the ND method,

1) Definition of **H** measurement matrix, selecting output variables and their derivatives as measurements, and SVD decomposition of **H** to define the observability and the system condition.

2) ND determines the periodic steady state for the network to remove the initial transient and obtains a more convenient initial condition to evaluate the TSE, avoiding divergence problems.

3) SVD solves the TSE including over, normal and under-determined cases. The estimated state variables, measurements and the physical laws are used to evaluate the rest of variables in the network.

4) ND obtains the new periodic steady state of the power system after the estimated transient condition.

The state space system model is,

$$\dot{\mathbf{x}} = \mathbf{A}\mathbf{x} + \mathbf{B}\mathbf{u} \tag{5.1}$$

$$\mathbf{y} = \mathbf{C}\mathbf{x} + \mathbf{D}\mathbf{u} \tag{5.2}$$

Where $\dot{\mathbf{x}}$ is the derivative of state vector, **y** the output vector and **u** the input vector.

The state estimation measurement equation can be structured with various options, Table 5.1 shows the variables that can be taken as measurements [Watson and Yu 2008].

Table 5.1 Variable Options as Measurements

Measurement	System Variable	Definition
y	**Cx**+**Du**	Output variable
*d***y**/*dt*	**CAx**+**CBu**+**Du**	Output variable derivative

A combination of output variables and their derivatives as measurements, ensures a linear measurement equation. If a state variable can be measured according to the proposed model, this variable can be used to set up the measurement equation. The measurement set defines the measurement equation, i.e.,

$$\mathbf{z} = \mathbf{H}\mathbf{x} \tag{5.3}$$

This equation is solved using the least squares criterion for the estimation error when the **H** matrix is non-singular, by means of the normal equation formulation [Watson 2010],

$$\mathbf{x} = (\mathbf{H}^T\mathbf{H})^{-1}\mathbf{H}^T\mathbf{z} \tag{5.4}$$

Equation (5.1) relates the state variables with the system dynamics; it can be linear or nonlinear depending of the system and its components. In this section the linear time invariant case is analyzed. Equation (5.3) can be added with a vector **w** representing the measurements noise [Arrillaga *et al.* 2000], and is related with the state space output (5.2) as,

$$\mathbf{z} = \mathbf{H}\mathbf{x} + \mathbf{w} \tag{5.5}$$

The state estimation error is $\mathbf{e} = \mathbf{z} - \mathbf{z}_{estimated} = \mathbf{z} - \mathbf{H}\mathbf{x}_{estimated}$.

5.2.1 State Variable Formulation

The time domain TSE formulation can be carried out in state variables using Equations (5.1)-(5.2). [Yu and Watson 2007] presents the state-space formulation of the TSE, as well as modeling of system components, this formulation can be used to find a switching load, so it can be applied also to identify the location of faults.

In this formulation to provide extra information to the measurement model, the derivative of measurements of voltage and current can be also used, which can be estimated using present and previous values. The measurements in relation to the state variables are:

Measurements of the state variables:

$$\mathbf{x}_{measured} = [1]\mathbf{x} \tag{5.6}$$

Derivative of the measured state variables:

$$\dot{\mathbf{x}}_{measured} = \mathbf{A}\mathbf{x} + \mathbf{B}\mathbf{u} \tag{5.7}$$

Values of the dependent variables using the state variables:

$$\mathbf{y}_{measured} = \mathbf{C}\mathbf{x} + \mathbf{D}\mathbf{u} \tag{5.8}$$

Derivative of the dependent variables using the state variables:

$$\dot{\mathbf{y}}_{measured} = \mathbf{C}\dot{\mathbf{x}} + \mathbf{D}\dot{\mathbf{u}} = \mathbf{C}\mathbf{A}\mathbf{x} + \mathbf{C}\mathbf{B}\mathbf{u} + \mathbf{D}\dot{\mathbf{u}} \tag{5.9}$$

The rows of the output Equation (5.2) corresponding to selected measurement points are used to form the measurement equation. After the formation of the measurement equation, its solution is carried-out:

$$\mathbf{x} = \left(\mathbf{H}^T\mathbf{H}\right)^{-1}\mathbf{H}^T\mathbf{z} \tag{5.10}$$

$$\mathbf{x} = \mathbf{H}^{+}\mathbf{z} \tag{5.11}$$

Where $\mathbf{H}^{+}$ is the pseudo-inverse.

Once the estimated state variables are known, the dependent variables can be computed, so that all the variables in the system can be determined. The estimated output variables ($\mathbf{y}$) can be also calculated, as well as its difference with respect to measured output variables ($\mathbf{y}_{measured}$). This difference or residue error of the estimated state is an indicative of the state estimation accuracy.

The methodology for the next case studies uses the singular value decomposition, introduced in Section 2.2.5.

5.2.2 Numerical Differentiation Method

The ND method is used in the TSE to efficiently calculate the periodic steady state in the time domain, an introduction to this technique is presented in Sections 3.4.2 and 3.4.3. If a first order ODE set is the mathematical model of a system and this has a periodic steady state solution, this can be calculated using the Poincaré Map and an extrapolation process of the state variables to the limit cycle through Newton methods [Parker and Chua 1989]. The ODE set is represented by,

$$\dot{\mathbf{x}} = \mathbf{f}(\mathbf{x}, t) \tag{5.12}$$

The state variables at the limit cycle x^{∞} can be evaluated as in [22], i.e.,

$$\mathbf{x}^{\infty} = \mathbf{x}^{i} + \mathbf{C}(\mathbf{x}^{i+1} - \mathbf{x}^{i}) \tag{5.13}$$

$$\mathbf{C} = (\mathbf{I} - \mathbf{\Phi})^{-1} \tag{5.14}$$

Where: $\mathbf{x}^i$ state vector at the base cycle beginning, $\mathbf{x}^{i+1}$ state vector at the base cycle ending, $\mathbf{\Phi}$ state transition matrix, $\mathbf{C}$ iteration matrix, and $\mathbf{I}$ unit matrix.

The ND is a Newton method used to identify the state transition matrix $\mathbf{\Phi}$ [Semlyen and Medina 1995]. It is applied to speed-up the state variables convergence to the limit cycle and thus to achieve a fast periodic state solution of the power system. The method can be summarized as follows: a base cycle $\mathbf{x}(t)$ is obtained, after the time domain state variables solution over a number of periods of time (cycles). With a perturbed value at the base cycle beginning, the differences between the last two values at the end of the cycle are then calculated to obtain $\Delta\mathbf{x}^{i+1}$, which allows to identify $\mathbf{\Phi}$ by columns; $\mathbf{C}$ is evaluated, to calculate $\mathbf{x}^{\infty}$, which represents an estimate of the state variables at the limit cycle. This process concludes once the difference between two consecutive evaluations of $\mathbf{x}^{\infty}$ meets a convergence criterion, e.g., 10^{-10}. For a detailed explanation of this numerical method please refer to [Semlyen and Medina 1995], [Segundo 2010].

For the following case studies, this technique is applied after the initial cycles, followed by a base cycle and one ND applications and again is applied after the transient is removed to reach the final periodic steady state; the initial state variable values are set to zero. After the initial application of the ND method, a conventional numerical integration method based on the trapezoidal rule (TR) is applied. The obtained results with the proposed TSE method are validated through direct comparison against the PSCAD/EMTDC response [Pscad 2005] and the actual system response, obtained with the TR conventional method. This limit cycle extrapolation allows a reduction of the processed cycles and the computation effort in the TSE solution, consequently, the program execution time is reduced, specifically when the system has long time constants or is under-damped. The ND method is useful when is of interest to simulate the transient condition without the influence of other system transients being the simulated transient the only one in the system [Watson & Arrillaga 2007].

5.2.3 Numerical Derivative

The measurements numerical derivative is approximately calculated, as,

$$\mathbf{f}'(\mathbf{x}) \approx (\mathbf{f}(\mathbf{x}+h) - \mathbf{f}(\mathbf{x}))/h \tag{5.15}$$

The accuracy of this expression depends on the $\mathbf{f}$ function and the time step h [Press *et al.* 2007]. The measurements and their derivatives are used to define the measurement equation, $\mathbf{z}=\mathbf{H}\mathbf{x}$, using the state space formulation, as it was illustrated in Table 5.1.

5.3 Case Studies

Figure 5.2 shows the IEEE 14 bus test system analyzed in the case studies detailed next, the system data are taken from [IEEE 2013], considering a base power of 100 MVA and a base voltage of 132 kV; real values are used to validate the results by direct comparison against the PSCAD/EMTDC simulation.

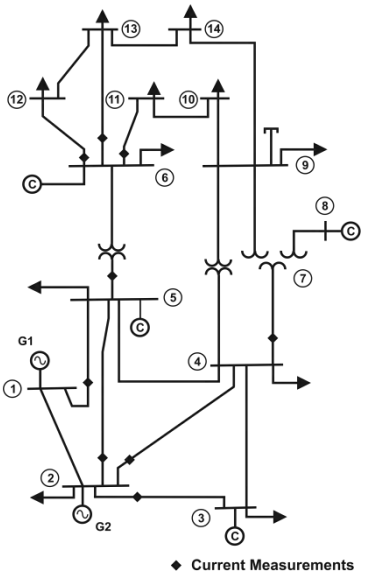

Figure 5.2 IEEE 14 Bus Test System

The lines 1-2, 1-5, 2-3, 2-4, 2-5, 3-4 and 4-5 are represented by a *pi* model and by a series impedance the rest of lines; the transformers 4-9, 5-6, 4-8-9, are represented by an inductive reactance, according to the IEEE 14 bus test system.

A transient condition is simulated with a fault at node 5, reducing the rated resistance load from 2320.1 to 74.4 ohms, starting at the 10th cycle (0.066 s) and ending at the 12th cycle (0.1 s) of simulation. This change originates a transient condition that can be estimated from a partial set of measurements.

The integration TR is used to solve the 31 ODE set, taking line currents and nodal voltages as state variables, and with a step size of 512 points per period, i.e., 32.5 μs, for a frequency of 60 Hz. The pre-fault plus fault time are 0.1 s. The ND method is applied once two initial periods of time (cycles) and a base cycle are calculated; then the state transition matrix $\mathbf{\Phi}$ is kept constant during subsequent applications of (5.13) to obtain $\mathbf{x}^{\infty}$, as shown in Table 5.2 using pu values. This will give the pre-fault periodic steady state solution of the power network. If the ND method is applied 35 cycles are processed, if TR method is used 1117 cycles must be processed for the considered case to fulfill a 10^{-10} tolerance (Table 5.2). After the fault is removed, an initial cycle and a base cycle are calculated before the ND is applied. With $\mathbf{\Phi}$ kept constant, (5.13) is applied twice to update $\mathbf{x}^{\infty}$ and to obtain the final periodic steady state, as shown in Table 5.3. For this case, 1134 full cycles (NC) were required by the TR method, while 35 were needed by the ND method, or just 3.08% of NC calculated with the conventional TR method to obtain the periodic steady state. For this particular case and using real quantities during the iterative solution of the assumed test case, the maximum error in the state variables using the conventional process based on the TR numerical integration method could not be reduced below 10^{-7}. The number of cycles to process depends on each case study and mainly of the system characteristics, i.e. if it is under, normal or over-damped system and of its component time constant values [Semlyen and Medina 1995]. The processed cycles vary for each case but if the system is under-damped, the

ND extrapolation to the limit cycle reduces the computational effort needed to obtain the TSE solution, prior to a periodic steady state condition.

Table 5.2 Pre-fault Conventional TR and ND Methods Convergence Process

NC	TR	ND
1	6.447332e-01	6.447332e-01
2	5.973785e-02	5.973785e-02
⋮	⋮	⋮
34	1.269982e-06	6.469466e-03
35	1.259118e-06	3.652759e-11
⋮	⋮	
1117	9.992150e-11	

Table 5.3 Final Conventional TR and ND Methods Convergence Process

NC	TR	ND
1	9.855697e-01	9.855697e-01
⋮	⋮	⋮
33	1.280940e-06	1.849277e-01
34	1.269982e-06	2.580195e-10
35	1.259118e-06	3.247402e-15
⋮	⋮	
1134	9.993077e-11	

The measurement equation $\mathbf{z}=\mathbf{H}\mathbf{x}$ is defined by selecting the output variables and their derivatives as measurements and defining elements of the **z** measurements vector, measurement matrix **H** and state vector **x**; relating the measurements with the state variables.

Figure 5.2 shows the measurements set; chosen to have an observable system condition, being enough to evaluate the TSE by means of the SVD using the pseudo-inverse solution (2.73). They are current measurements to estimate the set of state variables defined in the measurement equation [Madtharad *et al.* 2005]. With the measurements set, estimated variables and their derivatives, and using the Kirchhoff's and Ohm's laws, it is possible to calculate the rest of the system state and output variables. The complete system state can be estimated from a partial set of measurements [Shiying *et al.* 2006].

The measurement set is taken from a Matlab transient simulation using the ND method. The results obtained with the proposed TSE method are validated against the response given by the PSCAD/EMTDC simulator. A close agreement was obtained in all cases, as is illustrated in the following sections.

The measurement linear equation is solved using the SVD algorithm covering the over, normal and under-determined cases. The system observability and the numerical condition of the measurement matrix **H** are analyzed.

5.3.1 Over-determined Case

This case presents the condition when there are more available measurements from the power system than state variables to be estimated; normally the system is observable and all the state variables can be estimated. The measurements are correct and free of errors or excessive noise and the received values are adequate to solve the state estimation.

The TSE applies the SVD taking nine measurements from the time domain system solution and estimates eight state variables; with these measured and estimated state variables, the complete system solution can be determined using the equilibrium system equations, Kirchhoff's and Ohm's laws. The measurement points are indicated in Figure 5.2; the **z** vector is formed using expressions combining the measurements and their derivatives, as it was established in the methodology section. The following expressions define this measurement set,

$$\mathbf{z}_1 = \boldsymbol{v}_2 - \mathbf{x}_2 R_{23} - L_{23}\dot{\mathbf{x}}_2 = \mathbf{x}_{20} \tag{5.16}$$

$$\mathbf{z}_2 = \boldsymbol{v}_2 - \mathbf{x}_3 R_{24} - L_{24}\dot{\mathbf{x}}_3 = \mathbf{x}_{21} \tag{5.17}$$

$$\mathbf{z}_3 = \boldsymbol{v}_1 - \mathbf{x}_1 R_{15} - L_{15}\dot{\mathbf{x}}_1 = \mathbf{x}_{22} \tag{5.18}$$

$$\mathbf{z}_4 = \boldsymbol{v}_2 - \mathbf{x}_4 R_{25} - L_{25}\dot{\mathbf{x}}_4 = \mathbf{x}_{22} \tag{5.19}$$

$$\mathbf{z}_5 = L_{56}\dot{\mathbf{x}}_9 = \mathbf{x}_{22} - \mathbf{x}_{23} \tag{5.20}$$

$$\mathbf{z}_6 = \mathbf{x}_7 R_{47} + L_{47}\dot{\mathbf{x}}_7 = \mathbf{x}_{21} - \mathbf{x}_{24} \tag{5.21}$$

$$\mathbf{z}_7 = \mathbf{x}_{10} R_{611} + L_{611}\dot{\mathbf{x}}_{10} = \mathbf{x}_{23} - \mathbf{x}_{28} \tag{5.22}$$

$$\mathbf{z}_8 = \mathbf{x}_{11} R_{612} + L_{612}\dot{\mathbf{x}}_{11} = \mathbf{x}_{23} - \mathbf{x}_{29} \tag{5.23}$$

$$\mathbf{z}_9 = \mathbf{x}_{12} R_{613} + L_{613}\dot{\mathbf{x}}_{12} = \mathbf{x}_{23} - \mathbf{x}_{30} \tag{5.24}$$

Table 5.4 shows the measured and estimated variables.

Table 5.4 Over-determined Case

Measurement	Measured Variables Line current		Estimated Variables Node voltage	
$\mathbf{z}_1$	$\mathbf{x}_2$	2-3	$\mathbf{x}_{20}$	3
$\mathbf{z}_2$	$\mathbf{x}_3$	2-4	$\mathbf{x}_{21}$	4
$\mathbf{z}_3$	$\mathbf{x}_1$	1-5	$\mathbf{x}_{22}$	5
$\mathbf{z}_4$	$\mathbf{x}_4$	2-5	$\mathbf{x}_{22}$	5
$\mathbf{z}_5$	$\mathbf{x}_9$	5-6	$\mathbf{x}_{23}$	6
$\mathbf{z}_6$	$\mathbf{x}_7$	4-7	$\mathbf{x}_{24}$	7
$\mathbf{z}_7$	$\mathbf{x}_{10}$	6-11	$\mathbf{x}_{28}$	11
$\mathbf{z}_8$	$\mathbf{x}_{11}$	6-12	$\mathbf{x}_{29}$	12
$\mathbf{z}_9$	$\mathbf{x}_{12}$	6-13	$\mathbf{x}_{30}$	13

This definition gives the following linear measurement equation,

$$\begin{bmatrix} \mathbf{z}_1 \\ \mathbf{z}_2 \\ \mathbf{z}_3 \\ \mathbf{z}_4 \\ \mathbf{z}_5 \\ \mathbf{z}_6 \\ \mathbf{z}_7 \\ \mathbf{z}_8 \\ \mathbf{z}_9 \end{bmatrix} = \begin{bmatrix} 1 & 0 & 0 & 0 & 0 & 0 & 0 & 0 \\ 0 & 1 & 0 & 0 & 0 & 0 & 0 & 0 \\ 0 & 0 & 1 & 0 & 0 & 0 & 0 & 0 \\ 0 & 0 & 1 & 0 & 0 & 0 & 0 & 0 \\ 0 & 0 & 1 & -1 & 0 & 0 & 0 & 0 \\ 0 & 1 & 0 & 0 & -1 & 0 & 0 & 0 \\ 0 & 0 & 0 & 1 & 0 & -1 & 0 & 0 \\ 0 & 0 & 0 & 1 & 0 & 0 & -1 & 0 \\ 0 & 0 & 0 & 1 & 0 & 0 & 0 & -1 \end{bmatrix} \begin{bmatrix} \mathbf{x}_{20} \\ \mathbf{x}_{21} \\ \mathbf{x}_{22} \\ \mathbf{x}_{23} \\ \mathbf{x}_{24} \\ \mathbf{x}_{28} \\ \mathbf{x}_{29} \\ \mathbf{x}_{30} \end{bmatrix} \tag{5.25}$$

This over-determined linear measurement equation is solved using the SVD inverse (2.69) evaluating the state variable vector **x** (nodal voltages); the system is completely observable. Figure 5.3 shows the actual and estimated solutions and their difference. The maximum difference is negligible, only at the instant of the transient and in the voltage node with fault (node 5), it is of the order of 4%; this is due to the sudden change in the load condition of this node.

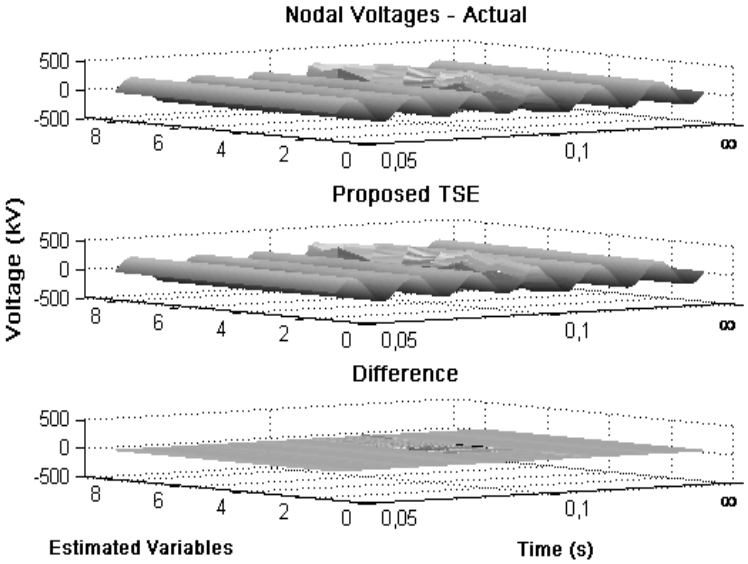

Figure 5.3 Actual, proposed TSE and difference for nodal voltages from 0.05 to 0.1 s of simulation, the transient starts at 0.066 s and ends at 0.1 s including the final cycles corresponding to the final ND method application, ∞ represents the limit cycle.

As selected variable, the estimated voltage at node 5 (x_{22}) is shown in Figure 5.4; this is the faulted node. The actual, estimated and PSCAD/EMTDC simulation results are shown, giving a close agreement between the waveforms.

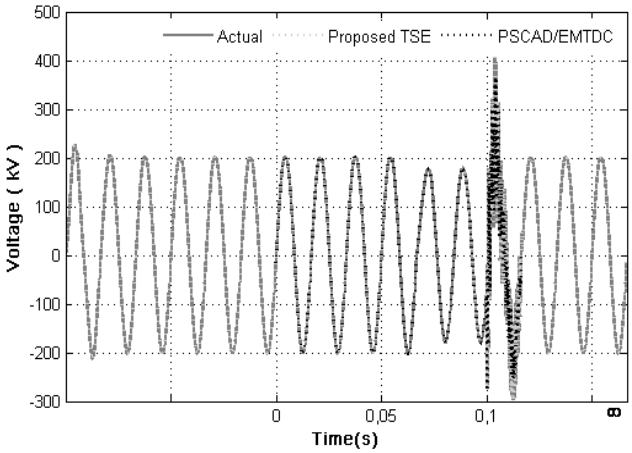

Figure 5.4 Actual, proposed TSE and PSCAD/EMTDC responses, voltage node 5, transient: 0.066-0.1 s.

Table 5.5 Applied Methods in Numerical Process

Cycle	Method	Condition
1-2	TR	Initial cycles
3	ND	Base cycle
4	ND	**Φ** constant
5-10	TR	Pre-fault
11-12	TR	Fault
13	TR	Initial cycle
14	ND	Base cycle
15-16	ND	**Φ** constant

Figure 5.4 and Table 5.5 show two initial cycles, a base cycle and a ND application to obtain the pre-fault periodic steady state; then the conventional TR of integration is applied to simulate the transient, after this a base cycle and two ND applications are applied to obtain the final periodic steady state. Table 5.2 and Table 5.3 show the ND convergence process for the pre-fault and final periods. The ND method process 35 cycles and the TR method process 1134 cycles to fulfill a 10^{-10} tolerance (Table 5.3). Figure 5.5 shows the waveforms for the line current 3-4, actual, estimated and PSCAD/EMTDC simulation. A close agreement between the responses is obtained. The PSCAD/EMTDC response is compared from 0 to 0.116 s, when the TR method is applied and the transient load condition is present.

The state variable 5, line current 3-4 is not a measured or estimated variable, it must be calculated taking into account the measured, estimated state variables and the equilibrium laws in the system.

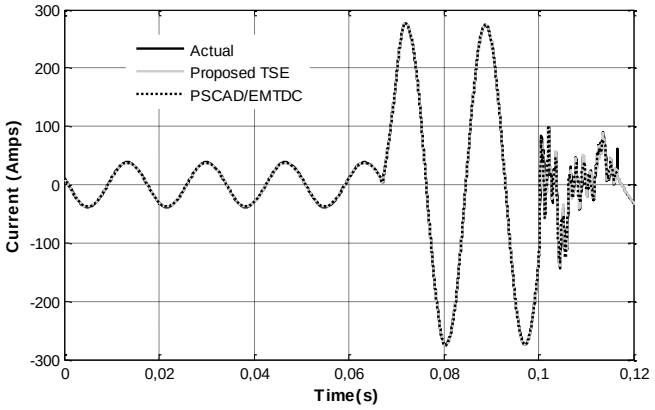

Figure 5.5 Calculated line current 3-4, state variable 5, over-determined system condition.

5.3.2 Normal-determined Case

This case is present when the available measurements are equal in number to the estimated state variables, regularly the system is observable and all the state variables can be estimated. This condition can be originated by measurement redundancy or lost measurements due to failures of instruments or communication links when initially the system is over-determined.

The measurement Equations (5.13)-(5.24) set, has a redundancy in the over-determined case; the measurements $\mathbf{z}_3$ and $\mathbf{z}_4$ are the same ($\mathbf{z}_3=\mathbf{z}_4=\mathbf{x}_{22}$). If the measurement $\mathbf{z}_4$ is eliminated, the number of measurements and the state variables is the same and equal to eight; this condition is the normal-determined case. The state estimation using the SVD gives the same results of Figures 5.3-5.5. The system has a complete observable condition with this normal-determined measurement set. Table 5.6 presents the measured and estimated variables.

Table 5.6 Normal-determined Case

Measurement	Measured Variables Line Current		Estimated Variables Node Voltage	
$\mathbf{z}_1$	$\mathbf{x}_2$	2-3	$\mathbf{x}_{20}$	3
$\mathbf{z}_2$	$\mathbf{x}_3$	2-4	$\mathbf{x}_{21}$	4
$\mathbf{z}_3$	$\mathbf{x}_1$	1-5	$\mathbf{x}_{22}$	5
$\mathbf{z}_4$	$\mathbf{x}_9$	5-6	$\mathbf{x}_{23}$	6
$\mathbf{z}_5$	$\mathbf{x}_7$	4-7	$\mathbf{x}_{24}$	7
$\mathbf{z}_6$	$\mathbf{x}_{10}$	6-11	$\mathbf{x}_{28}$	11
$\mathbf{z}_7$	$\mathbf{x}_{11}$	6-12	$\mathbf{x}_{29}$	12
$\mathbf{z}_8$	$\mathbf{x}_{12}$	6-13	$\mathbf{x}_{30}$	13

The TSE simulation can be used to determine the location or source of transients in a power system. Figure 5.6 shows the difference in nodal voltages as a function of time between the simulations of TSE, with

and without the disturbance. It can be observed from Figure 5.6 that the node with the largest change in voltage is the node 5, indicating that this node is the transient source. Both simulations, with and without transient, were simulated under a normal-determined condition.

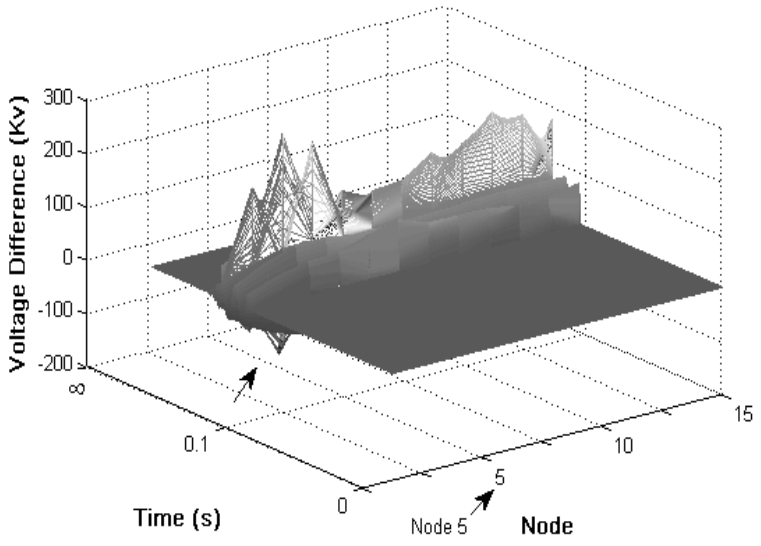

Figure 5.6 TSE nodal voltage difference, with disturbance minus without disturbance, indicating the node where the transient is originated, node 5 has the largest change.

5.3.3 Under-determined Case

This condition is present when the available measurements are fewer than the state variables to be estimated; in most cases the system is unobservable and the unobservable areas have to be delimited. Here only the observable state variables can be estimated, e.g., when the number of installed measurements is limited and less than the state variables or lost measurements due to instrument errors, communication faults or excessive noise when initially the system is normal or over-determined.

If the measurement $\mathbf{z}_8$ is eliminated, in reference to the normal-determined case, there are only seven measurements to estimate eight state variables; this condition gives the under-determined case. The SVD is able to obtain a solution under this condition for the first seven state variables, but the state variable 8, corresponding to the eliminated row in the measurement equation cannot be estimated, and consequently, the associated state variables cannot be calculated, creating an unobservable island in the system. The SVD estimation result is shown in Figure 5.7. It is observed that the state variable 8 is not estimated due to the measurement equation condition. Figure 5.8 shows the state variable 8, actual and estimated values, the estimated value is equal to zero. All the other state variables are well estimated under this condition, despite of the under-determined measurement equation and the unobservable system; again, a close agreement is observed. This is a SVD advantage with respect of normal equation formulation, i.e., that gives no solution with this condition. Table 5.7 shows the measured and estimated variables.

Table 5.7 Under-determined Case

Measurement	Measured Variables Line current		Estimated Variables Node voltage	
$\mathbf{z}_1$	$\mathbf{x}_2$	2-3	$\mathbf{x}_{20}$	3
$\mathbf{z}_2$	$\mathbf{x}_3$	2-4	$\mathbf{x}_{21}$	4
$\mathbf{z}_3$	$\mathbf{x}_1$	1-5	$\mathbf{x}_{22}$	5
$\mathbf{z}_4$	$\mathbf{x}_9$	5-6	$\mathbf{x}_{23}$	6
$\mathbf{z}_5$	$\mathbf{x}_7$	4-7	$\mathbf{x}_{24}$	7
$\mathbf{z}_6$	$\mathbf{x}_{10}$	6-11	$\mathbf{x}_{28}$	11
$\mathbf{z}_7$	$\mathbf{x}_{12}$	6-13	$\mathbf{x}_{29}$	12
			$\mathbf{x}_{30}$	13

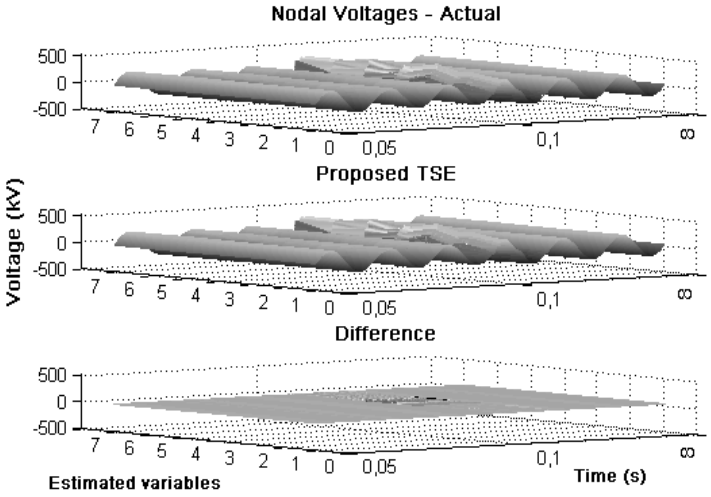

Figure 5.7 Actual, proposed TSE and difference values for the under-determined case from 0.05 to 0.116 s and the final period, ∞ represents the limit cycle.

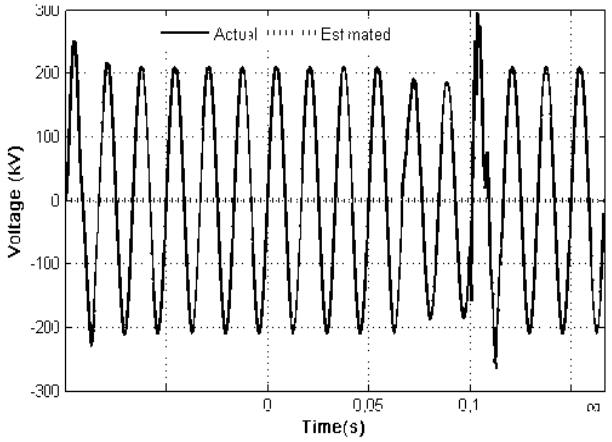

Figure 5.8 Voltage node 13, state variable 8, can not be estimated with the under-determined condition. The actual value is in reference to the high voltage side.

If the current measurement in line 6-12 ($\mathbf{z}_8$) is lost, an unobservable island is originated where the current lines and nodal voltages cannot be estimated, as shown in Figure 5.9. It can also be observed that if the measurements line 6-13 ($\mathbf{z}_9$), line 6-11 ($\mathbf{z}_7$), and line 5-6 ($\mathbf{z}_5$) are sequentially lost, unobservable islands are originated.

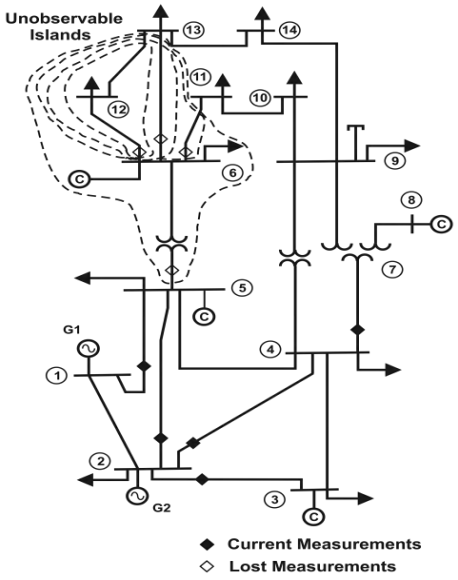

Figure 5.9 Unobservable islands due to lost measurements.

This under-determined case illustrates the special situation when the measurement matrix **H** is ill conditioned. If the original measurement in row 6 ($\mathbf{z}_6$) is repeated in row 7, as a redundant measurement and the SVD is applied; one of the singular values results equal to zero. The corresponding *rank* of **H** matrix is *rank=6* and the state variables are n=7; consequently, there is one singularity, the condition number is infinite. However, the SVD is able to estimate the state variables 1-6, but the state variables 7 and 8 cannot be estimated due to the singularity and the under-determined system condition. Figure 5.10 shows the actual, proposed TSE and their difference under this condition. The maximum difference is 8 kV or 4 % in transient state for the state variable 5.

The simulations were performed without measurement noise. However, during the measurements acquisition and transmission from the system to the control center, they are susceptible to be noise-contaminated, due to malfunctioning equipment or a noisy transmission environment. This noise adversely affects the state estimation accuracy, but it does not affect its solvability. Under this situation, the under-determined case for the TSE is again calculated. The results for the actual and estimated measurements are illustrated in Figure 5.11; these are calculated using (5.5) and $\mathbf{e} = \mathbf{z} - \mathbf{z}_{estimated} = \mathbf{z} - \mathbf{H}\mathbf{x}_{estimated}$; the measurements are contaminated with 1% of noise, which is generated by means of a stochastic process. From the results obtained and especially from the drawn overall difference, it is clear that the noise affects in a direct proportion the TSE evaluation. For this case, the estimated maximum difference is of 2.5 amps when

the peak current is of 270 amps; this represents an approximate average error of 0.93 % according with the 1% of measurements noise.

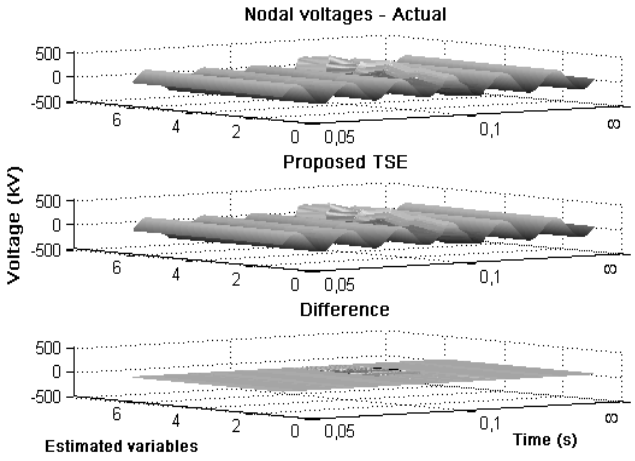

Figure 5.10 Proposed TSE with ill conditioned matrix H, the state variables 7 and 8 cannot be estimated due to a singularity and the under-determined system condition, ∞ represents the limit cycle.

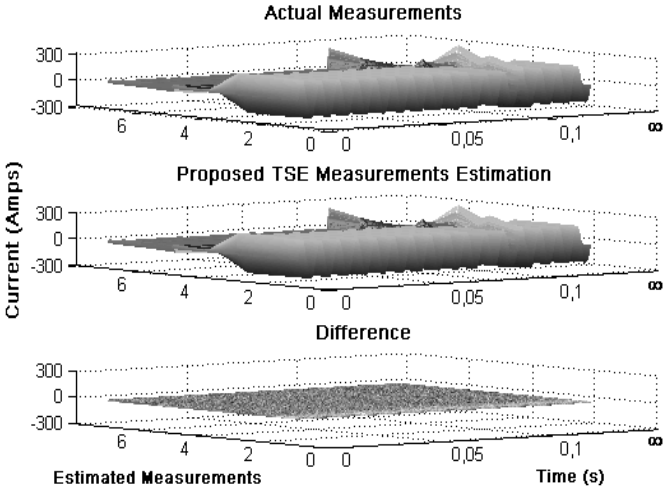

Figure 5.11 Proposed TSE measurements estimation from noisy measurements.

5.4 Transient State Estimation using the Enhanced Numerical Differentiation

A transient power system condition can be originated by faults, sudden load fluctuations or generation changes [Watson 2010]. The transient phenomena can be estimated using the END-KF methodology. In order to show this application, a short circuit fault is applied at node 5 in the IEEE 14 bus test system through the connection of a resistance of 0.52 pu between the node and ground; starting at cycle five and ending at cycle six of simulation. The END method is applied after two cycles of initial transient to obtain the periodic steady state, thus assuring that the only transient in the system is the associated with the application of the fault at

node 5. Under this condition, the KF allows the estimation of the line currents, a noise of 1% of SNR is added to measurements.

Figure 5.12 shows the line currents, for actual, KF estimate and difference values of state variables. The maximum difference is about of 2%. After the application of END method, during two cycles or 0.033 s, the KF method is applied during the next three cycles to solve the system model under the short circuit condition and to evaluate the transient state estimation.

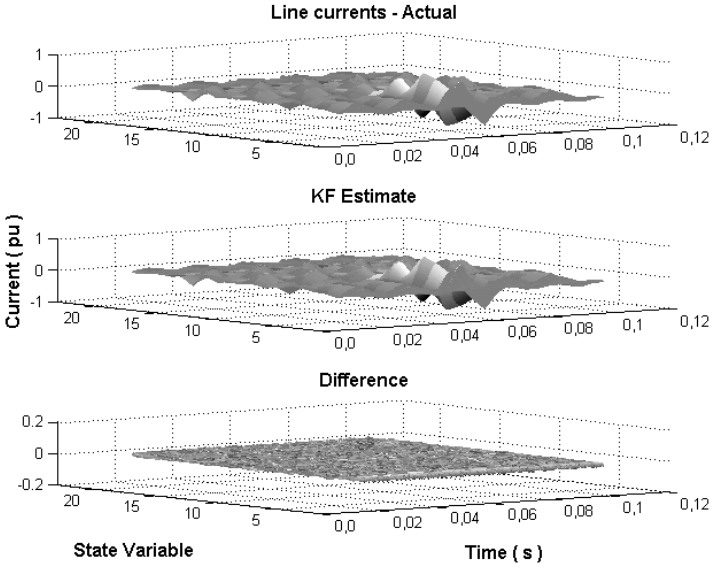

Figure 5.12 Actual, KF estimate and difference line currents for transient state estimation, short circuit node 5

Figure 5.13 shows the transient condition for currents lines 2-5 and 4-5, during the two cycles of periodic steady state, and three cycles of fault condition. The actual and KF estimate show a close agreement with the PSCAD/EMTDC simulation, thus validating the transient state estimation. The END method is applied in the pre-fault period, and the KF method is applied during the fault and post-fault periods.

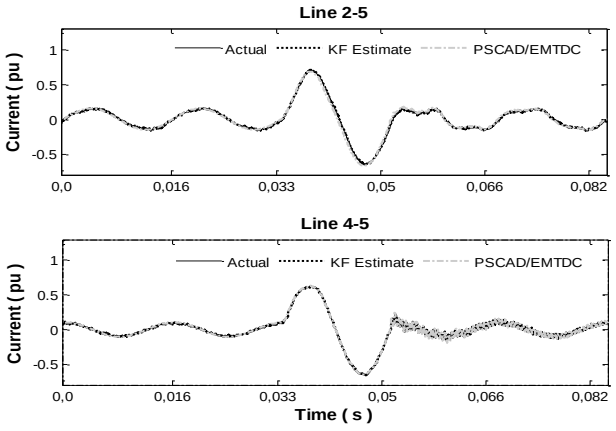

Figure 5.13 Actual, KF estimate, PSCAD/EMTDC response, line currents 2-5 and 4-5, transient state estimation using the END-KF method.

5.5 Conclusions

A time domain transient state estimator TSE has been developed and implemented using SVD to estimate the system transient state and to analyze the system observability, reviewing the singular values and the null space vectors to define the observable and unobservable areas in the analyzed system. From the obtained results, it has been clearly evident the possibility of using a combination of an output variable and its derivative to form the state estimation measurement equation. The ND Newton method has been applied to obtain the periodic steady state for the system under study when the initial and final transients are simulated, to provide convenient state variable values to efficiently obtain the pre-fault and the final periodic steady state solution, once the fault is removed, thus reducing the cycles to be numerically processed when is of interest to simulate the transient, prior to the periodic steady state, without the influence of other system transients and for a possible real time implementation, especially when the system is under-damped.

The over, normal and under-determined conditions of the system have been analyzed by means of the SVD, giving a solution for each condition. The condition number of the measurement matrix **H** must be analyzed to determine if this matrix is ill conditioned, and if this is the case, it is required to verify the system observability, establishing the observable and unobservable system areas.

The proposed TSE method has been compared against the actual system response obtained with the conventional numerical integration TR method and that obtained with the PSCAD/EMTDC simulator, yielding a close agreement between them.

It has been shown that the TSE can be applied to locate the sources of transients in a power system, by comparing the TSE solutions with and without the disturbance condition. From the difference in the state variables, the location of the transient source can be determined when the system is observable. When the system is partially observable, the comparison can be made by only considering the nodes that are in the observable part of the system; for this case, it is not possible to analyze the elements and nodes that are in the unobservable part of the system.

It has been illustrated that a noisy measurement condition adversely affects the TSE response, in direct proportion to the percentage of noise. Any condition of this type must be corrected as much as possible to avoid an inaccurate state estimation.

The transient state estimation can be evaluated using the periodic steady state obtained by the END method, and under this condition, the KF estimates the transient condition with only one transient in the system.

Chapter 6
Voltage Sags State Estimation

6.1 Introduction

This chapter presents the methodology to estimate voltage sags and their characteristics such as magnitude and duration in a power system, represented by a time domain nonlinear model, using the unscented Kalman filter algorithm. Partial and noisy measurements from a power network with nonlinear elements, used as data, are assumed. The characteristics of voltage sags can be calculated from the unscented Kalman filter estimate in a discrete form for all the nodal voltages; being possible to determine the *rms* nodal voltage, the sag starting and ending time in the voltage waveform. The results for the voltage sag state estimation can be used to obtain the power quality indices for monitored and unmonitored nodes in the power system and to design adequate mitigating techniques. The VSSE validation and the error are obtained by comparing the results against those of the complete time domain system simulation.

Power quality (PQ) is an important operation aspect of any electrical system. The utilities must comply with strict standards, relating primarily harmonics, transients and voltage sags. The PQ depends on the power supply, the transmission system and the load condition. The voltage sags are an essential issue for PQ; they can cause the malfunction of electronic loads, and can reset voltage-sensitive loads [Heydt 1991]. Voltage sags and interruptions are very critical power quality transients for customers due to their adverse effect on electronic equipment. They constitute the majority of power quality problems, representing about 60% of them [Dugan *et al.* 2002]. Voltage sags have increased due to the use of nonlinear varying loads, such as power electronic devices, smelters, arc furnaces and electric welders, the start of large electrical loads, switching transients, connection of transformers, faults and lightning strikes, among others [Arrillaga *et al.* 2000].

The Kalman Filter (KF) and the least square method have been used to estimate the voltage fluctuations in linear power systems [Watson 2010], [Yu and Watson 2007], [Watson and Yu 2008], [Farzanehrafat and Watson 2010]. The power quality state estimation based on the KF uses a linear model, partial and noisy measurements from the system. In [Espinosa-Juarez and Hernandez 2007] the number of sags is estimated using a limited number of monitored nodes, recording the number of sags during a determined period of time.

This work proposes a methodology based on the unscented Kalman filter (UKF) to assess the voltage sag state estimation (VSSE) in nonlinear power networks. The VSSE determines the magnitude and duration of sags with an observable system condition for the nodal voltages using the available measurements. Figure 6.1 illustrates the VSSE flowchart.

The state estimation collects measurements, through a wide area measurement system (WAMS) and evaluates the state vector, using algorithms such as the UKF. The practical implementation can be made using measurement instruments capable of recording the voltage and current waveforms during various cycles, being synchronized e.g., with the Global Positioning System (GPS) to time stamp the measurements [Baggini

2008], using adequate communication means like especially dedicated lines from the measurements points to the control center with high data updating rate, sufficient memory and adequate computational capability [Arrillaga *et al.* 2000], [Arrillaga *et al.* 2000a].

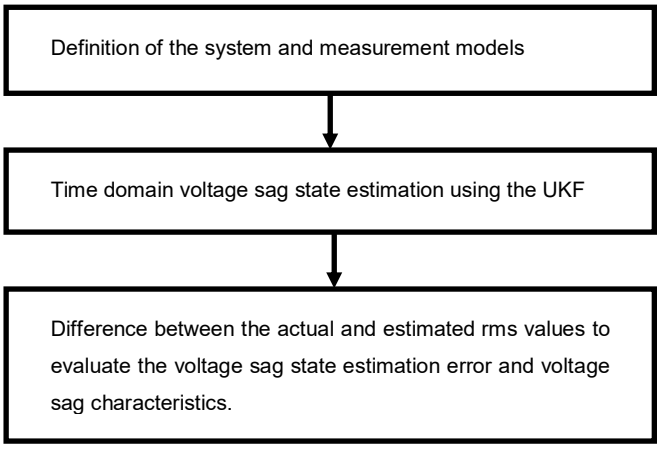

Figure 6.1 Time domain VSSE flowchart

Due to economic reasons, the measurement technology for VSSE is currently limited, making the system underdetermined,. The VSSE presents different problems from those of the traditional power system state estimation, where redundancy of measurements is possible [Moreno *et al.* 2009]. The VSSE solution can use some emerging technologies, such as automatic meter infrastructure (AMI) and smart meters.

The sags can be classified according to the unbalance, non-sinusoidal waveforms and phase shift. These factors are meaningful to determine the behavior of the system under study [Arrillaga *et al.* 2000]. The characteristics in magnitude and duration of the voltage sags are necessary to determine their effect on the sensitive electronic loads. This analysis uses the defined standards, as power quality graphs, such as the Computer Business Equipment Manufacturers Association (CBEMA) and the Information Technology Industry Council (ITIC) curves (magnitude to duration graphs) [Arrillaga *et al.* 2000a], to calculate power quality indices as the System Average Rms Frequency Index SARFIx [Heydt 1991], [Baggini 2008].

Section 6.2 details the dynamic state estimation, Section 6.3 presents the proposed UKF methodology to solve the VSSE and the evaluation of the *rms* value for a discrete waveform, Section 6.4 presents the VSSE case studies, and Section 6.5 describes the main conclusions from this chapter.

6.2 Dynamic State Estimation

The dynamic estimation problem data are the model with its inputs and a measurement set of outputs from the system, during a determined number of cycles to define the measurement equation. The measurements can be contaminated with noise or have measurement errors [Amit and Shivakumar 2009]; these measurements can be collected by means of WAMS [Wilson 2007].

The KF follows dynamically the variations in the power system states, currents and voltages. The difference with this approach from the static state estimation is that this method has the capability of tracking

the waveform variables. The KF detects changes in the voltage waveform within less than half of a cycle and is a good tool for instantaneous tracking and detection of voltage sags [Wang *et al.* 2012].

The dynamic state estimation problem can be solved using the KF; due to its recursive process [Tan *et al.* 2005], this filter is applied in the linear case, the extended Kalman filter (EKF) and the UKF are applied in the nonlinear case. In this work, the UKF is proposed to estimate the power system state under transient conditions e.g., voltage sags [Elnady and Salama 2005], [Wang *et al.* 2005], [Wang *et al.* 2004].

The EKF requires the derivation of Jacobian matrices and linear approximations for nonlinear functions; these matrices have to be evaluated and inverted at each time step; these approximations can originate numerical instability, in particular, when the time step is not small. Besides, the Jacobians can be of difficult implementation and evaluation. When the system is highly nonlinear, the EKF state estimation error can be of considerable magnitude as the covariance is propagated through the linearization process.

The UKF estimates the state of a process, minimizing the square of the expected estimation error between the real and the estimate state variables of a dynamic nonlinear system. The UKF uses a deterministic sampling technique: the unscented transform (UT), which takes a minimal set of sigma points near of their average [Valderde *et al.* 2011]. These points are propagated through the nonlinear model, evaluating the estimate average and covariance [Wang *et al.* 2012]. The main advantage of the UKF is the derivative free nonlinear state estimation, thus avoiding analytical or numerical derivative solutions [Ghahremani and Kamwa 2011]. Moreover, its computational complexity is a bit higher than the EKF, since includes a Cholesky decomposition to evaluate the sigma points, Equation (6.9) and a matrix inverse each time step.

The UKF and EKF state estimation errors increase when sudden fluctuations are present. The EKF can lead to divergence more easily than the UKF that shows good numerical stability properties [Julier and Uhlmann 2004].

The model parameter inaccuracies or fault impedances can be taken into account with a statistical term **v**, which is called the noise process. The metering devices have errors and noise; they are represented by a statistical term **w**. In most cases, **v** and **w** have a Gaussian distribution. The UKF is able to operate with partial, noisy, and inaccurate measurements [Ghahremani and Kamwa 2011].

6.3 Unscented Kalman Filter (UKF) Formulation

The next case studies apply the UKF method to VSSE, an introduction to this formulation is given in Section 2.2.4. The UT is based on the mean and covariance propagation by a nonlinear transform. The system and measurement nonlinear models are assumed as,

$$\dot{\mathbf{x}} = \mathbf{f}(\mathbf{x}, \mathbf{u}, \mathbf{v}) \tag{6.1}$$

$$\mathbf{y} = \mathbf{h}(\mathbf{x}, \mathbf{u}, \mathbf{w}) \tag{6.2}$$

UKF assumes a discrete time nonlinear system denoted by,

$$\mathbf{x}_{k+1} = \mathbf{f}(\mathbf{x}_k, \mathbf{u}_k, \mathbf{v}_k, t_k) \tag{6.3}$$

$$\mathbf{y}_k = \mathbf{h}(\mathbf{x}_k, \mathbf{u}_k, \mathbf{w}_k, t_k) \tag{6.4}$$

$$\mathbf{w}_k \sim \mathrm{N}(0, \mathbf{R}_k) \tag{6.5}$$

$$\mathbf{v}_k \sim \mathrm{N}(0, \mathbf{Q}_k) \tag{6.6}$$

v is the process noise and **w** is the measurement noise; they are assumed stationary, zero mean and uncorrelated, **Q** $n \times n$ order is the covariance matrix for **v** and **R** $m \times m$ order is the covariance matrix for **w**.

The algorithm has the following steps [Van der Merwe and Wan 2001]:

Initialization, k=0.

$$\hat{\mathbf{x}}_0^+ = \mathbf{E}(\mathbf{x}_0) \tag{6.7}$$

$$\mathbf{P}_0^+ = \mathbf{E}[(\mathbf{x}_0 - \hat{\mathbf{x}}_0^+)(\mathbf{x}_0 - \hat{\mathbf{x}}_0^+)^T] \tag{6.8}$$

Evaluation of sigma points.

$$\boldsymbol{\chi}_{k-1} = [\hat{\mathbf{x}}_{k-1} \quad \hat{\mathbf{x}}_{k-1} + \gamma\sqrt{\mathbf{P}_{k-1}} \quad \hat{\mathbf{x}}_{k-1} - \gamma\sqrt{\mathbf{P}_{k-1}}] \tag{6.9}$$

Update time step k from k-1.

$$\boldsymbol{\chi}^*_{k|k-1} = \mathbf{f}[\boldsymbol{\chi}_{k-1}, \mathbf{u}_{k-1}] \tag{6.10}$$

$$\hat{\mathbf{x}}_k^- = \sum_{i=0}^{2n} W_i^{(m)} \boldsymbol{\chi}^*_{i,k|k-1} \tag{6.11}$$

$$\mathbf{P}_k^- = \sum_{i=0}^{2n} W_i^{(c)} [\boldsymbol{\chi}^*_{i,k|k-1} - \hat{\mathbf{x}}_k^-][\boldsymbol{\chi}^*_{i,k|k-1} - \hat{\mathbf{x}}_k^-]^T + \mathbf{Q}_k \tag{6.12}$$

$$\boldsymbol{\chi}_{k|k-1} = [\hat{\mathbf{x}}_k^- \quad \hat{\mathbf{x}}_k^- + \gamma\sqrt{\mathbf{P}_k^-} \quad \hat{\mathbf{x}}_k^- - \gamma\sqrt{\mathbf{P}_k^-}] \tag{6.13}$$

$$\mathbf{y}^*_{k|k-1} = \mathbf{h}[\boldsymbol{\chi}_{k|k-1}] \tag{6.14}$$

$$\hat{\mathbf{y}}_k^- = \sum_{i=0}^{2n} W_i^{(m)} \mathbf{y}^*_{i,k|k-1} \tag{6.15}$$

Evaluate the error covariance matrices as,

$$\mathbf{P}_{\hat{y}k\hat{y}k} = \sum_{i=0}^{2n} W_i^{(c)} [\mathbf{y}^*_{i,k|k-1} - \hat{\mathbf{y}}_k^-][\mathbf{y}^*_{i,k|k-1} - \hat{\mathbf{y}}_k^-]^T + \mathbf{R}_k \tag{6.16}$$

$$\mathbf{P}_{xkyk} = \sum_{i=0}^{2n} W_i^{(c)} [\boldsymbol{\chi}_{i,k|k-1} - \hat{\mathbf{x}}_k^-][\mathbf{y}^*_{i,k|k-1} - \hat{\mathbf{y}}_k^-]^T \tag{6.17}$$

Evaluation of the filter gain, the state estimate and update the error covariance matrix,

$$\mathbf{K}_k = \mathbf{P}_{xkyk} \mathbf{P}_{\hat{y}k\hat{y}k}^{-1} \tag{6.18}$$

$$\hat{\mathbf{x}}_k^+ = \hat{\mathbf{x}}_k^- + \mathbf{K}_k(\mathbf{y}_k - \hat{\mathbf{y}}_k^-) \tag{6.19}$$

$$\mathbf{P}_k^+ = \mathbf{P}_k^- + \mathbf{K}_k \mathbf{P}_{\hat{y}k\hat{y}k} \mathbf{K}_k^T \tag{6.20}$$

The first four steps are the prediction stage, equations (6.9)-(6.17) and the last steps, equations (6.18)-(6.20) the KF update stage [Van der Merwe and Wan 2001].

The main objective of these sections is to use the UKF formulation to estimate the waveform of the nodal voltages to define the instantaneous voltage waveform at unmonitored nodes and to identify the voltage sags at these nodes [Rambabu *et al.* 2008].

The KF is able to identify the interval where the sags are present, as well as their magnitude, with an acceptable precision. By increasing the number of cycles in the simulation, the KF can identify before, during and after fault voltage amplitude.

The number of points per cycle is an important concern to evaluate the time domain state estimation with periodic inputs. This number defines the sampling rate for the measured variables in the system. The sampled signal is a sequence of values taken at defined time intervals and represents the measured variable. Interpolation can be used to adjust the number of points per cycle, linearly or nonlinearly. In addition, the interpolation should be carefully used with discrete signals satisfying the sampling theorem.

The sampling rate defines the speed at which the input channels are sampled and it is defined in samples per cycle. To detect transients, high sampling rates compared with the fundamental frequency may be necessary.

6.4 Case Studies

Figure 6.2 shows the modified IEEE 30 bus test system [IEEE 2013] used in the case studies described next, assuming a base power of 100 MVA and a base phase voltage of 132 kV. Lines 1-2, 1-4, 2-4, 2-5, 2-6, 4-6 and 5-6 are represented by a pi model and by a series impedance the rest of lines; the transformers 6-10, 4-12-13, 6-10-11, are represented by an inductive reactance, according to the IEEE 30 bus test system. Appendix D gives the additional system parameters.

The system is modified adding three nonlinear elements, i.e. an electric arc furnace (EAF) to node 2, a nonlinear inductance to node 5 and a thyristor controlled reactor (TCR) to node 6. The addition of these nonlinear elements gives the nonlinearity to the expressions (6.1) and (6.2). Appendix C shows the nonlinear models and differential equations for (6.1), the nonlinear function for the EAF real power and the nonlinear inductance current for (6.2).

The nodal voltages, line and load currents are selected as state variables to form the state space model for the power network in the time domain. The measurements are functions of these state variables, which are defined to obtain an observable condition for all the nodal voltages.

The generators are modeled as voltage sources connected to their respective busbars through a series inductance with constant fundamental frequency. The electrical loads are represented as constant impedances.

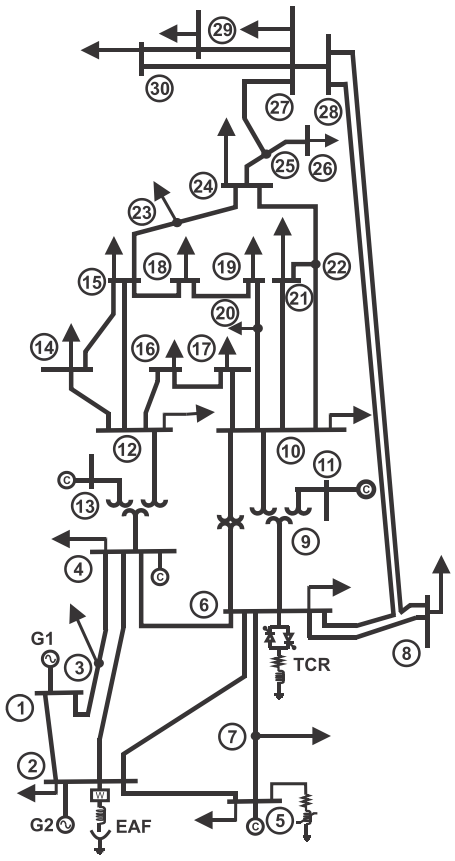

Figure 6.2 Modified IEEE 30 Bus Test System.

The installation points for the measurement instruments are selected in a way that the nodal voltages are observable. The measurements are 12 voltmeters, 27 ammeters and 1 wattmeter, giving 40 measurements. These are indicated in Table 6.2, the observation equation with this set of measurements has an observable condition for the nodal voltages, however, not all the line and load currents are observable. The EAF real power and the nonlinear inductance current are included as nonlinear functions in the measurement equation (**z**=**Hx**) represented in the formulation by (6.2). Table 6.1 and Table 6.2 show the **x** and **z** vectors, respectively, to form the measurement equation.

Table 6.1 State variables of vector **x**

Description	State Variable
Line current	1-41
Nodal voltage	42-71
Generator current	72-77
Nodal load current	78-106
Nonlinear inductance flux	107
EAF current and radius	108-109
TCR current	110

Table 6.2 Output measurement variables of vector **z**

Description	Measurement	Output Variable
Line current	1-14	1,4,5,10,13,16,19,22,25,28,31,34,37,40
Nodal voltage	15-26	42,43,46,49,52,54,55,58,61,64,67,70
Nodal load current	27-36	79,82,85,88,91,94,97,100,103,106
Generator current	37-38	73, 76
Nonlinear ind. current	39	107
EAF real power	40	108, 109

The measurement matrix **H** has *m* rows (measurements) and *n* columns (states). Each measurement is associated with its corresponding state variable (6.2), except for the nonlinear functions for the 39 and 40 measurements, which are evaluated with expressions (C.3) and (C.8) respectively in Appendix C.

The frequency of measurement sampling signals is at least of 30.72 kHz, to obtain 512 samples per cycle with a fundamental frequency of 60 Hz [Amit and Shivakumar 2009].

The trapezoidal rule of integration is used to solve the 110 ordinary differential equations set that represents the model of the power system, taking nodal voltages, line and load currents as state variables; with a step size of 512 points per period, i.e., 32.5 μs; the simulation time is set to 0.4s or 24 cycles. The measurements are taken from this simulation and then are contaminated with randomly generated noise.

6.4.1 Case Study: UKF VSSE fault at Node 4.

A transient condition is simulated with a ground fault at node 4, the fault impedance is of 0.05 pu, to simulate a short circuit, starting at the cycle 13 (0.216 s) and ending at the cycle 17 (0.283 s) of simulation. This fault generates voltage sags in the busbars, which can be estimated with the model of the system, partial noisy measurements and the UKF algorithm.

The measurement noise is assumed with a signal to noise ratio (SNR) of 0.025 pu or 2.5%; the noise process with a SNR of 0.001 pu or 0.1%. Figure 6.3 shows the nodal voltages 1-30, actual, the proposed UKF estimate and the difference values during the fault at node 4, corresponding to the 42-71 state variables.

The largest estimation error is present when the fault condition is removed at 0.283 s, this error is due to sudden changes in the nodal voltages. It is approximately of 7% but quickly decreases in the next cycles.

From the estimation process, the instantaneous voltage for nodes 4 and 6 are shown in Figure 6.4. Actual and UKF estimate values are illustrated, they closely agree. The presence of a voltage sag in these nodes can be observed, with duration of 4 cycles, while the fault condition is present, with a reduction in magnitude of 12% for node 4 and 8% for node 6.

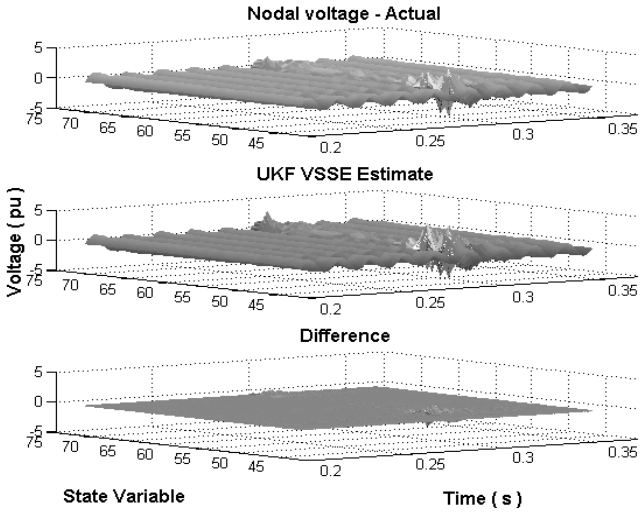

Figure 6.3 Actual, proposed UKF VSSE estimate and difference values for the nodal voltages with a fault at node 4 from 0.216 to 0.283 s.

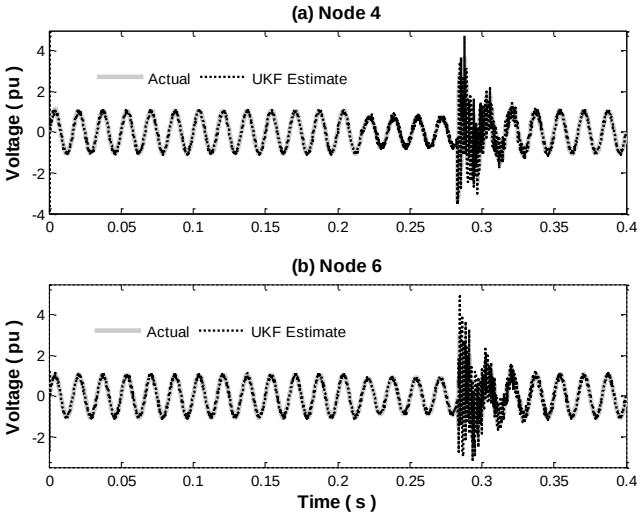

Figure 6.4 Actual, UKF estimate voltage for nodes 4 (a) and 6 (b) during the estimation process, voltage sag condition from 0.216 to 0.283 s.

Nodes 3-30 present the same behavior of nodes 4 and 6 during the transient system condition. The reduction in nodal voltage magnitude mainly depends on the network topology, the load system condition and the impedance values between the nodes. The fluctuations in the instantaneous voltage in both nodes are due to the noisy measurements used to evaluate the state estimation and the fault condition.

The line currents are shown in Figure 6.5, actual, UKF estimate and the difference values, with the fault condition from 0.216 to 0.283 s. The distribution of line currents in the system is shown during the interval of study, which includes a period of fault at node 4. The estimation error is of approximately 1%. After the fault is removed the error increases to 12% in the first cycle, but after this, the error decreases to around 1%.

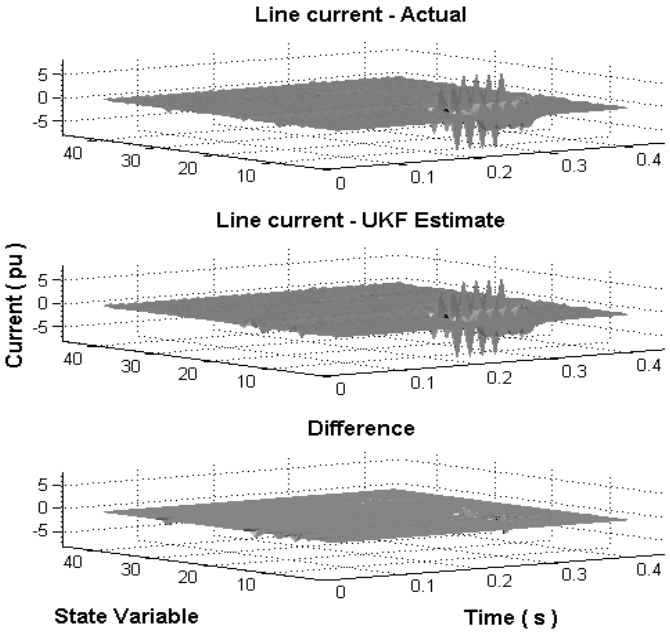

Figure 6.5 Actual, UKF estimate and difference values, line currents with a fault at node 4 from 0.216 to 0.283 s, state variables 1-41, interval of study 0-0.4 s.

Actual and estimate currents for nonlinear components are illustrated in Figure 6.6, e.g., the EAF, the nonlinear inductance and the TCR. These state variables show small variations due to the transient fault condition. Only in the post-fault period for the TCR current the values differ, but this difference decreases quickly after two cycles, to negligible proportions.

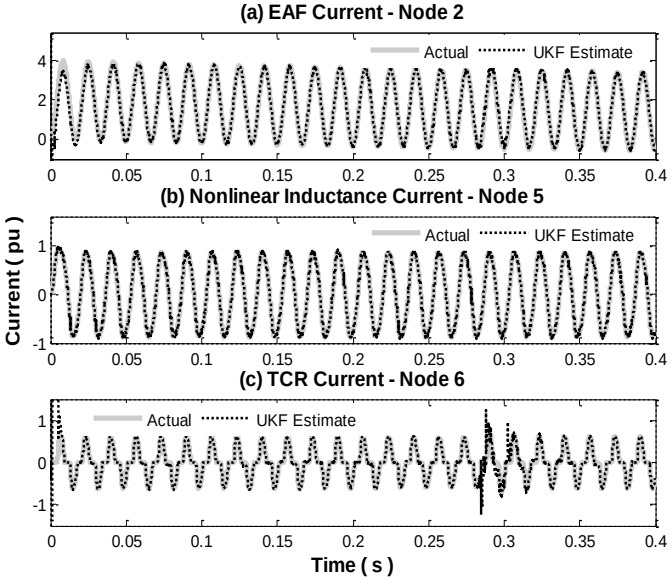

Figure 6.6 Actual, UKF estimate current for nonlinear components, nodes 2, 5, and 6.

6.4.2 RMS Nodal Voltages.

Figure 6.7 shows the *rms* voltage value for the faulty node 4 and for nodes 3, 6, 9, 12 and 14; these nodes are near to node 4 and present the largest voltage sags. These values are calculated using (2.66), which gives the *rms* value as a function of the values in a discrete waveform.

In Figure 6.7, the initial step when the voltage sag starts is due to fault; this time is at cycle 13 or 0.216 s. During the first cycle of the post-fault period, a noticeable difference is present in the *rms* voltage of the nearby nodes to the faulty node. The largest difference is of the order of 40% for node 6, but this error is reduced drastically in the next cycle to the order of 4.5%, and during the following cycles is reduced to negligible proportions. These effects are due to the sudden variations in the state variables after the fault is removed, which are difficult to follow exactly with the UKF algorithm.

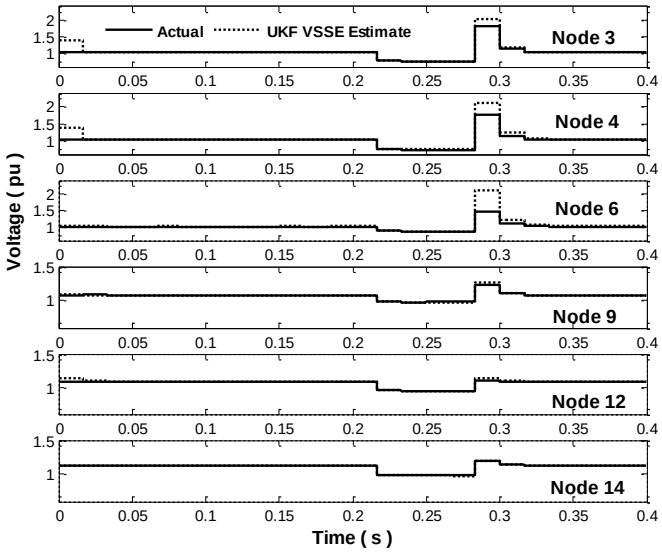

Figure 6.7 RMS UKF estimate voltage for nodes 3, 4, 6, 9, 12 and 14 during the state estimation process, voltage sags of different magnitude are present in each node due to the fault condition at node 4.

Table 6.3 shows the actual and estimate voltage sags present in the nodes in pu, with reference to the pre-fault value of the nodal voltage, due to the fault at node 4 during the 13-17 cycles or 0.216 to 0.283 s of the study interval. These values are calculated using (2.66), not listed nodes have a voltage variation of less than 0.01 pu, when the disturbance is present. The magnitude of the estimated voltage sag is close to the actual value, thus validating the UKF VSSE methodology.

6.4.3 Case Study UKF VSSE Fault at Node 15

This case study reviews the UKF VSSE when a short circuit fault is present at node 15; the fault impedance is of 0.35 pu. This impedance value is used to apply a different fault condition from the previous case study and to analyze the fault effect on the system condition. The node 15 has no voltage measurement, however, the

state estimation is able to estimate this voltage and of the nearby nodes with the same measurement points of the previous case.

Table 6.3 Actual and UKF Estimate Voltage Sags PU

Node	Actual	Estimate	Node	Actual	Estimate
3	0.752	0.753	20	0.889	0.890
4	0.713	0.717	21	0.892	0.892
6	0.858	0.860	22	0.892	0.893
7	0.908	0.910	23	0.893	0.893
10	0.890	0.900	24	0.887	0.888
12	0.870	0.880	25	0.888	0.889
14	0.880	0.885	26	0.892	0.892
15	0.872	0.873	27	0.891	0.892
16	0.880	0.890	28	0.880	0.881
17	0.892	0.895	29	0.884	0.885
18	0.875	0.880	30	0.907	0.909
19	0.889	0.89			

The measurements are contaminated with noise of a 3.5 % of SNR. Figure 6.8 shows the results under this condition for the voltages of nodes 15 and 23; these are the nodes that present the largest voltage sag during the examined transient condition. A close agreement between the actual and estimated signals including the post-fault period due to the decreased fault effect is achieved.

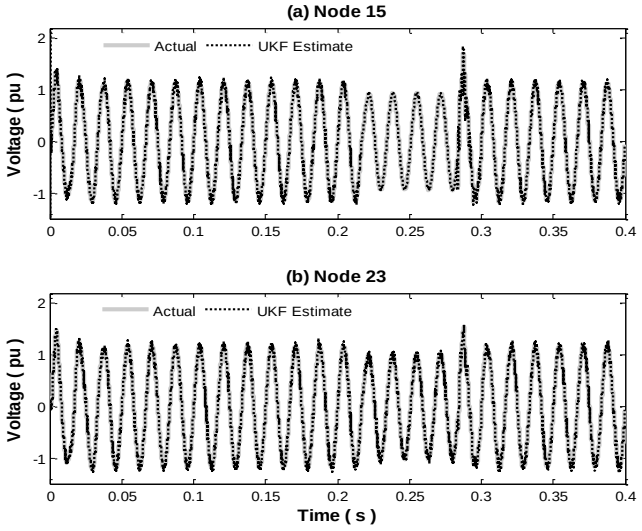

Figure 6.8 Actual, UKF estimate voltage for nodes 15 (a) and 23 (b) during the estimation process, voltage sag condition from 0.216 to 0.283 s, fault at node 15.

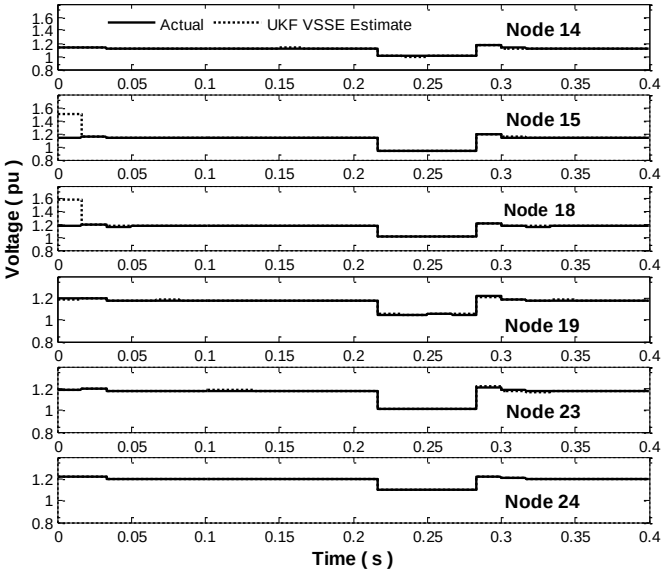

Figure 6.9 Actual, RMS UKF estimate voltage, nodes 14, 15, 18, 19, 23 and 24, a fault condition at node 15 is present during the 13-17 cycles generating sags.

Figure 6.9 shows the *rms* value for the nodal voltages near the node 15. The proposed UKF algorithm gives good estimates for the voltage sags magnitude and duration, mainly for the starting and ending time of the transient voltage sags. This data can be used to classify the type of voltage sags.

In reference to the previous case studies, the UKF algorithm implemented in Matlab is still slow to be used in real time applications. However, with adequate computational techniques such as parallel processing, the execution time can be reduced.

6.5 Conclusions

A state estimation methodology of power system voltage sags using the UKF has been proposed. A nonlinear system model and a nonlinear measurement equation have been used. The obtained results verify that the UKF can be used in power system voltage sag estimation. The method has been verified using a modified IEEE 30 bus test system and measurements with noises of 2.5% and 3.5% of SNR.

An important aspect is that the used sampling frequency for the measurements should satisfy the sampling theorem. When the power system presents fast transients, the UKF estimator error is more appreciable, but when the power system tends to the steady state, this error quickly decreases according with the damping degree of the system. In most cases, this period is short, compared with the voltage sag estimation interval. This condition is present during the post-fault period of the reviewed case studies.

The UKF estimator can be used to dynamically follow the generation of voltage sags in a power system, by executing the estimator continuously to count, record and classify the voltage sags originated during the power network operation; especially for the unmonitored nodes in the system. This requires an

accurate model of the system, a set of synchronized measurements, preferably without errors and noise, sufficient for an observable condition of nodal voltages in the power system.

The *rms* value for the nodal voltages can be calculated from the discrete values of the waveform for these voltages. These *rms* values give the information to define the voltage sag magnitude present in the nodes, delimiting the time interval of the voltage sag to classify the estimated event. The voltage sag characteristics can be determined according with the initial, duration, final time and magnitude.

The UKF VSSE method has been validated by comparing the obtained estimate values against the actual values taken from a simulation of the power system under the same fault condition. In all cases, for the analyzed voltage sags, the actual and estimate instantaneous or *rms* values closely agree.

Chapter 7

General Conclusions and Future Research

7.1 General Conclusions

This thesis has reported innovative time domain power quality state estimation implemented using normal, extended, unscented and parallel Kalman filter to estimate harmonic distortion, time-varying harmonics, inter-harmonics, transients and voltage sags under steady and transient state of electrical systems.

The power quality state estimation exploits numerical efficient techniques, such as the conventional numerical differentiation and the enhanced numerical differentiation method, to obtain the periodic steady state of the system in the harmonic and transient state estimation; this method uses the Poincaré map and extrapolation to the limit cycle techniques. The numerical differentiation finds the periodic steady state integrating complete cycles and the enhanced version uses the half wave symmetry property of the waveforms to integrate only during half cycles. This technique can be used to obtain a convenient initial condition to evaluate the power quality state estimation and to assure that there is only one transient in the system during the transient state estimation. The numerical differentiation method allows an efficient state estimation assessment in the time domain, by reducing the number of cycles to be numerically processed, when a transient of interest is simulated under a periodic steady state without the influence of other transients in the system, and for possible real-time implementation, especially when the system is under-damped.

Harmonic state estimation has been evaluated incorporating noisy measurements, by means of the Kalman filter formulation, the results show small differences compared against the PSCAD/EMTDC response. Case studies with balanced and unbalanced three-phase conditions have been reviewed, the harmonic content has been obtained by applying the discrete Fourier transform.

A harmonic state estimator based on the extended Kalman filter has been implemented and analyzed. This formulation requires a model and synchronized measurements from the system, it can be applied in case of nonlinear system and measurement models represented by a set of nonlinear differential equations. The extended Kalman filter results closely agree with those of the power system harmonic response.

The singular value decomposition of the measurement matrix has been used to determine the system observability. By examining the structure of the associated matrices, it is possible to establish the observable state variables and with these variables, to determine the observable area of a power system. This observability analysis is useful before and during the state estimation as the number of measurements can vary due to measurement errors or excessive noise. Under this condition, the singular value decomposition is convenient for the observability analysis. The conditions over, normal and under-determined have been analyzed using the SVD, giving a solution for each condition. The condition number of the measurement matrix must be analyzed to determine if the matrix is ill-conditioned, and if this is the case, it is required to review the system observability and to establish the observable and unobservable areas of the system.

The transient state estimation uses the numerical differentiation to obtain the periodic steady state following initial and final transients, to provide convenient values of the state variables for periodic steady state solution during the pre-fault and final periods. It has been shown that the transient state estimation may be applied to find the location of transients, through solutions of the TSE with and without disturbance condition. From the difference in the states, the transient location can be determined when the system is observable.

The time domain voltage sags state estimation can be assessed using the Kalman filters. The voltage sags can be classified by obtaining the *rms* value from the estimated discrete waveforms for each cycle of the nodal voltages in a network. The unscented Kalman filter has been applied to solve the voltage sags estimation in the time domain of a power system with nonlinear loads and short-circuit faults. The nonlinear system and measurement models are defined and solved, a particular case was analyzed when the measurement model has an underdetermined condition, this is a novelty application of the unscented Kalman filter in the estimation of power quality. This formulation determines the duration, starting and ending time of sags and if continuously executed can be used to record and classify the voltage sags.

A CPU-GPU configuration has been used to implement parallel processing techniques in order to evaluate the power quality state estimation. A parallel Kalman filter algorithm has been implemented to estimate harmonics, harmonic distortion, inter-harmonics and can be used to estimate transient conditions and voltage sags. The parallel Kalman filter execution time has been compared against the sequential code version, evidencing a speed up when the model is replicated to consider larger systems, showing an advantage of the parallel processing when the size of the power system become larger. This parallel computational technique can be used to implement real-time or near real-time applications of the state estimation.

7.2 Future Research

In reference to the research work reported in this thesis, the author proposes the following directions for future research:

1) Implementation of the time-domain algorithms of extended, and unscented Kalman filter including C++ code and parallel processing techniques, such as CUDA and CUBLAS on GPUs to evaluate the harmonic, transient and voltage sags state estimation.

2) Test of the state estimation results using actual data obtained from the operation of the power system, although this requires a suitable infrastructure, databases, communications, measurement instruments and adequate computational power. With the above, the verification can be carry out of the proposed algorithms by an application in real time or as close as possible to real time taking into account the limitations in measurements, communication channels and computational resources.

3) Definition of case studies considering numerous sources with diverse harmonic content, connected to different nodes in order to verify the combined effect on the power system.

4) Represent a power system with laboratory models of the components and take the measurements from this experiment using them in the state estimation to evaluate the unmonitored variables, to compare the actual with the estimated values.

5) Implementation of case studies including the optimal location of meters and evaluate the erroneous data analysis to filter the incoming measurement gross errors.

Appendices

Appendix A Power Quality Adverse Phenomena

There are several effects related to power quality, each of them is originated from different causes and may occur simultaneously, alternately or randomly. Following there is a summary of the typical problems associated to power quality.

A.1 Frequency

The grid operates at 60 Hz, by the size of the network is rare to find problems with frequency. Moreover, nearly all electrical devices are capable of operating appropriately with low frequency variations greater than those that occur practically.

Stable frequency concept does not apply for systems where electricity is generated on site. Diesel generators of considerable power can present frequency problems. The isolated renewable energy systems such as wind and solar have problems with considerable variation in frequency at which they are operated, backing itself into a diesel generator or other type of generation [Dugan *et al.* 2002].

A.2 Harmonics

The harmonics are reflected as recurring voltage or current distortion waveform that can be caused by various devices, such as variable speed drives, variable nonlinear power sources or electronic ballasts, nonlinear loads as thyristor controlled reactors, arc furnaces, Figure A.1 shows harmonic distortion. Certain types of power conditioners, such as ferroresonant transformers or constant voltage can significantly increase the harmonic waveform distortion [Emanuel 2000].

The waveform distortion may also be related to uninterruptible power supplies (UPS) or other devices and inverters. UPS does not add distortion, but as digitally synthesized waveform, the latter may be square or distorted; to some extent away from the sinusoidal waveform.

The effects of harmonic distortion include overheating, increased engine load and operational problems on the equipment or electrical loads and generators.

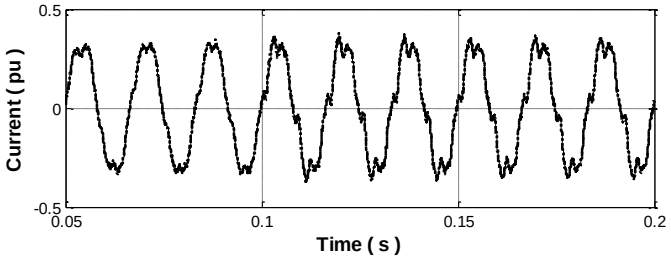

Figure A.1 Harmonic distortion

A.3 Inter-harmonics

The inter-harmonics are components of a voltage or current waveform, these components have a frequency not integer multiple of the fundamental frequency, which can be discrete frequencies or have a wide spectrum. They have an adverse effect on the power quality originating heating, flicker, control and communications interference and magnetic saturation [Testa *et al.* 2007]. Sub-harmonics are components with a frequency under the fundamental. The inter-harmonics are generated by nonlinear loads such as frequency converters, cyclo-converters, speed drives, arc furnaces and arc welders [Gunther 2001]. Figure A.2 shows an example of a current signal with an inter-harmonic of 90 Hz and a sub-harmonic of 30 Hz.

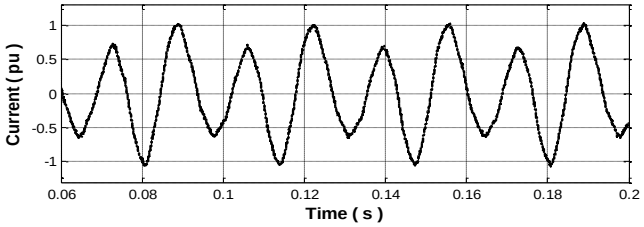

Figure A.2 Inter-harmonics

A.4 Interruption

An interruption or blackout occurs when the voltage falls below 10% of rate value [Bollen 2000]. Interruptions are classified into three types: momentary (lasting 30 cycles to 3 seconds), temporal (duration of 3 seconds to 1 minute) and sustained (lasting more than 1 minute) [IEEE 1995].

While interruptions are one of the most severe problems in the power system; they rarely occur during operation. The voltage sags are mistakenly taken as interruptions, as the connected equipment reboots or the lighting loads turn off, as a result of the voltage falling below the value of operation of these devices [Dugan *et al.* 2002], Figure A.3 shows an interruption.

Figure A.3 Interruption

A.5 Noise

The noise is a high frequency distortion in the voltage or current waveform; its origin is the disturbances in the power system or connected equipment, such as welders, arc furnaces, switches, interference with other electromagnetic sources and transmitters; noise can often go unnoticed [Heydt 1991].

The high frequency noise can cause poor operation of the equipment, overheating and reduction of its operation life. Figure A.4 shows a current signal with noise.

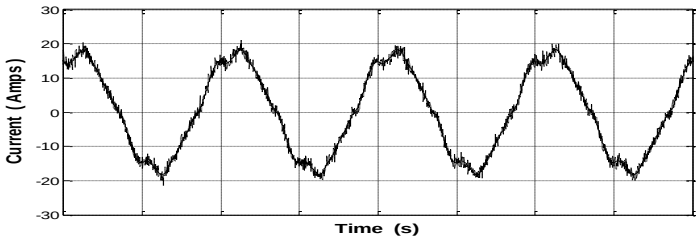

Figure A.4 Noise

A.6 Notching or Deformation

Notching is a disturbance of normally opposite polarity to the voltage waveform, which is subtracted from the waveform; the duration is at least a half cycle. The deformation or notching is often caused by poor operation of electronic switches or power conditioners. In practice, this effect is not generally a problem of greater consideration, yet the deformation can cause the equipment to operate improperly, especially the electronic equipment [Bollen 2000]. Figure A.5 shows a waveform with notching.

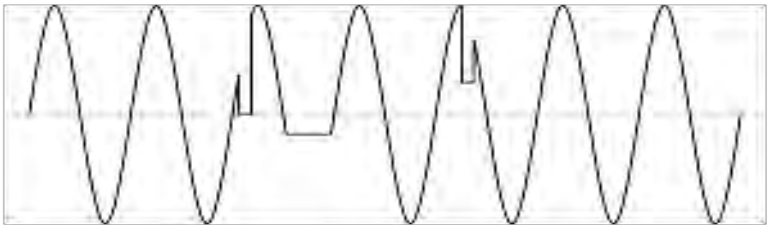

Figure A.5 Notching or deformation

A.7 Over-voltage

The over-voltage is an increment above 110% of the nominal value lasting from half cycle to more than one minute [IEEE 1995], Figure A.6. It can be caused by a permanent surge from the utility or by the user, if they have adjusted the tap of a transformer to a very high value. This adjustment can be made to compensate for the voltage drop experienced by users farther from the point of supply of the transformer. However, those closest to the transformer may experience a surge, as a result of this adjustment. The surge is set by the voltage regulation standards by the utility. Over-voltages adversely affect most electronic devices since they can cause overheating during operation [Dugan *et al.* 2002].

Although over-voltages, surges or swells do not occur as frequently as voltage sags; they can cause the equipment to not work properly and reduce its life span. The over-voltage can also be caused by commutation of capacitor banks.

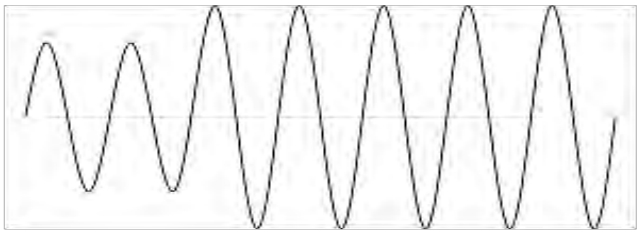

Figure A.6 Over-voltage

A.8 Voltage depression or sag

The voltage sag is a voltage decrement between 10 and 90% of its nominal value by one cycle to a minute [IEEE 1995], Figure A.7. Voltage sags are between the power problems experienced by the majority of users. These sags can be generated internally and externally, with reference to the user installations.

External causes of voltage dips mainly come from the transmission and distribution network, which are caused by lightning, normal and abnormal operation of electrical equipment. The voltage sags generated in the transmission or distribution network can be spread hundreds of kilometers and can affect thousands of users during a single event.

Sometimes externally generated voltage sags may be caused by nearby users. The starting of large electrical loads or switching of parallel capacitor banks can generate voltage sags of significant magnitude to affect a local area. If the end user is permanently subjected to a low voltage, a sag of relatively small magnitude voltage can have adverse effects on the system operation.

The sags caused internally within the end user installation is typically generated by the large starting electrical loads, such as motors or magnets. The required starting current is high to start this type of load, which depresses the voltage level available to other loads that share the same wiring. Similarly to the voltage sags caused externally, internally generated sags can worsen an already existing low voltage problem [Bollen 2000].

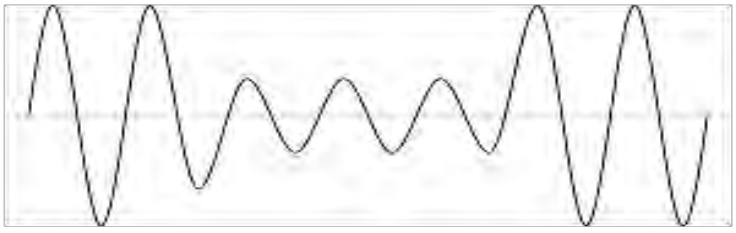

Figure A.7 Voltage sag

A.9 Transients

Transients are events of short duration, with a variable magnitude. An example is a fault to ground, the most common transient is lightning. Figure A.8 shows a voltage transient due to a ground fault.

Transients can be caused by the commutation of loads, failures, or by operation events. Even low voltage transients can damage electrical components if they occur with some frequency [Dugan *et al.* 2002]. A proper surge protection is usually chosen against the negative effects of high voltage transients.

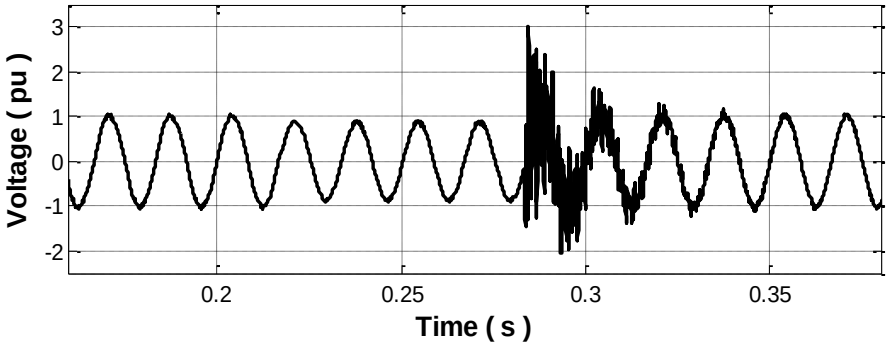

Figure A.8 Transient

A.10 Low voltage

Low voltage is a decrement below 90% of nominal value by more than a minute [IEEE 1995]. The low voltage is also known as blackout, and it is used when the utility deliberately reduces the voltage in the system to supply a high demand or other operating problems, such as shedding load [Dugan *et al.* 2002], Figure A.9.

Symptoms of low voltage can range from none, to the equipment always working improperly or the equipment failure prematurely. A low voltage may not be noticed until the new equipment is installed or the electrical system is adapted and the new combination of loads; it depresses the voltage to a point where symptoms are noticeable, the equipment malfunction by low constant voltage can cause excessive stress on certain devices, such as motors, since they tend to work overheated.

A low voltage is usually a permanent problem, aggravated by a number of factors beyond the control of the end user. The utility companies try to maintain voltage levels suitable for consumers in ± 5%. However, factors such as the weather, high demand and other causes can originate that the voltage be within a range of ± 10%. Even under ideal operating conditions, most users experience a voltage drop during the day when demand begins to increase.

The characteristics of the distribution circuits may contribute to causing low voltage, e.g., end users connected to a long distribution line may be subject to a permanent low-voltage due to line voltage drop and voltage variations in the power system.

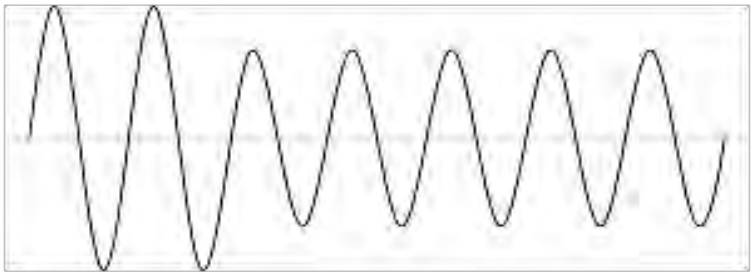

Figure A.9 Low voltage

A.11 Power Conditioning

The power conditioning refers to modifying the power, in order to improve its quality. An uninterruptible power supply (UPS) can be used to remove the principal power transients that occur along the line. However, cheaper UPS can create a low power quality by themselves, due to the imposition of a high frequency waveform with low amplitude square attached to the sinusoidal waveform. The high quality UPS units use a double conversion topology which converts the power from alternating current (AC) to direct current (DC), charge the batteries, then the DC is converted back to AC sinusoidal waveform of higher quality than the AC original waveform [Heydt 1991].

Overvoltage protection, a capacitor or a varistor can protect against most over-voltages while an arrester protects against severe peak pulses. Active and passive electronic filters can remove or filter the harmonics.

A.12 Smart grids and Power Quality

Meters and sensors called phasor measurement units (PMU) have been in use in power systems, distributed throughout the network to monitor power quality and in some cases to automatically respond to changes, to improve power quality. The smart grid is characterized by a fast measurement and automatic control and correction, thus allowing better power quality and a shorter duration of faults, taking better support for intermittent power sources and distributed generation, such as wind power and solar energy, which if not adequately supported, can degrade to a greater extent the network power quality.

Appendix B Ordinary Differential Equations Solution Methods

The periodic steady state of a power network can be determined in the time domain, by integrating the set of non-autonomous ODEs representing the dynamic model of the system, i.e.,

$$\dot{\mathbf{x}} = \mathbf{f}(\mathbf{x}, t) \tag{B.1}$$

The numerical methods to solve the model can be classified into explicit and implicit methods. A concise description about these methods is given next.

a) Explicit Methods.

a.1) Forward Euler. The solution depends only on the previous step between these methods are the forward Euler and Runge-Kutta methods. The formulation of the forward Euler method is

$$\mathbf{x}_{k+1} = \mathbf{x}_k + h\mathbf{f}(\mathbf{x}_k, t_k) \tag{B.2}$$

Where:

$\mathbf{x}_k$ state vector, step k

t_k step time k

h is the integration step

This method is equivalent to use the first two terms of the Taylor series expansion for $\mathbf{x}$ around the point $(\mathbf{x}_0, t_0)$, i.e.,

$$\mathbf{x}_{k+1} = \mathbf{x}_k + h\dot{\mathbf{x}}_k + \frac{h^2}{2!}\ddot{\mathbf{x}}_k + \frac{h^3}{3!}\dddot{\mathbf{x}}_k + \ldots \tag{B.3}$$

To obtain the solution with sufficient accuracy h has to be small, consequently the computational effort required is generally high.

a.2) Runge-Kutta. These methods are based on the approximation of the function $\mathbf{f}(\mathbf{x},t)$ by its Taylor series expansion. The fourth order Runge-Kutta method uses intermediate time steps to compute the state at time t_{k+1}. The recursive formulation is,

$$\mathbf{x}_{k+1} = \mathbf{x}_k + \frac{h}{6}(\mathbf{k}_1 + 2\mathbf{k}_2 + 2\mathbf{k}_3 + \mathbf{k}_4) \tag{B.4}$$

Where:

$$\mathbf{k}_1 = \mathbf{f}(\mathbf{x}_k, t_k) \tag{B.5}$$

$$\mathbf{k}_2 = \mathbf{f}(\mathbf{x}_k + \frac{h}{2}\mathbf{k}_1, t_k + \frac{h}{2}) \tag{B.6}$$

$$\mathbf{k}_3 = \mathbf{f}(\mathbf{x}_k + \frac{h}{2}\mathbf{k}_2, t_k + \frac{h}{2}) \tag{B.7}$$

$$\mathbf{k}_4 = \mathbf{f}(\mathbf{x}_k + h\mathbf{k}_3, t_k + h) \tag{B.8}$$

a.3) Predictor-corrector methods. They are based on two processes:

1) Predictor: where an initial value $\mathbf{x}^p_{k+1}$ is determined using an explicit method.

2) Corrector: This step obtains $\mathbf{x}_{k+1}$ by applying an implicit method, which uses the predicted value to assess $\mathbf{f}(\mathbf{x}_{k+1}, t_{k+1})$,

Predictor:

$$\mathbf{x}^p_{k+1} = \mathbf{x}_k + h\mathbf{f}(\mathbf{x}_k, t_k) \tag{B.9}$$

Corrector:

$$\mathbf{x}_{k+1} = \mathbf{x}_k + \frac{h}{2}\left[\mathbf{f}(\mathbf{x}_k, t_k) + \mathbf{f}(\mathbf{x}^p_{k+1}, t_{k+1})\right] \tag{B.10}$$

These methods require more computational effort because each integration step becomes an iterative process.

In explicit methods, numerical stability is associated with the stiffness of the set of differential equations modeling the system. The stiffness depends of the range of time constants in the system; it can be measured by the ratio of the largest to smallest time constants or eigenvalues of the linearized system [Kundur 1994].

b) Implicit Methods

b.1) Backward Euler. This method is an example of an implicit algorithm, as needs to solve x_{k+1} which can be considered as feedback. The implicit methods are more accurate and stable compared with the explicit methods. The backward Euler formula is given by,

$$\mathbf{x}_{k+1} = \mathbf{x}_k + h\mathbf{f}(\mathbf{x}_{k+1}, t_{k+1}) \tag{B.11}$$

b.2) Trapezoidad rule. The modified Euler method or trapezoidal rule is an implicit method, whose expression is:

$$\mathbf{x}_{k+1} = \mathbf{x}_k + \frac{h}{2}\left[\mathbf{f}(\mathbf{x}_k, t_k) + \mathbf{f}(\mathbf{x}_{k+1}, t_{k+1})\right] \tag{B.12}$$

The equation shows that it is necessary to use a solution for finding an approximation for $\mathbf{f}(\mathbf{x}_{k+1},t_{k+1})$; this is a feature of all the implicit methods. An approximation of $\mathbf{f}(\mathbf{x}_{k+1},t_{k+1})$ can be obtained by the forward Euler method.

Appendix C Nonlinear Load Models

C.1 Nonlinear inductor

The magnetic flux is defined as the state variable, the current can be represented with a *n* order polynomial of the flux to model a nonlinear inductor [Acha and Madrigal 2001]. Figure C.1 illustrates a nonlinear inductor circuit.

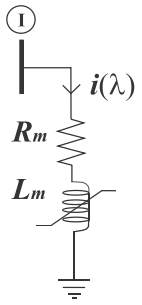

Figure C.1 Nonlinear inductor.

According to KVL,

$$v_I = v_{Rm} + v_{Lm} = R_m i(\lambda) + d\lambda / dt \tag{C.1}$$

$$d\lambda / dt = v_I - R_m i(\lambda) \tag{C.2}$$

The nonlinear function is represented by $i(\lambda)$ as,

$$i(\lambda) = \lambda^n \tag{C.3}$$

Where *n* is an odd number due to the odd symmetry of (C.3). This non linearity can be also modeled as [Chang *et al.* 2004],

$$i(\lambda) = a\lambda + b\lambda^n \tag{C.4}$$

C.2 Electric Arc Furnace

The EAF transient state has influence over the system dynamic behavior [Acha and Madrigal 2001]. Figure C.2 shows the EAF model. The electric arc model can be expressed mathematically by two first order differential equations based on the energy conservation law, where the state variables are the radius and current. The power balance equation is,

$$P_1 + P_2 = P_3 \tag{C.5}$$

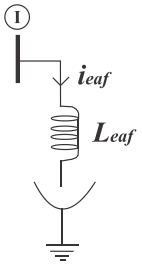

Figure C.2 Electric arc furnace.

P_1 is the heat power going to the external environment, P_2 the power which increases the internal energy arc affecting its radius, and P_3 is the total power converted into heat [Chang *et al.* 2004]. It is assumed that the cooling effect depends of the arc radius r, as,

$$P_1 = k_1 r_{eaf}^{n} \tag{C.6}$$

P_1 also depends of the arc temperature, this dependency is less significant and is ignored, to keep a simple model. n=0 if the arc cooling do not depend on its radius when the environment is hot. When the arc is long, the cooling area is its lateral surface, in this case n=1 and when the arc is short, the cooling is proportional to cross-section arc at the electrodes, then n=2 [Acha and Madrigal 2001], [Chang *et al.* 2004]. P_2 is proportional to the derivative of the arc energy which is proportional to r^2,

$$P_2 = k_2 r_{eaf}(dr_{eaf} / dt) \tag{C.7}$$

P_3 is the total power demanded by the EAF,

$$P_3 = v_{eaf} i_{eaf} = (R_{eaf} i_{eaf}) i_{eaf} = (k_3 r_{eaf}^{(-m-2)}) i_{eaf}^2 \tag{C.8}$$

The arc column resistivity is inversely proportional to r^m, where m=0…2, to consider that the arc may be hotter in the interior if it has a larger radius [Acha and Madrigal 2001].

Substitution of (C.6), (C.7) and (C.8) into (C.5) and solving for the derivative gives the first EAF nonlinear differential equation, radius is the state variable,

$$dr_{eaf} / dt = (k_3 / k_2) r_{eaf}^{(-m-3)} i_{eaf}^2 - (k_1 / k_2) r_{eaf}^{(n-1)} \tag{C.9}$$

From (B.8), voltage is,

$$v_{eaf} = (k_3 r_{eaf}^{(-m-2)}) i_{eaf} \tag{C.10}$$

Applying KVL to the EAF circuit gives the second differential equation, EAF current is the state variable,

$$v_I = v_{Leaf} + v_{eaf} = L_{eaf}(di_{eaf} / dt) + (k_3 r_{eaf}{}^{(-m-2)}) i_{eaf} \tag{C.11}$$

$$di_{eaf} / dt = (1 / L_{eaf})(v_I - k_3 r^{(-m-2)} i_{eaf}) \tag{C.12}$$

A.3 Thyristor Controlled Reactor

The TCR is represented by a thyristor pair back to back connection, in series with a RL circuit. The thyristor conduction interval is controlled with the firing angle α. The TCR current is the state variable, the TCR model is shown in Figure C.3.

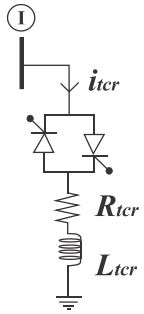

Figure C.3 Thyristor controlled reactor.

According to KVL,

$$v_I = v_{Rtcr} + v_{Ltcr} = i_{tcr}R_{tcr} + L_{tcr}(di_{tcr}/dt) \tag{C.13}$$

$$di_{tcr}/dt = (v_I - i_{tcr}R_{tcr})/L_{tcr} \tag{C.14}$$

The TCR current is dependent of the thyristor firing angle α, representing this dependency by *s*, the TCR nonlinear differential equation is,

$$di_{tcr}/dt = s(v_I - i_{tcr}R_{tcr})/L_{tcr} \tag{C.15}$$

Appendix D Additional system parameters modified IEEE 30 bus test system

Additional System Parameters (pu).

Nonlinear inductance node 5: Rm=4.0, Lm=1.0, pow=n=5.0, b=0.3

EAF node 2: Leaf=0.5, k1=0.004, k2=0.0005, k3=0.005, m=0.0, n=2.0, initial condition radius EAF=0.1

TCR node 6: Rtcr=1.0, Ltcr=0.5, firing angle α=100 deg.

Node Loads (Rl resistance load, Ll inductance load, number indicates the node where load is connected).

Rl2=36.88, Ll2=1.57, Rl3=260.0, Ll3=240.0, Rl4=520.0, Ll4=480.0, Rl5=21.2,

Ll5= 1.05, Rl6=920.0, Ll6=880.0, Rl9=33200.0, Ll9=30800.0, Rl10=67.8,

Ll10=12.04, Rl11=64400.0, Ll11=61600.0, Rl12=17.86, Ll12=2.66, Rl13=128800.0,

Ll13=123200.0, Rl14= 32.78, Ll14=12.5, Rl15=29.64, Ll15=3.45, Rl16= 57.14,

Ll16=11.12, Rl17=22.2, Ll17=3.45, Rl18=130.4, Ll18=20.0, Rl19=201.0, Ll19=30.0,

Rl20=268.0, Ll20=40.0, Rl21=536.0, Ll21=80.0, Rl22=128800.0, Ll22=123200.0,

Rl23=536.0, Ll23=80.0, Rl24=536.0, Ll24=80.0, Rl25=128800.0, Ll25=123200.0,

Rl26=536.0, Ll26=80.0, Rl27=128800.0, Ll27=123200.0, Rl28=128800.0,

Ll28=123200.0, Rl29=536.0, Ll29=80.0, Rl30=670.0, Ll30=100.0

Appendix E Measurement System

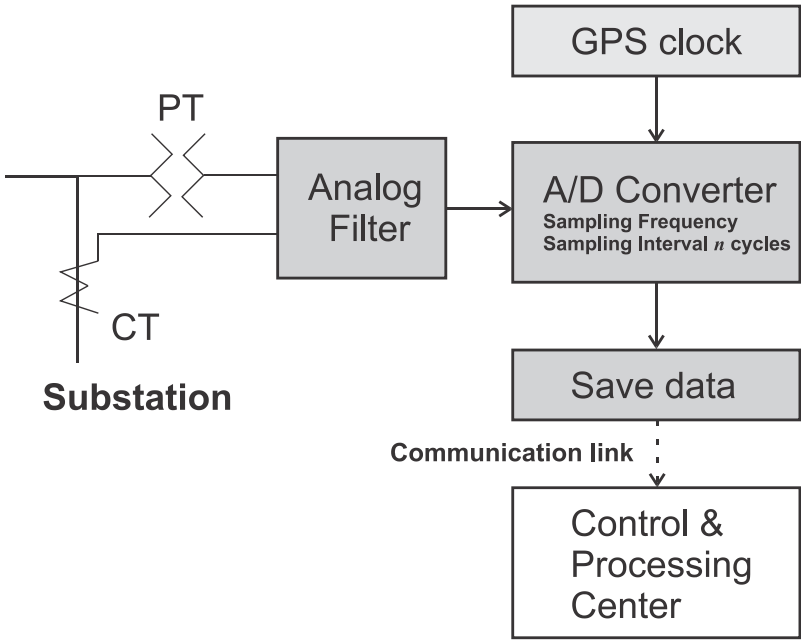

Figure E.1 Measurement System

Voltage and current signal are sampled from lines and nodes with potential and current transformers. These instrument transformers must be of wide spectrum to sense harmonics and transients, the signals are analog filtered , then analog/digital converted after this, they are saved to be sent to the control and processing center, the measurements from various points are synchronized by means of a radio signal or the GPS clock with this time signal the measurements are time stamped to be numerically processed [Arrillaga *et al.* 2000a], [Kanao *et al.* 2005], [Meliopoulos *et al.* 1994], [IEEE 1995].

References

[Abur and Exposito 2004]

Abur A., Exposito A. G., *Power System State Estimation: Theory and Implementation,* Marcel Dekker, USA, 2004.

[Acha and Madrigal 2001]

Acha E., Madrigal M., *Power Systems Harmonics Computer Modelling and Analysis,* John Wiley & Sons, 2001.

[Acha *et al.* 1990]

Acha E., Semlyen A., Rajakovic N., *A Harmonic Domain Computational Package for Nonlinear Problems and its Application to Electric Arcs*, IEEE Trans. on Power Delivery, vol. 5, no. 3, July 1990, pp. 1390-1397.

[Albu and Heydt 2003]

Albu M., Heydt, G.T., *On the Use of RMS Values in Power Quality Assessment*, IEEE Trans. on Power Delivery, vol. 18, No. 4, October 2003, pp. 1586-1587.

[Amit and Shivakumar 2009]

Amit J., Shivakumar N. R., *Power System Tracking and Dynamic State Estimation*, IEEE Power Systems Conference and Exposition, PSCE, March 2009, pp. 1-8.

[Aprille and Trick 1972]

Aprille T.J., Trick T.N., *A Computer Algorithm to Determine the Steady-State Response of Nonlinear Oscillators*, IEEE Trans. on Circuit Theory, CT-19(4), 1972, pp. 354-360.

[Arabkhaburi et al., 2006]

Arabkhaburi D., Kazemi A., Yari M., Aghaei J., *Optimal Placement of UPFC in Power Systems Using Genetic Algorithm*. IEEE Int. Conf. on Industrial Technology, 15-17 Dec. 2006, pp. 1694-1699.

[Arefi *et al.* 2011]

Arefi A., Haghifam M.R., Fathi S.H., *Observability analysis of electric networks considering branch impedance*. International Journal of Electrical Power and Energy Systems, vol. 33, No. 4, May 2011, pp. 954-960.

[Arrillaga *et al.* 2000]

Arrillaga J., Watson N. R., Chen S., *Power System Quality Assessment,* John Wiley & Sons 2000.

[Arrillaga *et al.* 2000a]

Arrillaga J., Bollen M.H.J., Watson N. R., *Power Quality following deregulation,* IEEE Proceedings, vol. 88, No. 2, Feb. 2000.

[Arrillaga *et al.* 2000b]

Arrillaga J., Smith Bruce C., Watson N. R., Wood Alan R., *Power System Harmonic Analysis* John Wiley & Sons, 2000.

[Arrillaga and Watson 2001]

Arrillaga J., Watson N. R., *Computer Modelling of Electrical Power Systems*, John Wiley & Sons, 2001.

[ATP 2002]

Prikler L., Hoidalen H. K., *ATPDRAW version 3.5 Users' Manual*, October 2002.

[Bay 1999]

Bay J. S., *Fundamentals of Linear State Space Systems,* McGraw-Hill, 1999.

[Baggini 2008]

Baggini A., *Handbook of Power Quality*, John Wiley & Sons Inc., 2008.

[Beides and Heydt 1991]

Beides H. M., Heydt G. T., *Dynamic state estimation of power system harmonics using Kalman filter methodology,* IEEE Trans. on Power Delivery, vol. 6, No. 4, Oct. 1991, pp. 1663-1670.

[Blood *et al.* 2008]

Blood E. A., Krogh B. H., Ilic M.D., *Electric Power System Static State Estimation through Kalman Filtering and Load Forecasting,* PES General Meeting, 20-24 July 2008.

[Bollen and Gu 2006]

Bollen Math H. J., Gu Irene Y. H., *Signal Processing of Power Quality Disturbances,* IEEE Press 2006.

[Bollen 2000]

Bollen Math H. J., *Understanding Power Quality Problems,* IEEE Press, 2000.

[Bollen *et al.* 1998]

Bollen Math H. J., Yalcinkaya G., Hazza G., *The use of Electromagnetic Transient Programs for Voltage Sag Analysis,* PES 8th Int. Conf. on Harmonics and Quality of Power, Athens, Greece, October 14-16, 1998.

[Bonner *et al.* 1996]

Bonner A., Grebe T., Gunther E., Hopkins L., Marz M.B., Mahseredjian J., Miller N.W., Ortmeyer T.H., Rajagopalan V., Ranade S.J., Ribeiro P.F., Spherling B.R., Sims T.R., Xu W., *Modeling and Simulation of the Propagation of Harmonics in Electric Power Networks Part II: Sample systems and examples,* IEEE Trans. on Power Delivery, vol 11, No. 1, Jan. 1996, pp. 466-474.

[Brigham 1988]

Brigham E. O., *The Fast Fourier Transform and its Applications,* Prentice Hall, Inc., 1988.

[Chang *et al.* 2004]

Chang G., Hatziadoniu C., Xu W., Ribeiro P., Burch R., Grady W.M., Halpin M., Liu Y., Ranade S., Ruthman D., Watson N, Ortmeyer T., Wikston J., Medina A., Testa A., Gardinier R., Dinavahi V., Acram F., Lehn P., *Modeling Devices With Nonlinear Voltage-Current Characteristics for Harmonic Studies,* IEEE Trans. on Power Delivery, vol 19, No. 4, Oct. 2004, pp. 1802-1811.

[Charalampidis and Papavassilopoulos 2011]

Charalampidis A.C., Papavassilopoulos G.P., *Development and numerical investigation of new non-linear Kalman filter variants,* IET Control Theory and Applications, vol. 5, No. 10, 2011, pp. 1155-1166.

[Chen *et al.* 2010]

Chen C.I., Chang, G.W., Hong R.C., Li H.M., *Extended real model of Kalman filter for time varying harmonic estimation,* IEEE Trans. on Power Delivery, vol. 25, No. 1, Jan. 2010, pp. 17-26.

[Crow 2003]

Crow, Mariesa, *Computational methods for electric power systems,* CRC Press, 2000.

[Dash *et al.* 2012]

Dash P.K., Padhee M., Barik S.K., *Estimation of power quality indices in distributed generation systems during power islanding conditions*, International Journal of Electrical Power and Energy Systems, vol. 36, No. 1, March 2012, pp. 18-30.

[Domijan *et al.* 1993]

Domijan A., Heydt G.T., Meliopoulos A.P.S., Venkata S.S., West S., *Directions of Research on Electric Power Quality*, IEEE Trans. on Power Delivery, vol. 8, No. 1, January 1993, pp. 429-436.

[Dommel 1969]

Dommel H. W., *Digital Computer Solution of Electromagnetic Transients in Single and Multiphase Networks*, IEEE Trans. on Power Apparatus and Systems, PAS-88, No. 4, April 1969, pp. 388-399.

[Du *et al.* 1996]

Du Z. P., Arrillaga J., Watson N. R., *Continuous harmonic state estimation of power systems,* IEE Proc. Gener., Transm. and Distrib., vol. 143, No. 4, July 1996, pp. 329-336.

[Du *et al.* 1998]

Du Z. P., Arrillaga J., Watson N. R., Chen S., *Implementation of Harmonic State Estimation*, 8th Int. Conf. on Harmonics and Quality of Power ICHQP'98, Athens, Greece, October 14-16, 1998.

[Du *et al.* 1999]

Du Z. P., Arrillaga J., Watson N. R., Chen S., *Identification of harmonic Sources of Power Systems Using State Estimation,* IEE Proc. Part C, Gener., Transm. and Distrib., vol. 146, No. 1, Jan. 1999, pp. 7-12.

[Dugan *et al.* 2002]

Dugan Roger C., McGranaghan Mark F., Santoso Surya, Wayne Beaty H., *Electrical Power Systems Quality* 2nd Edition, McGraw-Hill, 2002.

[El-Rewini and Abd-El-Barr 2005]

El-Rewini H., Abd-El-Barr M., *Advanced Computer Architecture and Parallel Processing,* John Wiley & Sons, 2005.

[Elnady and Salama 2005]

Elnady A., Salama M.M.A., *Unified Approach for Mitigating Sag and Voltage Flicker Using the DSTATCOM,* IEEE Trans. on Power Delivery, vol. 20, No. 2, April 2005, pp. 992-1000.

[Emanuel 2000]

Emanuel A. E., *Harmonic in the Early Years of Electrical Engineering: A Brief Review of Events, People and Documents,* IEEE 9th Int. Conf. on Harmonics and Quality of Power, vol. 1, Orlando, FL, 1-4 Oct. 2000.

[EMTDC 2005]

EMTDC User's Guide, Manitoba HVDC Research Centre, Inc., Version 4.2.0, 4th printing, April 2005.

[EMTPTB 1981]

Electro-Magnetic Transients Program (EMTP) Theory Book, Branch of System Engineering Bonneville Power Administration, Portland, Oregon 97208-3621, USA, 1981.

[Espinosa-Juarez and Hernandez 2007]

Espinosa-Juarez E., Hernandez A., *A Method for Voltage Sag State Estimation in Power Systems,* IEEE Trans. on Power Delivery, vol. 22, No. 4, October 2007, pp. 2517-2526.

[Farach *et al.* 1993]

Farach J. E., Grady W. M., Arapostathis A., A*n optimal procedure for placing sensors and estimating the locations of harmonic sources in power systems,* IEEE Trans. on Power Delivery, vol. 8, No. 3, pp. 1303-1310, 1993.

[Farzanehrafat and Watson 2010]

Farzanehrafat A., Watson N. R., *Review of Power Quality State Estimation,* 20th Australasian Universities Power Engineering Conf., AUPEC, 2010.

[Gao and Wang 2010]

Gao W., Wang S., *On-line Dynamic State Estimation of Power Systems*. North American Power Symposium NAPS 2010; Arlington, TX, Sept. 26-28.

[Ghahremani and Kamwa 2011]

Ghahremani E., Kamwa I., *Dynamic State Estimation in Power System by Applying the Extended Kalman Filter With Unknown Inputs to Phasor Measurements*, IEEE Trans. On Power Syst., vol. 26, no. 4, Nov. 2011, pp. 2556-2566.

[Ghahremani and Kamwa 2011a]

Ghahremani E., Kamwa I., *Simultaneous State and Input Estimation of a Synchronous Machine Using the Extended Kalman Filter with Unknown Inputs*, IEEE Int. Electric Machines & Drives Conf. (IEMDC), 2011, pp. 1468-1473.

[Grainger and Stevenson 1996]

Grainger John J., Stevenson William D., *Power System Analysis,* McGraw-Hill, 1996.

[Grewal and Andrews 2001]

Grewal M. S., y Andrews A.P., *Kalman Filtering: Theory and Practice using Matlab,* Second Edition, John Wiley & Sons, 2001.

[Gunther 2001]

Gunther E. W., *Interharmonics in power systems,* IEEE PES Summer Meet., vol. 2, 2001, pp. 813-817.

[Hajian *et al.* 1989]

Hajian M., Ranjbar A.M., Amraee T., Mozafari B., *Optimal placement of PMUs to maintain network observability using modified BPSO algorithm*. International Journal of Electrical Power and Energy Systems, vol. 33, No. 1, January 2011, pp. 28-34.

[Handschin *et al.* 1975]

Handschin E., Schweppe F.C., Kohlas J., Fiechter A., *Bad Data Analysis for Power System State Estimation*. IEEE Trans. on Power Apparatus and Systems, vol. PAS-94, No. 2, March/April 1975.

[Heydt 1991]

Heydt G. T., *Electric Power Quality,* 2nd Edition, Stars in a Circle Publications, 1991.

[Heydt and Jewel 1998]

Heydt G. T., Jewell W. T., *Pitfalls of Electric Power Quality Indices,* IEEE Trans. on Power Delivery, vol. 13, No. 2, April 1998, pp 570-578.

[Heydt 1989]

Heydt G. T., *Identification of harmonic sources by a state estimation technique*, IEEE Trans. on Power Delivery, vol. 4, No. 1, Jan. 1989, pp. 569-576.

[Huang *et al.* 2011]

Huang M., Wei S., Huang B., Chang Y., *Accelerating the Kalman Filter on a GPU,* IEEE 17th. Int. Conf. on Parallel and Distributed Systems, ICPADS 2011, pp. 1010-1020.

[IEC 2008]

International Electrotechnical Commission, IEC 61400-21, Edition 2.0, 2008-08.

[IEEE 2013]

IEEE Test Systems, Power Systems Test Case Archive. http://www.ee.washington.edu/research/pstca.

[IEEE 1995]

IEEE Recommended Practice for Monitoring Electric Power Quality, IEEE Std. 1159.

[IEEE 1992]

IEEE Recommended Practices and Requirements for Harmonic Control in Electrical Power Systems, IEEE Std. 519.

[Jinghe *et al.* 2011]

Jinghe Z., Welch G., Bishop G., *LoDiM: A Novel Power System State Estimation Method with Dynamic Measurement Selection*, IEEE PES General Meeting, 2011, pp 1-7.

[Julier and Uhlmann 2004]

Julier S.J., Uhlmann J.K., *Unscented Filtering and Nonlinear Estimation*. Proceedings IEEE vol. 92, 2004, pp. 401-422.

[Julier and Uhlmann 1997]

Julier S.J., Uhlmann J.K., *A new extension of the Kalman filter to nonlinear systems*. Proceedings Aerosense: 11th Int. Symposium Aerospace/Defense Sensing, Simulation and Controls, 1997, pp. 182-193.

[Kalman 1960]

Kalman R. E., *A New Approach to Linear Filtering and Prediction Problems,* Trans. of the ASME, Series D, Journal of Basic Engineering, vol. 82, 1960, pp. 35-45.

[Kanao *et al.* 2005]

Kanao N., Yamashita M., Yanagida H., Mizukami M., Hayashi Y., and Matsuki J., *Power System Harmonic Analysis using State-Estimation Method for Japanese Field Data,* IEEE Trans. on Power Delivery, vol. 20, No. 2, April 2005, pp. 970-977.

[Kennedy *et al.* 2003]

Kennedy K., Lightbody G. and Yacamini R., *Power System Harmonic Analysis using the Kalman Filter,* IEEE PES General Meeting, vol. 2, 2003, pp. 752-757.

[Kuang-Rong and Shyh-Jier 2002]

Kuang-Rong S., Shyh-Jier H., *Application of a Robust Algorithm for Dynamic State Estimation of a Power System*. IEEE Trans on Power Systems, vol. 17, No. 1, February 2002, pp. 141-147.

[Kumar *et al.* 2006]

Kumar A., Das B., Sharma J., *Robust dynamic state estimation of power system harmonics*. International Journal of Electrical Power and Energy Systems, vol. 28, No. 1, January 2006, pp. 65-74.

[Kundur 1994]

Kundur, P., *Power System Stability and Control,* McGraw-Hill, California, 1994.

[Lobos *et al.* 1998]

Lobos T., Kozina T., Osowski S., *Detection of Remote Harmonics Using SVD,* Int. Conf. on Harmonics and Quality of Power ICHQP 98, Athens, Greece, October 14-16, 1998.

[Ma and Girgis 1996]

Ma H. and Girigs A. A., *Identification and tracking of harmonic sources in a power system using a Kalman filter,* IEEE Trans. on Power Delivery, vol. 11, No. 3, 1996, pp. 1659-1665.

[Madrigal 2003]

Madrigal M., *Calidad de la Energía y Análisis Armónico en Sistemas Eléctricos,* PGIIE, ITM 2003.

[Madtharad *et al.* 2003]

Madtharad C., Premrudeepreechacharn S., and Watson N. R., *Power System State Estimation using Singular Value Decomposition,* Electric Power System Research, vol. 67, Nov. 2003, pp. 99-107.

[Madtharad *et al.* 2005]

Madtharad C., Premrudeepreechacharn S., Watson N. R., Saeng-Udom R., A*n Optimal Measurement Placement Method for Power System Harmonic State Estimation,* IEEE Trans. on Power Delivery, vol. 20, No. 2, April 2005, pp. 1514-1421.

[Mahmoud *et al.* 2000]

Mahmoud M.S., Xie L., Soh Y.C., *Robust Kalman filtering for discrete state-delay systems,* IEE Proc. Control Theory Appl., vol. 147, No. 6, November 2000.

[Manson and Targosz, 2008]

Manson, J., Targosz, R., *European Power Quality Survey Report*, Leonardo Energy, Nov. 2008. Available: http://www.leonardo-energy.org/european-power-quality-survey-report

[Matair *et al.* 2000]

Matair S. S., Watson N. R., Wong K. P., Pham V. L., Arrillaga J., *Harmonic state estimation:*

a method for remote harmonic assessment in a deregulated utility network, Electric Utility Deregulation and Restructuring and Power Technologies, Proceedings DRPT 2000.

[Medina *et al.* 2013]

Medina, A., Segundo-Ramirez J., Ribeiro P., Xu W., Lian K. L., Chang G. W., Dinavahi V., Watson N.R., IEEE Task Force on Harmonics Modeling and Simulation, *Harmonic Analysis in Frequency and Time Domain*, IEEE Trans. on Power Delivery, vol. 28, No. 3, 2013, pp. 1813-1821.

[Medina *et al.* 2003]

Medina, A., Ramos-Paz, A., Fuerte-Esquivel, C.R., *Swift Computation of the Periodic Steady State Solution of Power Systems Containing TCSCs*, International Journal on Electrical Power and Energy Systems, vol. 25, 2003, pp. 689-694.

[Medina *et al.* 2003a]

Medina, A., Ramos-Paz, A., Fuerte-Esquivel, C.R., *Periodic Steady State Solution of Electric Systems With Nonlinear Components Using Parallel Processing*, IEEE Trans. on Power Systems, vol. 18, No. 2, May 2003, pp. 963-965.

[Medina and Ramos-Paz 2005]

Medina, A., Ramos-Paz, A., *Newton Techniques for the Steady State Solution of Nonlinear Electric Networks*, WSEAS Trans. on Circuits and Systems, vol. 4, No. 8, August 2005, pp. 842-849.

[Meliopoulos *et al.* 1994]

Meliopoulos A. P. S., Zhang F., Zelingher S., *Power system harmonic state estimation,* IEEE Trans. on Power Delivery, vol. 9, No. 3, July 1994, pp. 1701-1709.

[Miller and Dewe 1992]

Miller A. J. V., Dewe M. B., *Multichannel Continuous Harmonic Analysis in Real-Time,* IEEE Trans. on Power Delivery, vol. 7, No. 4, October 1992, pp. 1813-1819.

[Moghadasian *et al.* 2010]

Moghadasian M., Mokhtari H., Baladi A., *Power System Harmonic State Estimation using WLS and SVD*; A practical Approach, IEEE 14th Int. Conf. on Harmonics and Quality of Power, ICHQP, 2010.

[Monticelli 1999]

Monticelli A., *State Estimation in Electric Power Systems: A Generalized Approach,* Kluwer Academic Publishers, USA, 1999.

[Monticelli 2000]

Monticelli A., *Electric Power System State Estimation,* IEEE Proceedings, vol. 88, No. 2, February 2000.

[Moreno *et al.* 2009]

Moreno V. M. and Pigazo A., *Kalman Filter: Recent Advances and Applications*, In-Teh, I-Tech Education and Publishing KG, Vienna, Austria, 2009.

[Nvidia Cuda C 2012]

NVIDIA, CUDA C Programming Guide, Version 5.0, October 2012.

[Nvidia Cuda API 2012]

NVIDIA, CUDA API Reference Manual, Version 5.0, October 2012.

[Nvidia Cublas 2012]

NVIDIA, CUDA Toolkit 5.0 CUBLAS Library, April 2012.

[Ogata 2002]

Ogata K., *Modern Control Engineering,* Pearson Prentice Hall, 4th Ed., 2002.

[Owen 1998]

Owen E. L., *A history of harmonics in power systems,* IEEE Industry Applications Magazine, vol. 4, no. 1, Jan.-Feb. 1998, pp. 6-12.

[Owens *et al* 2008]

Owens J. D., Houston M., Luebke D., Green S., Stone J.E., Phillips J.C., *GPU Computing,* Proc. of the IEEE, vol. 96, no. 5, May 2008, pp. 879-899.

[Parker and Chua 1989]

Parker T. S., Chua L. O., *Practical Numerical Algorithms for Chaotic Systems,* Springer-Verlag New York Inc., 1989.

[Peng *et al.* 2011]

Peng J.C.H., Mead A., Nair N. K. C., *Exploring Parallel Processing for Wide Area Measurement Data Applications,* PES General Meeting, 24-29 July 2011.

[Pham *et al.* 2000]

Pham V. L., Wong K. P., Watson N. R., Arrillaga J., *Sub-harmonic state estimation in power systems,* Proc. of PES Winter Meeting, vol. 2, Jan. 2000, pp. 1168-1173.

[Press *et al.* 2007]

Press W. H., Teukolsky S. A., Vetterling W. T., Flannery B. P., *Numerical Recipes The Art of Scientific Computing*, 3rd Edition, England, Cambridge University, 2007.

[PSCAD 2005]

Pscad User's Guide, Versión 4.2.0, Manitoba HVDC Research Centre Inc., Abril 2005.

[Rambabu *et al.* 2008]

Rambabu K., Bjarne F., Lars I., *Applying the unscented Kalman filter for nonlinear state estimation*. Journal of Process Control, Elsevier, vol. 18, Nos. 7-8, August-September 2008, pp. 753-768.

[Rakpenthai *et al.* 2010]

Rakpenthai C., Premrudeepreechacharn S., Uatrongjit S., Watson N.R., *An interior point method for WLAV state estimation of power systems with UPFCs*. International Journal of Electrical Power and Energy Systems, vol. 32, No. 6, July 2010, pp. 671-677.

[Ramos 2006]

Ramos Paz Antonio, *Metodología Unificada en el dominio del tiempo para el Análisis en Estado Estacionario y Estado Transitorio de Sistemas Eléctricos No Lineales,* Tesis Doctoral, División de Estudios de Posgrado, Facultad de Ingeniería Eléctrica, Universidad Michoacana de San Nicolás de Hidalgo, Morelia, Michoacán, México, 2006.

[Ranade *et al.* 1996]

Bonner A., Grebe T., Gunther E., Hopkins L., Marz M. B., Mahseredjian J., Miller N. W., Ortmeyer T. H., Rajagopalan V., Ranade S. J., Ribeiro P. F., Shperling B. R., Sims T. R., Xu W., *Modeling and Simulation of the Propagation of Harmonics in Electric Power Networks*, Task Force on Harmonics Modeling and Simulation, IEEE Trans. on Power Delivery, vol. 11, No. 1, Jan. 1996, pp. 452-465.

[Saha *et al.* 2012]

Saha Roy B.K., Sinha A.K., Pradhan A.K., *An optimal PMU placement technique for power system observability*. International Journal of Electrical Power and Energy Systems, vol. 42, No. 1, November 2012, pp. 71-77.

[Schweppe *et al.* 1970]

Schweppe F. C., Wildes J. C., Rom D., *Power system static state estimation, Part I, II and III*, IEEE Trans. Power Apparatus and Systems, vol. PAS-89, No. 1, January 1970, pp. 120-135.

[Segundo 2010]

Segundo Ramírez Juan, *Nonlinear Analysis of Power Systems including FACTS and Custom Power Devices Based on Bifurcation Theory and Newton Methods*, Doctoral Thesis, Universidad Michoacana de San Nicolás de Hidalgo, Morelia, Michoacán, México, 2010.

[Segundo and Medina 2010]

Segundo-Ramírez J., Medina A., A*n Enhanced Process for Fast Periodic Steady State Solution of Nonlinear Systems by Poincaré Map and Extrapolation to the Limit Cycle*, International Journal of Nonlinear Sciences & Numerical Simulation, vol. 11, No. 8, 2010, pp. 659-668.

[Segundo and Medina 2008]

Segundo J., Medina A., *Periodic Steady State Solution of Electric Systems including UPFC by Extrapolation to the Limit Cycle*, IEEE Trans. on Power Delivery, vol. 23, No. 3, July 2008, pp. 1506-1512.

[Semlyen and Medina 1995]

Semlyen A., Medina A., *Computation of the Periodic Steady State in Systems with Nonlinear Components Using a Hybrid Time and Frequency Domain Methodology,* IEEE Trans. on Power Systems, vol. 10, No. 3, August 1995, pp. 1498-1504.

[Shiying *et al.* 2006]

Shiying Hou, Zhixiang Xu, Houyu Lv, Zejia Jiang and Lingyi, *Research into Harmonic State Estimation in Power System Based on PMU and SVD*, IEEE Int. Conf. on Power System Technology, Powercon, 2006.

[Short *et al.* 2003]

Short T. A., Mansoor A., Sunderman W., Sundaram A., *Site Variation and Prediction of Power Quality,* IEEE Trans. on Power Delivery, vol. 18, No. 4, October 2003, pp. 1369-1375.

[Stagg and El-abiad 1968]

Stagg G. W., El-Abiad A. H., *Computer Method in Power System Analysis,* Mc Graw Hill, Japón 1968.

[Strang 1988]

Strang G., *Linear Algebra and its Applications*, 3rd Edition, Harcourt Brace Jovanovich, Inc., 1988.

[Tan *et al.* 2005]

Tan T. L., Chen S., Choi S. S., *An Overview of Power Quality State Estimation*, IEEE 7th. International Power Engineering Conference, IPEC, 2005.

[Testa *et al.* 2007]

Testa A., Akram M. F., Burch R., Carpinelli G., Chang G., Dinavahi V., Atziadonin C., Grady W. M., Gunther E., Halpin M., Lehn P., Liu Y., Langella R., Lowenstein M., Medina A., Ortmeyer T., Ranade S., Ribeiro P., Watson N., Wikston J., and Xu W., *Interharmonics: Theory and Modeling,* IEEE Task Force on Harmonics Modeling and Simulation, IEEE Trans on Power Delivery, vol. 22, No. 4, Oct. 2007, pp. 2335-2348.

[Ueda *et al.* 1975]

Ueda R., Takata H., Nakagaki S., Takata S., *On the estimation of transient state of power system by discrete of nonlinear observer,* IEEE Trans. on Power Apparatus and Systems, vol. 94, No. 6, 1975, pp. 2135-2140.

[Ueda *et al.* 1977]

Ueda R., Takata H., Yoshimura S., Takata S., *Estimation of transient state of multi-machine power system by extended linear observer,* IEEE Trans. on Power Apparatus and Systems, vol. 96, No. 2, pp. 681-687, 1977.

[Valderde *et al.* 2011]

Valverde G., Kyriakides E., Heydt GT., Terzija V. *Nonlinear Estimation of Synchronous Machine Parameters using Operating Data.* IEEE Trans. on Energy Conversion, vol. 26, pp. 831-839, 2011.

[Valderde and Terzija 2011]

Valverde G., Terzija V., *Unscented Kalman filter for power system dynamic state estimation.* IET Gener., Transm. and Distrib., vol. 5, No. 1, 2011, pp. 29-37.

[Van der Heijden *et al.* 2004]

Van der Heijden F., Duin R.P.W., de Ridder D., Tax D.M.J., *Classification, Parameter Estimation and State Estimation,* John Wiley & Sons, 2004.

[Van der Merwe and Wan 2001]

Van der Merwe R., Wan E.A. *The square-root unscented Kalman filter for state and parameter estimation.* IEEE Int. Conf. on Acoustics, Speech, and Signal Processing (ICASSP), vol. 6, pp. 3461-3464, 2001.

[Volkov and Demmel 2008]

Volkov V., Demmel, J.W., *Benchmarking GPUs to tune dense linear algebra,* Int. Conf. for High Performance Computing, Networking, Storage and Analysis, 2008, pp. 1-11.

[Wang *et al.* 2012]

Wang S., Gao W., Meliopoulos A.P.S., *An Alternative Method for Power System Dynamic State Estimation Based on Unscented Transform*. IEEE Trans. on Power Systems, vol. 27, 2012, pp. 942-950.

[Wang *et al.* 2004]

Wang B., Xu W., Pan Z., *A Method to Estimate Voltage Sag Profile for Power Distribution Systems* 2004 Int. Conf. on Power System Technology POWERCON 2004, Singapore, 21-24 November 2004.

[Wang *et al.* 2005]

Wang B., Xu W., Pan Z., *Voltage Sag State Estimation for Power Distribution Systems* IEEE Trans. on Power Systems, vol. 20, pp. 806-812, 2005.

[Watson 2010]

Watson N. R., *Power Quality State Estimation*, European Trans. Electrical Power; vol. 20, No 1, Jan. 2010, pp. 19-33.

[Watson & Arrillaga 2007]

Watson N. R., Arrillaga J., *Power Systems Electromagnetic Transients Simulation,* IET Power and Energy Series 39, 2007.

[Watson *et al.* 2000]

Watson N. R., Arrillaga J., Du Z. P., *Modified Symbolic Observability for Harmonic State Estimation,* IEE Proc. Part C, Gener., Transm. and Distrib., vol. 147, No. 2, March 2000, pp. 105-111.

[Watson and Yu 2008]

Watson N.R., Yu K.K.C., *Transient State Estimation,* 13th Int. Conf. on Harmonics and Quality of Power. ICHQP, 2008.

[Wilson 2007]

Wilson D.H., *Wide-Area Measurement and Control for Dynamic Stability,* PES General Meeting, 24-28 June 2007.

[Wu *et al.* 1988]

Wu F. F., Liu W. E., Lun S., *Observability Analysis and Bad Data Processing for State Estimation with Equality Constraints,* IEEE Trans on Power Systems, vol. 3, No. 2, May 1988, pp. 541-548.

[Yu *et al.* 2004]

Yu K. K. C., Watson N. R., Arrillaga J., *Three Phase Harmonic State Estimation using SVD for Partially Observable Systems*, Proceedings of PowerCon 2004, Singapore, Nov. 2004.

[Yu 2005]

Yu K. K. C., *Harmonic State Estimation and Transient State Estimation,* Tesis Doctoral, Electrical and Computer Engineering, University of Canterbury, Chrischurch, New Zealand 2005.

[Yu *et al.* 2005a]

Yu K. K. C., Watson N. R., Arrillaga J., *An Adaptive Kalman Filter for Dynamic Harmonic State Estimation and Harmonic Injection Tracking*, IEEE Trans. on Power Delivery, vol. 20, No. 2, April 2005, pp. 1577-1584.

[Yu *et al.* 2005b]

Yu K. K. C., Watson N. R., Arrillaga J., *Error Analysis in Static Harmonic State Estimation : A Statistical Approach.*, IEEE Trans. on Power Delivery, vol. 20, No. 2, April 2005, pp. 1045-1050.

[Yu and Watson 2007]

Yu K. K. C., Watson N. R., *An Approximate method for Transient State Estimation*, IEEE Trans. on Power Delivery, vol. 22, No. 3, July 2007, pp. 1680-1687.

[Zamora 2004]

Zamora Cárdenas Enrique Arnoldo, *Estimación de Estado en Sistemas Flexibles de Transmisión de Corriente Alterna*, Thesis, Universidad Michoacana de San Nicolás de Hidalgo, Morelia, Michoacán, México, 2004.

[Zhang J. *et al.* 2011]

Zhang J., Welch G., Bishop G., *LoDiM: A Novel Power System State Estimation Method with Dynamic Measurement Selection*, PES General Meeting, 24-29 July 2011.

[Zill 2002]

Zill Dennis G., *Differential Equations with Modeling Applications*, 9a. Edition International Thomson Editors, 2009.